NEAR-FIELD INVESTIGATION OF UNIFORMLY PERIODIC MONOPOLE ARRAYS

by
EDWARD HUDOCK

30 May 1963

Technical Report No. 1

Contract No. NOBSR 85243
Index Number SS024001

Sponsored by
BUREAU OF SHIPS
DEPARTMENT OF THE NAVY
Washington 25, D.C.

ANTENNA LABORATORY
DEPARTMENT OF ELECTRICAL ENGINEERING
ENGINEERING EXPERIMENT STATION
UNIVERSITY OF ILLINOIS
URBANA, ILLINOIS

NEAR-FIELD INVESTIGATION OF UNIFORMLY PERIODIC MONOPOLE ARRAYS

by

Edward Hudock

30 May 1963

Technical Report No. 1

Contract No. NOBSR 85243
Index Number SS024001

Sponsored by

BUREAU OF SHIPS
DEPARTMENT OF THE NAVY
Washington 25, D.C.

ANTENNA LABORATORY
ENGINEERING EXPERIMENT STATION
UNIVERSITY OF ILLINOIS
URBANA, ILLINOIS

ABSTRACT

The amplitude and phase characteristics of waves traveling along various uniformly periodic arrays of monopoles have been investigated. It is found that these structures usually exhibit regions of frequency where the propagation constant is complex. Over these regions the structure may function as an effective radiator, the directional characteristics of which depend upon the relative phase and amplitude distribution of the wave(s) on the array. Of prime importance in the determination of the structure's directional properties is the sign of the phase constant over the first cell or two.

This study led to extensive use of the Brillouin, or k-β, diagram and its utility in the analysis and summation of the measured near-field data is shown. The measured far-field patterns illustrate the correlation between the actual and expected directional properties of the respective structures.

The results of this study provide additional insight to the fundamental principles which underlie frequency independent antennas, and, thus, have application to successful designs of log-periodic monopole arrays. These results demonstrate that under appropriate conditions of phasing, backfire radiation may be established, and, further, that the rate of attenuation or decay of the near field depends upon the geometry of the structure.

ACKNOWLEDGEMENT

The author is indebted to the Antenna Laboratory of the University of Illinois for the opportunity given to conduct this work, and to the members of the laboratory staff for their support. The guidance and counsel of the author's advisor, Professor P. E. Mayes, are particularly appreciated.

Gratitude is due also to Messrs. Samuel A. Guccione and Richard C. Griswold for their assistance in the construction of the models, measurements, data reduction, and preparation of illustrations for this report. Their patience and interest are sincerely appreciated.

This work was conducted under the sponsorship of the United States Navy Department, Bureau of Ships, Contract Number NOBSR 85243.

CONTENTS

LIST OF ILLUSTRATIONS

LIST OF ILLUSTRATIONS (Continued)

LIST OF ILLUSTRATIONS (Continued)

1. INTRODUCTION

There have evolved over the past few years many successful, practical and useful designs from the log-periodic class of frequency independent antennas. It is safe to say, however, that for every successful design there preceded several, if not many, unsuccessful attempts. While much has been written by the engineer on his particular successful design, very little has been published regarding the fundamental principles which govern the successful operation of some structures and the unsuccessful performance of others. This is evidence of the fact that there does not yet exist a thorough knowledge of the basic principles which underlie successful frequency independent, or, more correctly, quasi frequency-independent, performance from the adequately designed practical log-periodic structure. This fact, together with the requirement by the sponsoring agency for an improved antenna system for wideband radio direction finding application, prompted the subject investigation.

In May 1961, Mayes, Deschamps and Patton[1] suggested that a knowledge of the near-field properties of the uniformly periodic structure whose geometry is the counterpart of that of the log-periodic device may lead to a better understanding of the elements which govern successful frequency-independent performance. Using the concept of backward-wave radiation, they introduced several basic requirements for frequency independence. Backward wave radiation is that which is directed toward the point of excitation, a trait which appears to be inherent in most unidirectional log-periodic antennas, and is believed to be the result of a space wave traveling along the structure in the backward direction. It is further believed that the backward traveling wave is due to effective coupling between the forward traveling feeder wave and the proper

(backward) space harmonic(s). In order for this condition to exist it was shown that the feeder wave medium must be such to produce only waves which are quite slow at the frequencies where radiation is not intended. At the frequencies where radiation is intended one or more of the space harmonic waves should be fast or almost fast. Thus, for the tapered (log-periodic) structure, the feeder wave progresses toward the active region under slow wave conditions. Upon reaching the active region, space harmonics are generated, the dominant of which is one propagated in the backward direction. For a slow wave, $\beta > k$, where β is the phase constant of the feeder (guided) wave and k is the intrinsic phase constant of free space. The near-field characteristic of fundamental interest, therefore, is the relative phase velocity of the feeder wave, or, more precisely, the k-to-β relationship.

With the uniformly periodic structure, the k-to-β relation is observed as a function of frequency of the source of the feeder wave. An invaluable method for displaying the k-to-β relation is by means of the Brillouin or k-β diagram. Its utility extends beyond the convenience it offers for summarizing the near-field data in that the diagram also affords a useful tool for analyzing the radiation properties of the uniformly periodic antenna structure. Consequently, extensive use has been made of the Brillouin diagram throughout the project.

There is, of course, a large number of periodic antenna structures which differ enough in their geometry to warrant individual attention. However, it would be highly impractical for one effort to explore more than a particular class of structures. The class of periodic structures of interest here is that of the vertically polarized monopole arrays. With the current state of the antenna art, a system of vertically polarized log-periodic monopole arrays comes nearest to meeting the requirements of a broadband wide aperture radio

direction finding system for the h-f (2-30 Mc) range. Even with the area of research reduced to this class of antennas, it was necessary to further limit the investigation to structures of practical interest and to those which would appear not to yield redundant information. In like manner, it could not be expected that all vertically polarized periodic monopole arrays that may be of practical interest are covered herein.

By the nature of the project, it was largely an experimental effort. Consequently, this report contains a rather large amount of experimental data. Yet, the data presented herein represent only a small portion of the total taken and is considered to be the minimum necessary to exhibit the properties of the various structures. In addition to the near-field measurements, far-field pattern measurements were made on the various structures to examine the correlation between the actual and expected radiation properties of each. Although the impedance properties of frequency independent antennas are as important as their radiation properties, the problem of impedance was not considered here. This would appear to constitute its own area of research. It is hoped that the efforts expended in this project will offer experimental evidence to theories that may have been postulated heretofore, and that the data will be of supplemental aid to a better understanding of the frequency-independent antenna.

2. A BRIEF REVIEW OF THE BRILLOUIN DIAGRAM AND ITS APPLICATION TO PERIODIC STRUCTURES

It is instructive, first, to review some of the basic properties of the uniform periodic transmission system. In so doing, the utility of the Brillouin diagram in analyzing the near-field data of the periodic monopole array will be also illustrated. The application of the Brillouin diagram to the analysis of several other types of periodic structures has been reported heretofore. Mayes and Ingerson, for example, have demonstrated the usefulness of the diagram in reporting near-field measurements on the uniformly periodic counterpart of the log-periodic dipole array.[2] Dyson, Patton and Greiser, of the University of Illinois Antenna Laboratory, have used the diagram in their work with the log-spiral, bifilar helix and the zigzag antennas, respectively. The near-field characteristics of the periodic monopole array differ enough from these earlier structures to warrant this distinct effort. It is important to note that this work with the monopole arrays does not duplicate the efforts expended on the dipole array; that is, the log-periodic monopole array cannot in general be treated simply as one-half of the log-periodic dipole array. These two structures achieve their backward-wave characteristics through different mechanisms. Accordingly, the respective Brillouin diagrams can be expected to be somewhat different.

In discussing periodic transmission systems, it is advisable to clarify the term "period". A period is defined here to involve only the property of axial translation. That is, a displacement of the structure along its axis by one period results in a configuration which does not differ from that of the original. Thus, for the structure (UPM(2)C) shown in Figure 1, the period is the dimension, a; the region between two points separated by a is sometimes

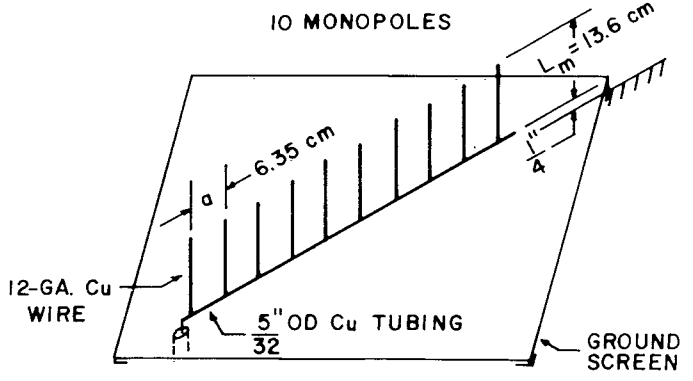

UPM(2)C

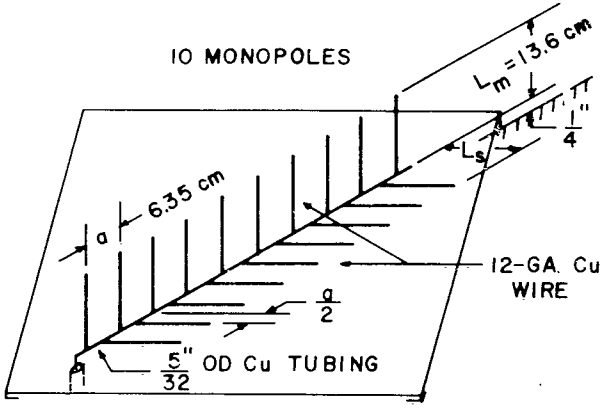

	UPM(2)	UPM(2)A	UPM(2)B
L_s (cm)	13.6	12.6	14.6

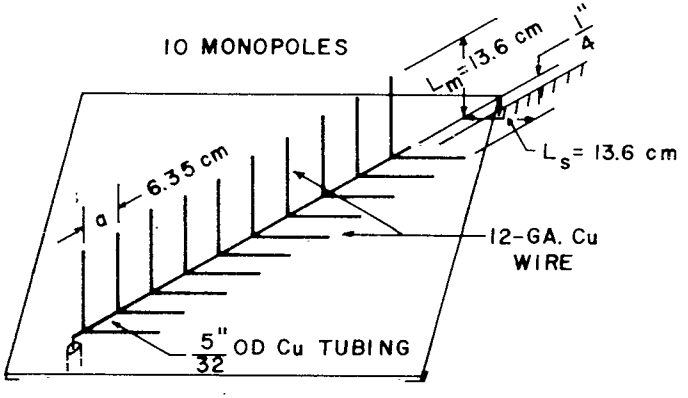

UPM(2)D

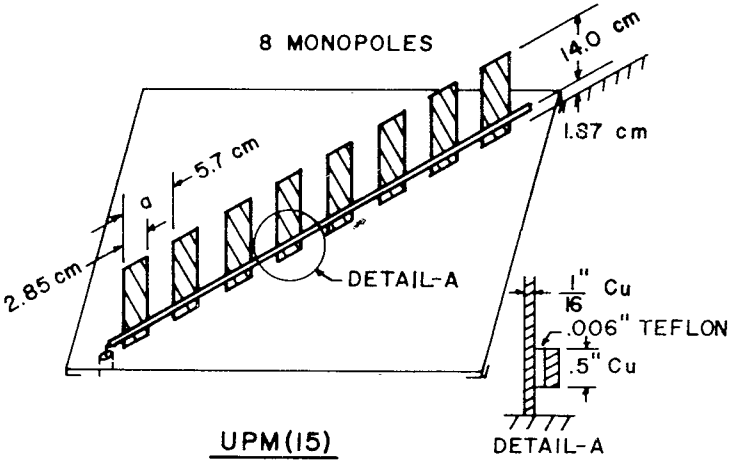

UPM(15)

Figure 1. Details of Model Construction for UPM(2)C, UPM(2), UPM(2)A, UPM(2)B, UPM(2)D and UPM(15).

referred to as a cell. However, it is worthwhile to note the more generalized form of periodicity suggested by Professor G. A. Deschamps,[3] where the additional symmetrical properties of glide rotation, glide reflection, etc., are included to define periodicity. For example, the period of the structure (UPM(10)C) shown in Figure 2 may be defined as $\frac{a}{2}$ instead of a.

The theorem of Floquet applied to periodic transmission systems infinite in length provides a basis for analyzing the uniformly periodic antenna structure. This theorem states that for a given frequency and a given mode of propagation the fields at a particular cross section of one cell will differ from the fields at the same cross section of any other cell only by a complex constant. This constant can be written as the exponential, $\exp(-\gamma a)$, where γ is the usual propagation constant and a is the period of the structure as defined above. Although Floquet's theorem is strictly true only for structures of infinite length, experiment indicates that the theorem does provide grounds for analyzing the periodic antenna structure whose length is finite.

As a consequence of Floquet's theorem stated above, the fields associated with a periodic structure can be written in the form

$$f(z) = \exp(-\gamma z)\, g(z) \tag{1}$$

where $g(z)$ is a periodic function with period a; that is, $g(z + a) = g(z)$.

Thus,

$$f(z + a) = \exp[-\gamma (z + a)]\; g(z + a)$$

or

$$= \exp(-\gamma a)\; f(z) \tag{2}$$

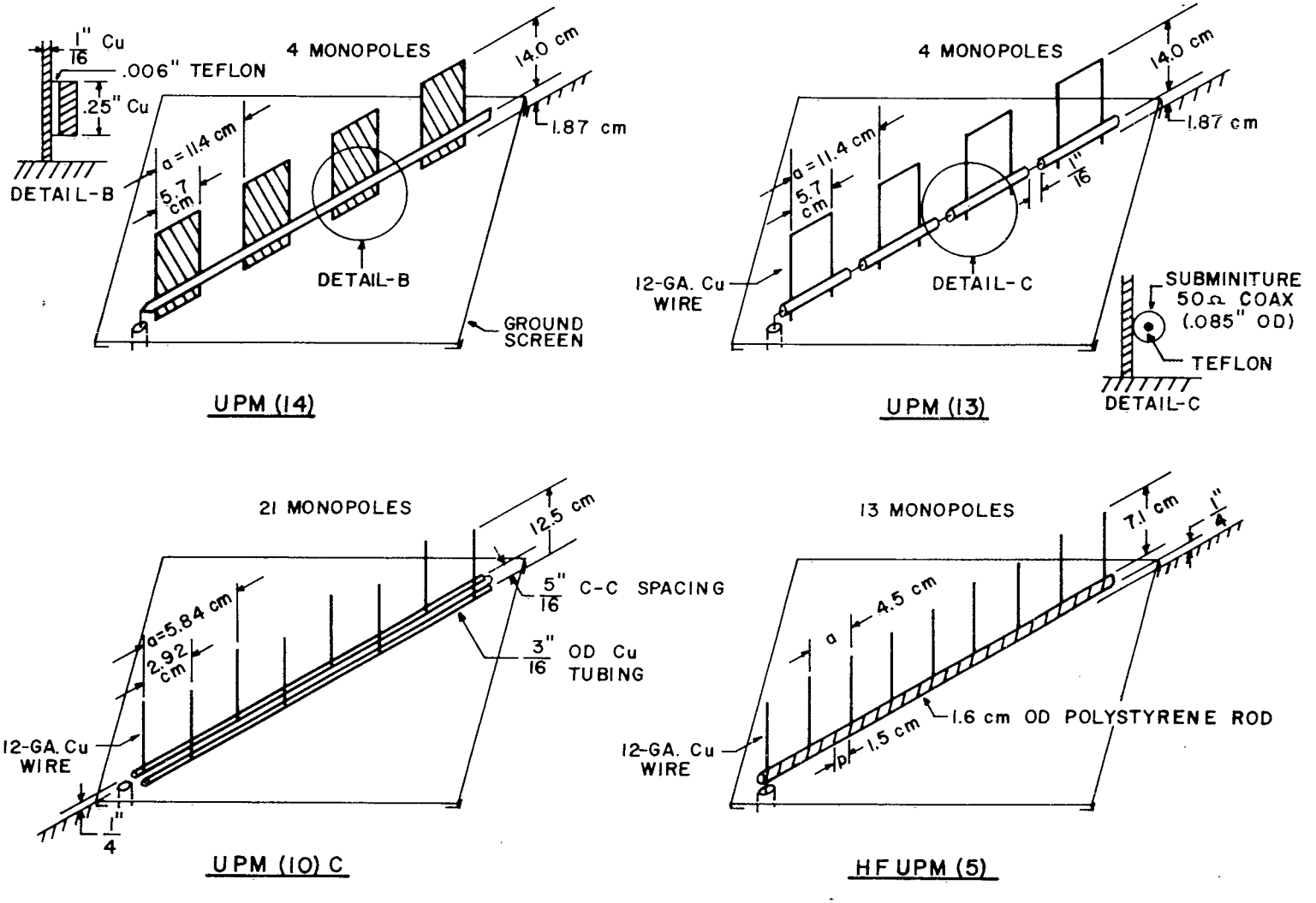

Figure 2. Details of Model Construction for UPM(14), UPM(13), UPM(10)C and HFUPM(5).

Since g(z) is periodic, it can be expanded in a Fourier series,

$$g(z) = \sum_{m=-\infty}^{\infty} A_n \exp\left(-j \frac{n\pi}{a} z\right) \tag{3}$$

and Equation (1) becomes

$$f(z) = \sum_{m=-\infty}^{\infty} A_m \exp\left[-\left(\gamma + j \frac{n\pi}{a}\right) z\right] \tag{4}$$

Each term of the series represents a discrete wave or so-called space harmonic, each of which is characterized by its own phase velocity. The corresponding propagation constant, γ_n, for the nth space harmonic is given by

$$\gamma_n = \gamma + j \frac{n\pi}{a} \tag{5}$$

where n is any integer (positive or negative), a is the period of the structure and γ is the propagation constant of the fundamental wave. Thus, for a given mode, the field at any cross section of the structure is described as the sum of the fundamental wave and an infinite number of space harmonics. For the practical structure only a finite number of space harmonics are of significance. These are the larger magnitude Fourier coefficients, A_n, and usually correspond to the lower order space harmonics. The remaining harmonics are highly suppressed. It can be seen from Equation (5) that phase data obtained from near-field probing would be difficult to interpret unless one or another of the propagating waves strongly predominates. Furthermore, more than one value of γ may exist for the structure, each value of which corresponds to a separate mode. That this is so will be seen from some of the experimental data presented later. It is

characteristic of most periodic antenna structures, however, to exhibit one dominant wave throughout most of the frequency spectrum of interest, so an "effective" phase constant usually can be derived. The dominant wave need not necessarily remain the same throughout this spectrum. In fact, for the monopole arrays it appears that the fundamental wave may dominate up to frequencies where the monopoles approach a quarter-wave in height, and a lower order space harmonic may dominate at the upper frequencies. Since measurement of the phase cannot distinguish between the fundamental and a particular space harmonic, this deduction admittedly may be somewhat of a guess. But upon comparing the measured far-field patterns with the phase-constant data displayed on the Brillouin diagram, the guess tends to be a little more of an educated one. Actually, the nomenclature assigned to the particular wave whose phase constant is measured is not of practical importance. The k-to-β relationship (i.e., the locus of the phase constant on the Brillouin diagram) is the information of interest, whether the curve be due to the fundamental wave, a particular space harmonic or any combination thereof.

This brings to the forefront the k-β, ω-β or Brillouin diagram. As mentioned previously, it relates the phase constant, β, of the wave propagation along the structure to the intrinsic phase constant, k, of free space. This, of course, assumes that there exists a single (or perhaps two)[2] predominant wave on the structure whose discrete phase velocity can be determined. The k-β diagram as employed in the treatment of wave transmission in periodic structures is described, for example, by Watkins.[4] Structures considered there, however, are those intended for guiding the fields and not those for radiating. Of pertinent interest is the so-called open structure (i.e., a structure having

one or more infinite transverse dimensions), which, thus, resembles the periodic antenna system. The k-β diagram for the open periodic structure is shown to possess regions designated as "forbidden". These regions are forbidden in the sense that they correspond to frequencies at which there is power flow away from the structure. In these regions the propagation constant is complex; that is, the wave undergoes decay as it travels along the structure away from the point of excitation. The decay or attenuation of the wave corresponds to coupling of energy from the structure to the space wave. The space wave in the forbidden region is a fast wave (i.e., $\beta < k$) and yields a condition for the wave energy to "leak" off of the structure. A wave which is launched along an open-boundary structure will propagate along the surface as a bound (trapped) wave, or as an oblique (leaky) wave which couples energy away from the surface. Whether the open-boundary structure functions as a waveguide or as a radiator depends upon its surface impedance. The impedance can effect a slow wave ($\beta > k$) which will be trapped to the surface, or it can effect a fast wave ($\beta < k$) which will leak away from the surface. Thus, the so-called forbidden region of the k-β diagram corresponds to fast waves which in turn are associated with radiation. Similarly, the slow wave region represents ordinary wave transmission.

It is not quite appropriate that the term "forbidden" should designate the region of most interest in antenna work. Instead, this region is often referred to as the "visible" or, simply, the "radiation" region. The Brillouin diagram of Figure 3 classifies these regions and illustrates sample phase constant loci for a fundamental ($n = 0$) and several of the lower order space harmonics. The higher order harmonics are represented in a similar manner. The curves shown are not intended to represent any particular structure. These

are shown merely to illustrate that for a given frequency (i.e., k) the corresponding (measured) phase constant could be that of the fundamental or any of the associated space harmonics. Hence, it is necessary to use only a portion of the diagram to illustrate the phase characteristics of a given periodic structure. For the work with the monopole arrays, the portion of the diagram from $-\pi$ to π is considered adequate.

Having associated certain regions of the k-β diagram with radiation and others with transmission, it is now suitable to establish additional significance to various portions of the radiation region. It was pointed out above that at frequencies in the radiation region energy leaves the structure via oblique or leaky waves. The direction of propagation for each oblique wave is given by

$$\theta = \cos^{-1} \frac{\beta}{k} \tag{6}$$

where θ is measured from the axis of the structure. It can be seen from Equation (6) that the angle of departure will vary with frequency, and for values of β such that $\left|\beta/k\right| \leq 1$ (i.e., fast wave) the angle θ is real and can take on any value from 0 to $\pm \pi$ radians. Assigning this added significance to the Brillouin diagram, Figure 4 can be drawn.

Thus, after having plotted the characteristic phase constant curve on the Brillouin diagram, it should be possible to predict the radiation properties of the particular periodic structure under investigation. One of the purposes of this project was to test the validity of this theory ..... at least for the case of the monopole arrays. An important fact to note is that the above discussions are based on the uniformly periodic structures of infinite length.

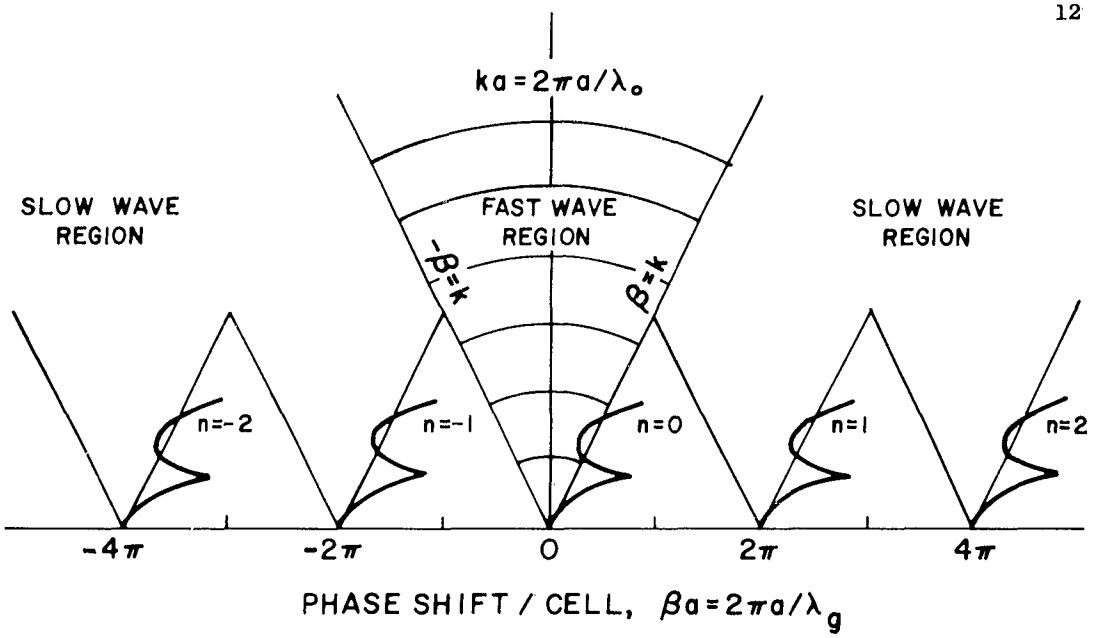

Figure 3. Brillouin Diagram for the Uniformly Periodic Transmission System.

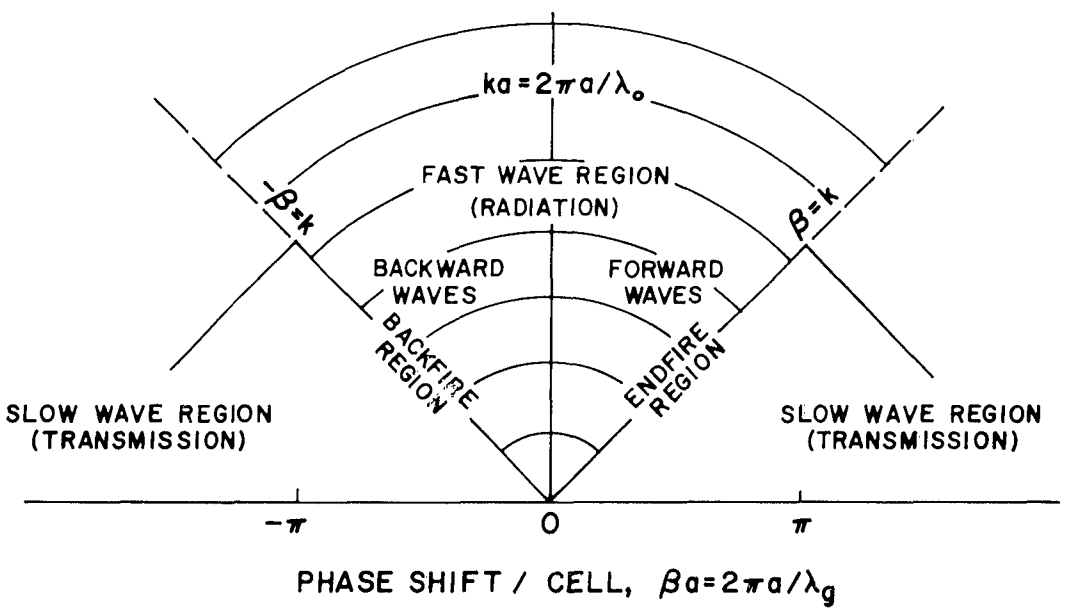

Figure 4. Brillouin Diagram and Regions of Interest for the Uniformly Periodic Monopole Array.

Since the practical structure is of finite length, its current distribution usually will differ from the infinitely long structure and some deviations or discrepancies in the expected behavior discussed above can be expected to occur. Specifically, the boundary lines between the various regions shown in Figure 4 should not be considered as absolute limits. For example, effective radiation may occur at frequencies where the phase constant lies within the slow wave region, but near the boundary. Similarly, it can be expected that some deviation may occur in the expected directional characteristics.

3. MEASUREMENT TECHNIQUES

The primary purpose of making near-field measurements is to determine the propagation constant of the wave on the periodic structure. For the case where the periodicity is uniform, the propagation constant is measured as a function of frequency. At frequencies below which the monopoles (or other loading devices) are near their quarter-wavelength resonance, the feeder wave travels along the structure with little or no decay. Here the structure functions simply as a "loaded" transmission line, and the propagation constant can be determined by measuring the effective or guide-wavelength. This is most easily accomplished by terminating the end of the structure in an open or short circuit and measuring the resultant standing wave pattern. For the structures reported here, a satisfactory standing wave pattern usually was established simply by leaving the end of the structure feed system open. In cases where the short circuit (field-type) was employed, care had to be taken not to interfere with the periodicity of the structure. Specifically, the shorting plate must be large compared to monopole height and positioned so that it creates the proper image. A common and straightforward method for making the relative amplitude measurements is indicated in Figure 5. The ground plane upon which the structures were mounted was a 6 ft. x 6 ft. solid aluminum sheet oriented vertically so that it formed one wall of an anechoic cubical. Except for the model under test, the near-field sampling probe and probe-driving mechanism, all other equipment was located external to the cubical. The step-by-step procedure employed for this measurement is outlined below. Typical standing wave plots can be seen by referring to the experimental data presented in the next section. It will be noted that the amplitude plots begin at the first monopole. The reason for this is discussed below. Thus, with the guide-

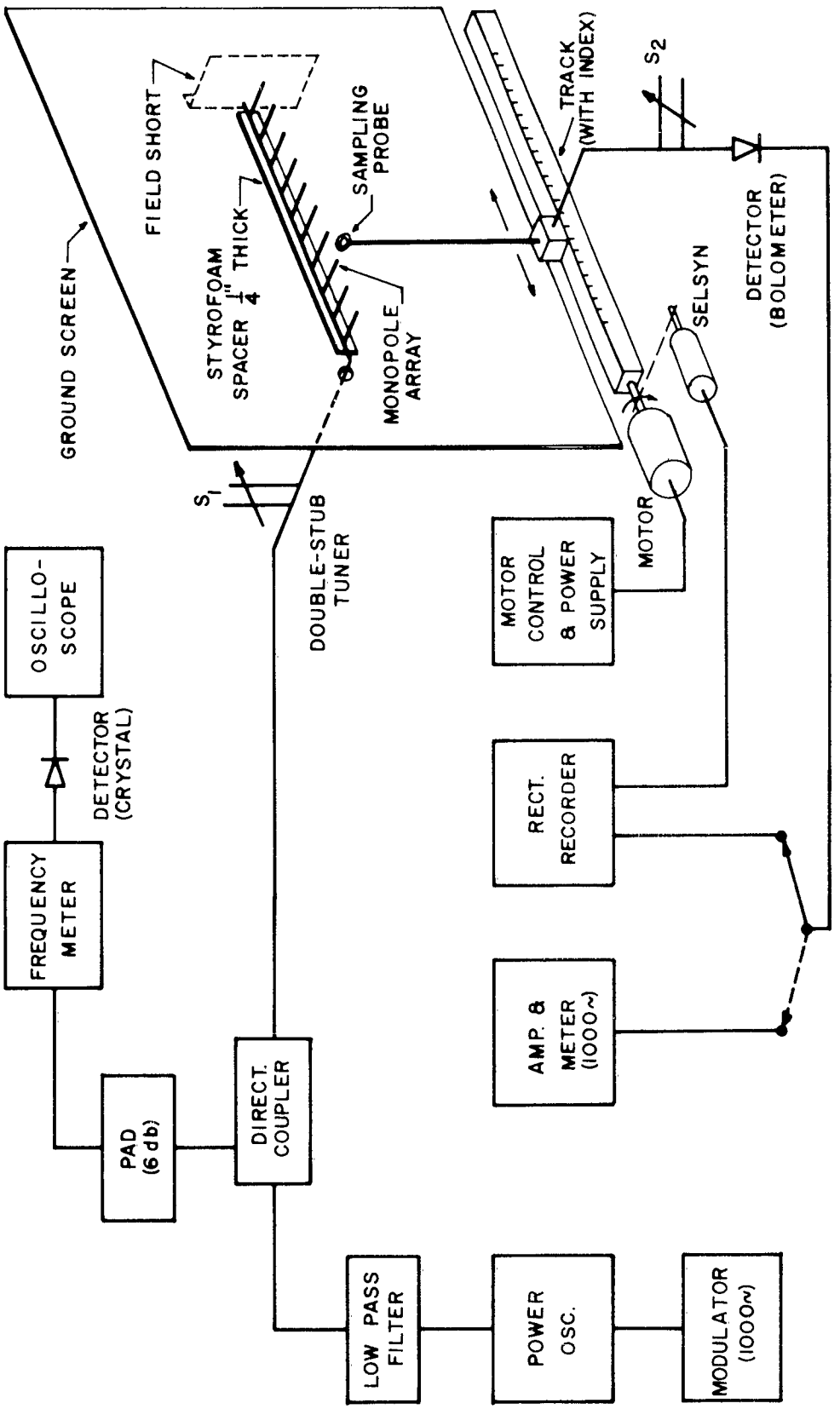

Figure 5. Block Diagram of Equipment Set-up for Measurement of Amplitude Distribution.

wavelength known, the phase constant, β, is determined. For simplicity, attenuation due to losses on the structure was assumed to be negligible.

It is worthwhile to note several details regarding the probe employed for sampling the near fields. In the beginning of the measurement program some difficulty was encountered in achieving satisfactory data, both for the simple measurement of amplitude and for the more involved measurement of phase. Without delving into the many details, it can be concluded that for the amplitude measurements most of the trouble was due to the type, location and orientation of the probe. Early measurements were made with a voltage-type probe inserted through a narrow slot in the ground plane. This proved unsatisfactory for most structures because the slot would often radiate or "leak". Further, it was found that in order to use a voltage probe with the set-up shown in Figure 5, the probe usually had to be placed very close to the structure. With such close positioning the localized fields due to the fine structure (i.e., fields around the individual monopoles or other loading devices) would cause variations in the total field and create superfluous nulls in the standing wave pattern. Subsequent endeavors found that the probe configuration shown in Figure 6 was the most satisfactory for the measurements of interest here. The probe was a single turn loop enclosed by an electrostatic shield and oriented so that it coupled primarily to the magnetic field of the monopoles. As a general rule, locating the probe approximately one-half of a monopole length away from the plane of the monopoles yielded adequate signal strength without significant detection of the fine structure fields.

As the frequency of excitation is increased to where the monopoles or other loading devices approach resonance, the structure no longer functions

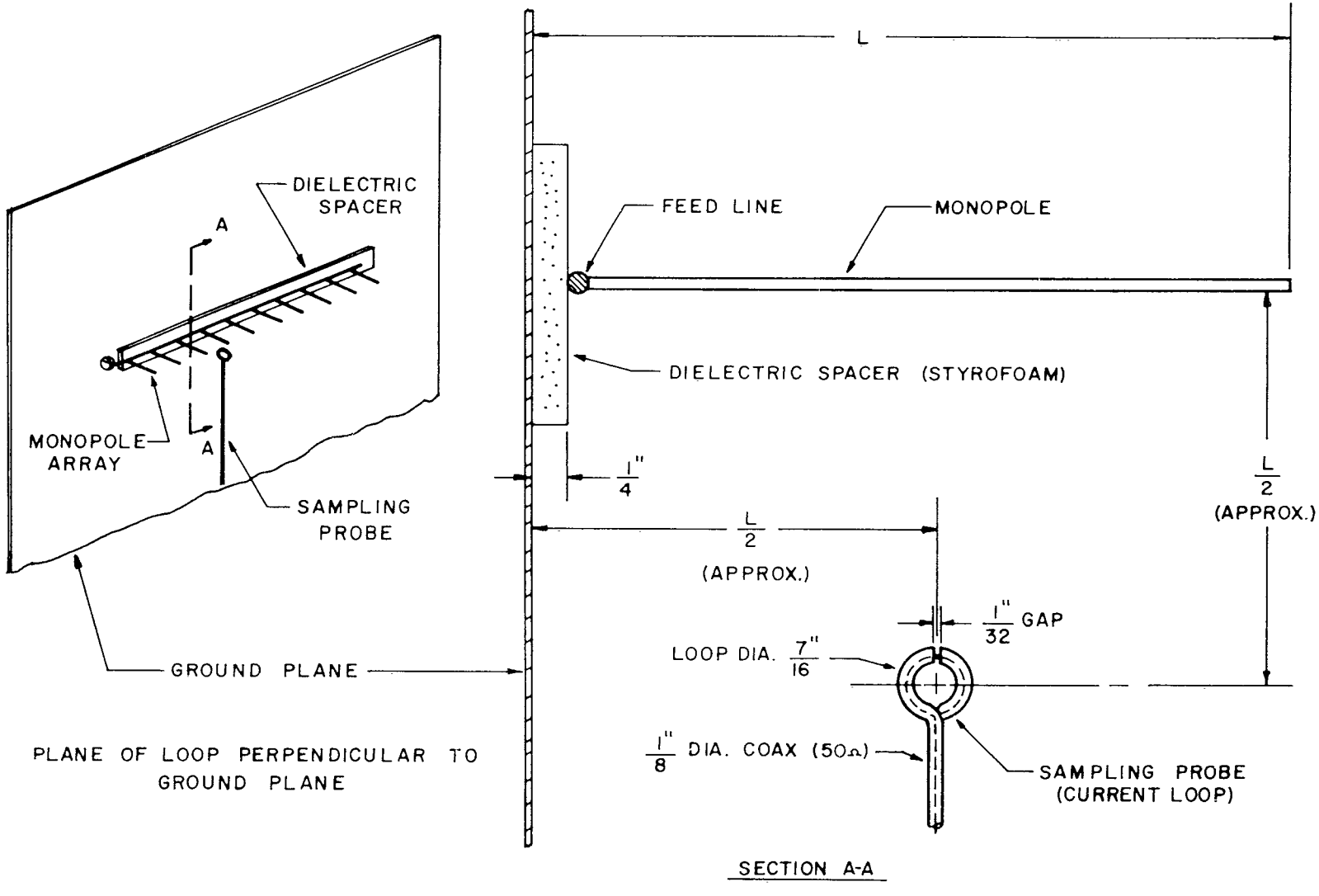

Figure 6. Details of the Near-Field Sampling Probe.

as a simple loaded transmission line. The feeder wave undergoes decay or "attenuation" as it travels along the structure away from the point of excitation. The magnitude of the reflected wave then becomes insufficient to create a distinct standing wave. Consequently, the propagation constant can no longer be determined by merely observing the null spacing on the standing wave pattern.

At frequencies above the first quarter-wavelength resonance of the monopoles little or no reflected wave exists. The incident wave is then of the form of a traveling wave, and there is a resultant progression of phase with distance. Here the determination of the propagation constant involves the measurement of the relative phase of the traveling wave. This measurement is considerably more intricate than the measurement of the standing wave pattern, and as will be shown later it often involves a certain amount of judicious analysis of the data.

All measurements of phase are based on the concept of comparison. That is, the value of the phase angle of the wave at a particular point on the structure is meaningful only if it is related to some other point on the structure. The problem of the reference point is discussed below. Although all measurements of phase are based on a common general method, each measurement usually presents requirements that are unique with the specific area of endeavor. Let it suffice here to say that after experimenting with a number of different ramifications to the basic method, the measurement set-up shown in Figure 7 proved to be the most satisfactory in so far as the data of interest, convenience and simplicity are concerned. Basically, this technique consists of combining two signals of the same frequency, one of which is the test signal sampled from the structure and the other is a phase reference

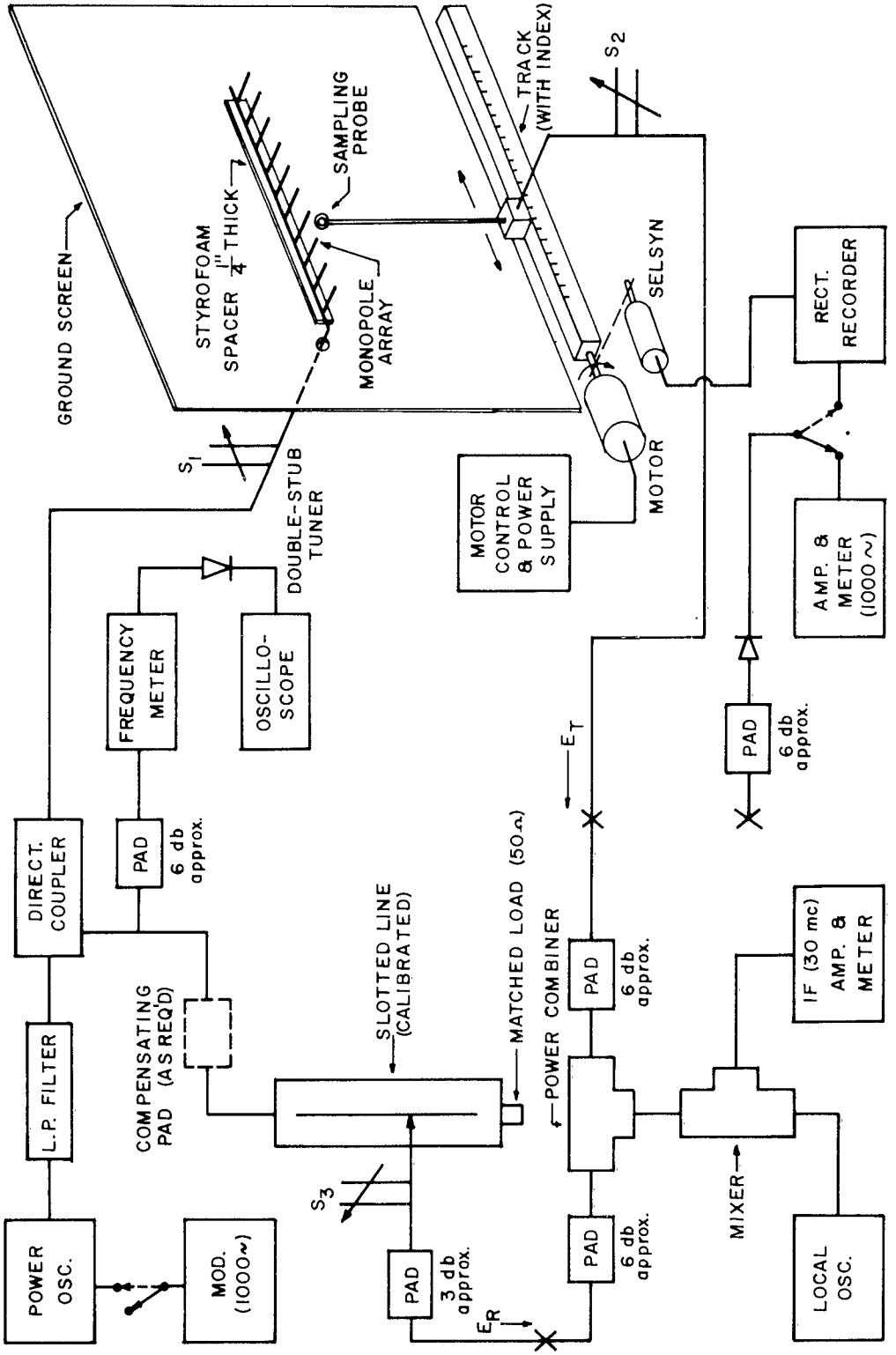

Figure 7. Block Diagram of Equipment Set-Up for Measurement of Relative Phase.

signal. The relative phase of the test signal is determined by comparison with that of the reference. A calibrated slotted line whose end is terminated in a matched load provides a good source of variable phase. The degree of error in the reference phase introduced by an imperfect termination is discussed in the Appendix. The two signals are fed into a power combiner, the output of which is the phasor sum of the two signals and is a minimum when the signals are 180° out of phase. For a null, the two signals should be, of course, also equal in magnitude. This would yield the ideal condition for null detection. Unfortunately, this is not the usual case during measurements. Distinct minima can be achieved providing the magnitudes of the two signals do not differ by more than about 6 db. When the signals differ by much more than this, the minima become broad and difficult to locate precisely. This is the reason for the use of the compensating pad shown in Figure 7. When the magnitude of the signal sampled from the structure under test decreases to where the position of the minima are no longer readable, the pad is inserted into the reference signal line for compensation. The undesirable effect here, of course, is the phase shift introduced in the reference line by the addition of the pad. However, this shift can be accounted for by carefully noting the position of a particular null before and after the pad is inserted. Such calibration should be done prior to the time when the pad is required, that is, while distinct minima still exist. It is important to note that this procedure must be done for each frequency, for the amount of phase shift introduced by the pad(s) will vary with frequency and even some with power level. Actually, for most structures, if the step-by-step procedure outlined below is followed, the compensating pad will be only seldom required. The output of the combiner is then fed into the mixing circuit for amplification and null detection. Thus,

for an incremental movement of the sampling probe along the structure, the reference probe in the slotted line is moved by some corresponding increment to bring about the 180° phase difference at the combiner inputs. The size of the increments at which the phase is sampled and the total distance along the structure over which measurements are made depend upon the particular structure under test and upon the frequency region in which the structure is operating. For the frequency range of interest here, approximately 400 to 2,000 Mc, sampling increments of one centimeter were usually adequate to establish a phase curve.

The matter of the reference point on the structure, or where to begin the measurement, warrants some discussion. First, so that all phase and amplitude data have a basis for comparison, a common reference point should be chosen where possible. It will be seen from the experimental data in the next section that this reference point should not be too distant from the feed point of the structure. For convenience, the reference point was chosen as the first monopole, or the edge of the first monopole nearest the feed point in cases where the monopole was of significant width. If it were not for the effects of the localized fields at the feed point, it would have been advantageous to begin the measurements even before the first monopole. Early in the measurement program measurements began as far down the structure as the second or third monopole. It was discovered later, however, that much of the pertinent amplitude and phase data was not acquired. In other words, the action of the first cell or two is of considerable importance.

There are always narrow regions of frequencies between those where the amplitude distribution is of the pure standing wave form and of the pure traveling wave form. In these regions it is practically impossible to ascer-

tain a value for the propagation constant. Typical amplitude distributions in these regions can be seen by referring to some of the experimental data shown in the next section. It is characteristic of the periodic monopole array to exhibit these regions at the so-called "turnover"; that is, a narrow range of frequencies where the phase velocity represented by the k-β curve undergoes a change from slow to fast. These regions correspond to the frequencies at which the monopoles or other loading devices are at their resonant conditions. For the monopoles, this occurs near the $1/4\lambda$, $3/4\lambda$, etc., resonances. With most of the structures investigated, this turnover region was relatively narrow, indicating rather high Q systems. From the viewpoint of measurement data this was fortunate, because it would not result in large gaps in the characteristic k-β curve.

Early in the measurement program attempts were made to "smooth out" the amplitude distribution in these turnover regions so that a successful phase measurement may be made and the propagation constant determined. The reflected wave could be significantly damped to effect a smooth amplitude distribution by terminating the end of the monopole array in a dissipative load, and a subsequent phase measurement appeared successful. (This technique was suggested by the author in Reference 4). It was found later, however, that because of the finiteness of the structure and its extreme sensitivity in the turnover region, the termination affected the propagation constant. Consequently this technique could not be employed. Several other attempts yielded similar results. It appeared, therefore, that a distinct propagation constant could not be measured in the turnover region.

With several of the structures the system-Q was so high that the turnover region often would differ slightly between that measured on the near-field

measurement set-up and that observed from radiation pattern measurements. (The connection between turnover and patterns is discussed in the next section). This change was found to be due to slight differences in the physical positioning of the structure between the two measurements set-ups. To establish a more definite relation between near-field data and far-field patterns, two small sampling probes for detecting the relative front-to-back ratio in field intensity were incorporated into the near-field measurement set-up. This system is shown in Figure 8. It offers a crude but simple and adequate means for determining when the structure under test is clearly firing in the forward or backward direction. When the structure exhibits radiation in the backward direction, it must be remembered that only the first several cells are contributing. Hence, the relative distances between the source and pick-ups must be weighted. The procedure for this measurement is discussed in the step-by-step procedure outlined below.

The following is a detailed step-by-step outline of the procedure employed for making the near-field measurements of amplitude, phase and front-to-back ratio. The normal attention given to measurements of this type is assumed. A matter which warrants specific mention is that of the physical alignment of the sampling probe. The probe must travel parallel to both the ground plane and to the plane of the monopoles so that the received signal will not be a function of other than axial translation. Far-field pattern measurements were made by conventional ground-plane techniques.

Measurement of Amplitude Distribution:

Refer to Figure 5.

1) Position the sampling probe at the first monopole. Refer to Figure 6 for the approximate location of the probe with respect to the mono-

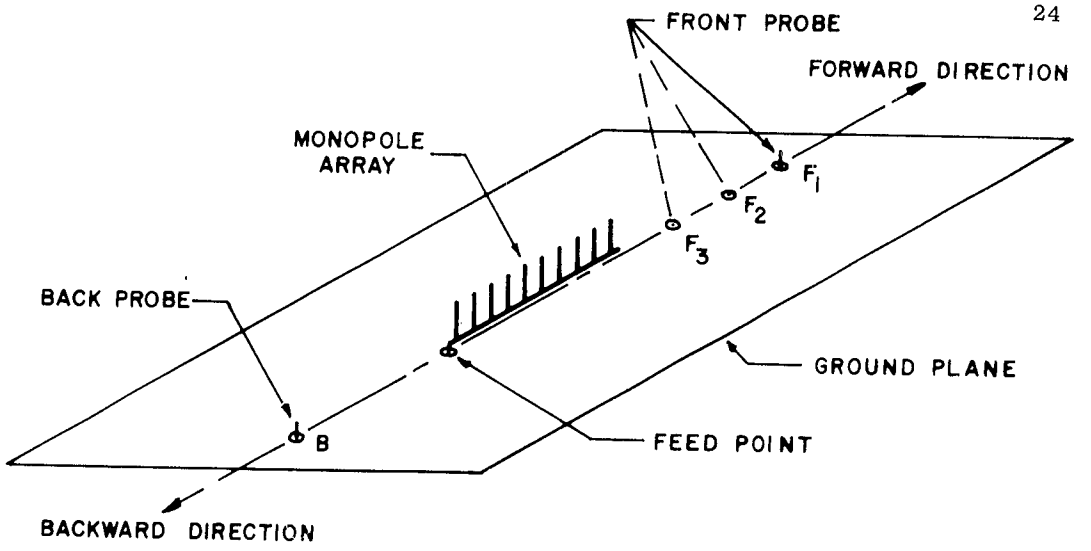

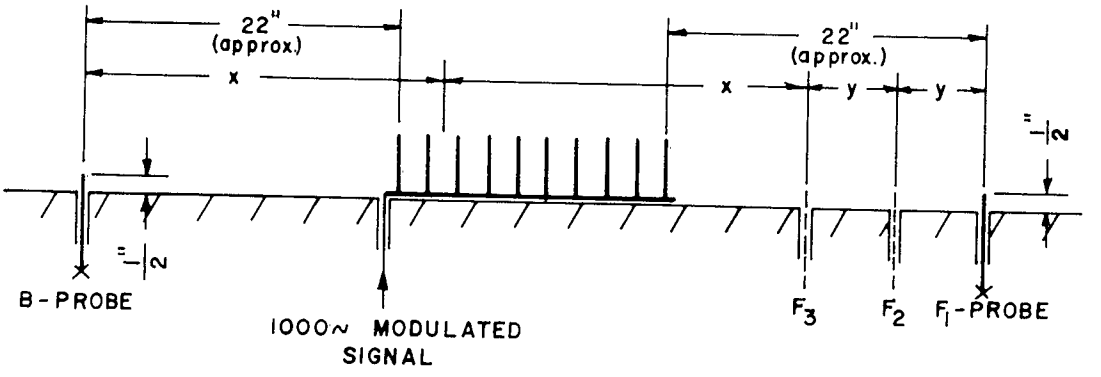

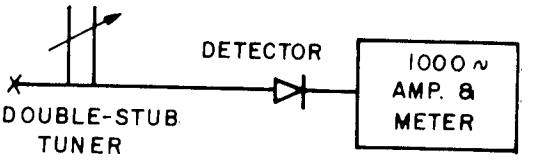

METERING CIRCUIT

Figure 8. Details for Measurement of Approximate Front-to-Back Ratio.

pole structure under test.

2) With the output from the sampling probe circuit connected to the 1000-cycle amplifier/meter (eg., HP-415B amplifier/VSWR meter), adjust the double-stub tuners S_1 and S_2 for maximum indication on the meter. For the amplitude measurement, a bolometer-type detector should be used at the sampling probe when power level permits. If a crystal detector must be used, care should be taken not to overdrive (or underdrive) the crystal beyond its square-law region. Otherwise, the recorded amplitude data will not indicate the true decay of the near-field.

3) Connect the probe signal to the recorder input. Activate the probe-driving mechanism and record the amplitude distribution.

4) Repeat the above steps for each frequency of measurement.

Measurement of Relative Phase:

An amplitude measurement preceded each potential measurement of phase. In so doing, the adjustments described below were facilitated, or it could be seen that a satisfactory standing wave pattern existed from which the guide-wavelength could be determined directly, or, conversely, it could be seen that a successful measurement of phase was hopeless.

Refer to Figure 7.

1) Observe the amplitude plot for the degree of attenuation. For most practical purposes the phase need not be measured beyond the distance where the amplitude of the near field has decayed or attenuated by about 20 db. In fact, experiment indicates that phase data are usually unnecessary beyond about the 10 db point. However, it is advisable to make measurements over at least 5 or 6 cells even though the attenuation rate is rapid.

If the amplitude has not decayed by more than about 6 db over the distance which the phase is to be measured, distinct minima can be located on the slotted line without the need for the compensating pad nor the adjustment for compensation described below. If the amplitude has decayed by more than about 6 db and no greater than about 15 db, it is usually possible to establish minima that are reasonably distinct after making an initial compensating adjustment, but still without the use of the compensating pad. However, when the amplitude has attenuated by more than the above, the compensating pad is normally required.

2) For the case where the attenuation is on the order of 6 db or less, the following applies:

   a) With the sampling probe at the first monopole and modulation applied to the power oscillator, connect the test signal E_T to the 6 db pad-detector-amplifier/meter combination and note the signal level. S_2 may require retuning. Reconnect E_T to the pad and power combiner. The power combiner used here was a Microlab Type DA. The two 6 db pads are for additional isolation.

   b) Connect the reference signal E_R to the metering circuit and adjust S_3 so that the signal level is approximately that of E_T. Reconnect E_R as shown. It is to be noted that E_R is an RF signal; that is, the pick-up probe in the slotted line does not contain the usual detector element. For the slotted line employed here (HP 805A), the tuner S_3 is an integral part of the probe mechanism. The 3 db pad is for the purpose of an

additional isolation and should be located immediately adjacent to the tuner and probe.

c) Disconnect modulation from the power oscillator.

d) Tune the local oscillator for the proper IF signal output from the mixer. A GR Type 874-MR mixer was used here.

e) Move the slotted line probe for a minimum indication on the IF amplifier/meter (eg., GR Type 1216-A). This represents minimum output from the power combiner; that is, E_T and E_R are 180° out of phase. The corresponding location of this minimum on the slotted line is the phase reference. Record this together with the position of the sampling probe.

f) Move the sampling probe to the next sampling position, usually in increments of 1 cm, and locate the corresponding minimum on the slotted line. The amount of shift of the minimum from that of the preceding reading represents the change in phase of the wave over the incremental movement of the sampling probe. The minimum may shift either toward (leading phase) or away from (lagging phase) the source end of the slotted line.

g) Repeat part (f) for each increment of measurement.

h) Plot data to establish a curve showing relative phase vs. distance along the structure. Refer to the next section of this report for such plots.

i) Repeat the above for each frequency of measurement.

3) For the case where attenuation is between about 6 and 15 db, the following applies:

a) Determine from the amplitude plot where along the structure

the amplitude has decayed to approximately one-half of the total. Position the sampling probe at this point and follow the calibration procedure as otherwise outlined in 2(a) and 2(b) above.

b) Return the sampling probe to the first monopole and follow steps 2(c) through 2(i) above.

4) For the case where the attenuation is greater than about 15 db, the following applies:

a) Determine from the amplitude plot where along the structure the amplitude has decayed by approximately 6 db from the maximum (i.e., maximum is presumably near the first monopole). Position the sampling probe at this point and follow the calibration procedure as otherwise outlined in 2(a) and 2(b) above.

b) Return the sampling probe to the first monopole and follow steps 2(c) through 2(g) above.

c) At the point along the structure where the amplitude has decayed to the order of 12 to 15 db, the minima will be broad and difficult to locate. Just prior to this, that is, when a reasonably distinct minimum still exists, insert the compensation pad (about 6 db). The locations of the minimum before and after the pad is inserted should be noted so that the amount of phase shift introduced by the pad may be accounted for.

d) Continue and complete the phase measurements.

e) Follow steps through 2(i) above.

Measurement of Front-to-Back Ratio:

The measurement employed here for determining the front-to-back ratio of field intensity is rather crude but simple, and yields information of a relative nature only. However, it offers a convenient means to observe and to confirm when the structure is actually radiating in the backfire or in the endfire direction. It will be seen later in the next section that the directional properties of the uniformly periodic monopole array usually change from multidirectional to unidirectional in the matter of a few megacycles, or, equivalently, in a frequency change on the order of one percent. Since far-field radiation patterns are not usually recorded at such fine intervals, the frequency at which this change in directivity takes place may not be observed. Also, as mentioned earlier, the effect of the structure's sensitivity in the region of turnover may cause apparent differences between the actual (measured) far-field patterns and those predicted from near-field data. A simple test of the front-to-back ratio during the near-field measurements affords closer correlation between these two sets of data. Of course, the front-to-back ratio test needs to be made only at frequencies where abrupt changes in directivity are expected to occur, that is, at the turnover region. It is desirable to have recorded the far-field patterns prior to making the near-field measurements. In this way the turnover region can be estimated by referring to the far-field data.

Refer to Figure 8.

1) Observe the amplitude plot for the nature of the current distribution. For most practical purposes the distribution can be classified as non-attenuated, slowly-attenuated or rapidly-attenuated.
2) With modulated signal applied to the monopole array (eg., see

Figure 5), connect the metering circuit shown in Figure 8 to the B-probe and note the signal level.

3) Connect the metering circuit to either F_1-, F_2- or F_3-probe, according to the amplitude distribution; that is, to F_1-probe for negligible attenuation, to F_2-probe for slow attenuation and to F_3-probe for rapid attenuation. The difference between the signal levels from the two probe connections is then an approximation of the front-to-back ratio.

The various dimensions indicated in Figure 8 are not inflexible; they were chosen merely for convenience. The two probes should be short so not to interfere with the fields of the structure under test, and they must be identical to accommodate the common tuning circuit.

4. EXPERIMENTAL DATA AND INTERPRETATION

In this section of the report results of the measurements on various periodic monopole structures are presented. An attempt is also made to correlate the various data and to deduce from these data the points of significance. The data shown herein represents only a portion of the total acquired from the many measurements, and, in addition, the particular structures reported do not constitute the total number investigated. However, the results presented here are typical, and are considered adequate for illustrating the near-field properties which appear to be characteristic of the monopole class of periodic structures. Each structure with its corresponding data is discussed below. With reference to the information presented in the preceding sections of this report, the data shown should be self-explanatory in most respects. The points of significance will be identified as the discussion of the various structures progresses.

Before proceeding to these discussions, it is necessary first to clarify several points regarding the measured data and their analysis. In reviewing the measured data it will be noted that radiation patterns are not shown for frequencies below about 400 Mc, yet there are illustrated amplitude and phase data at frequencies below this. Pattern range limitations precluded adequate measurements below approximately 400 Mc. It was not considered wise to perform the near-field measurements on higher frequency models, nor was it desirable to make the near and far-field measurements on separate models. Most of the measurements were made on models whose monopole elements were quarter-wave resonant at approximately 500 Mc.

No elevation plane (ie., E-plane) patterns are included in this report, and only seldom were they recorded. Knowing the azimuth plane patterns for

the linear monopole array, the vertical plane patterns can be estimated to a sufficient degree not to warrant the additional effort required for their measurement. Suffice it to say that elevation patterns were occasionally recorded and were in good agreement with those expected from the azimuthal plots.

It was mentioned earlier that a certain amount of judgement was occasionally required in analyzing the measured data. This had reference primarily to the phase data. In observing the plots of phase on the following pages, it will be seen that the progression of phase often does not yield a smooth curve with a well defined slope from which the phase shift per cell can be readily and accurately determined. In order to deduce a value for the phase constant from these types of phase distributions, the associated amplitude plot was first observed for the distance from the feed point of the structure to where the current decayed by 10 db. This distance was then designated as being the most important over which the phase should be analyzed. With this 10 db weighting factor, a reasonably good slope could usually then be drawn and, hence, a phase constant determined. The phase data are plotted so that a positive slope corresponds to a leading phase and a negative slope to a lagging phase.

The final point to clarify is that of relating the sense of the phase (ie., sign of the slope) to the k-β diagram. A negative slope corresponds to a lagging phase which in turn yields propagation of a forward wave. Thus, β is positive and is plotted to the right of the $\beta a=0$ axis. Similarly, a positive slope corresponds to a leading phase which in turn yields a backward wave. Here, β is negative and is plotted to the left of the $\beta a=0$ axis.

4.1 UPM(2)C — Simple Monopole Array

The uniformly periodic structure on which near-field measurements began was a simple linear array of vertical monopoles fed in shunt from a single wire line. By simple here it is meant that the structure incorporates no mechanism for phasing other than that which the monopoles themselves provide through self-loading of the feed line. A detailed sketch of UPM(2)C is shown in the upper-left of Figure 1. For an array of this type it is well known that the phase of the dipole currents progresses along the array in the same direction as the feeder wave progresses along the transmission line. This is the condition of phase retardation with reference to the point of excitation, and, further, it is the condition for endfire-type directivity when the structure is operating near its radiation region.

With this structure being the first on which the measured results are reported, it is instructive to review briefly the experimental data shown in the respective figures. Thence, in the discussions of the structures which follow, it will be necessary to elaborate only on those data which differ significantly from those for the UPM(2)C structure. The k-β and attenuation curves of Figure 9, which actually summarize the measured phase and amplitude data, will be reviewed after the data shown in the figures which follow are discussed. Figures 10, 11 and 12 contain some of the recorded amplitude data (solid line curves) and measured phase data (dashed line curves) for UPM(2)C. The small circles appearing on the phase curve represent the points along the structure at which phase measurements were made (normally at 1-cm increments). The relative magnitude of phase in degrees is shown along the left ordinate of each diagram and the relative magnitude of near-field current in db along the right ordinate. The monopole locations are indicated along the abscissa,

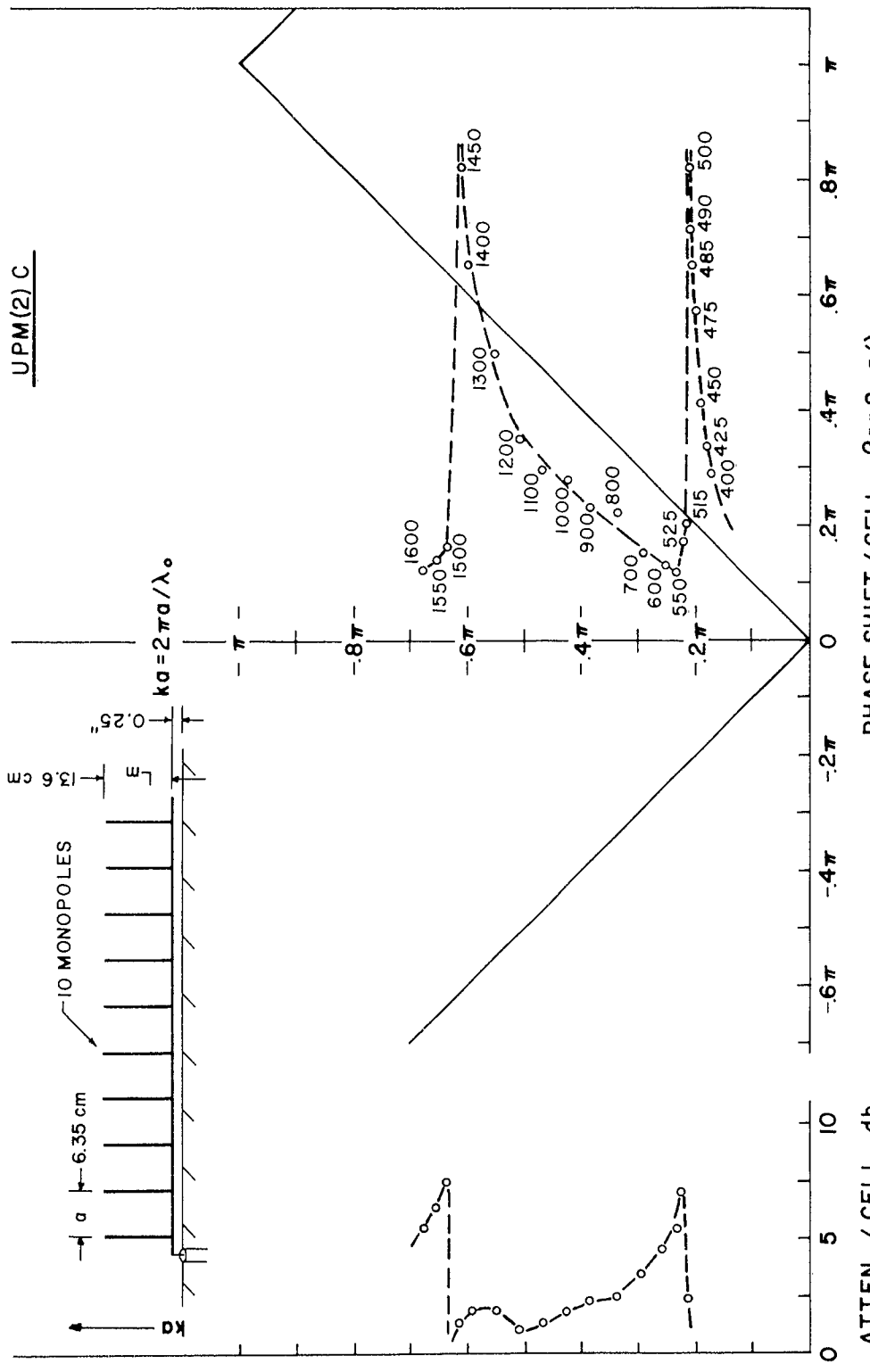

Figure 9. The k-β /Attenuation Diagram for the Simple Monopole Array, UPM(2)C.

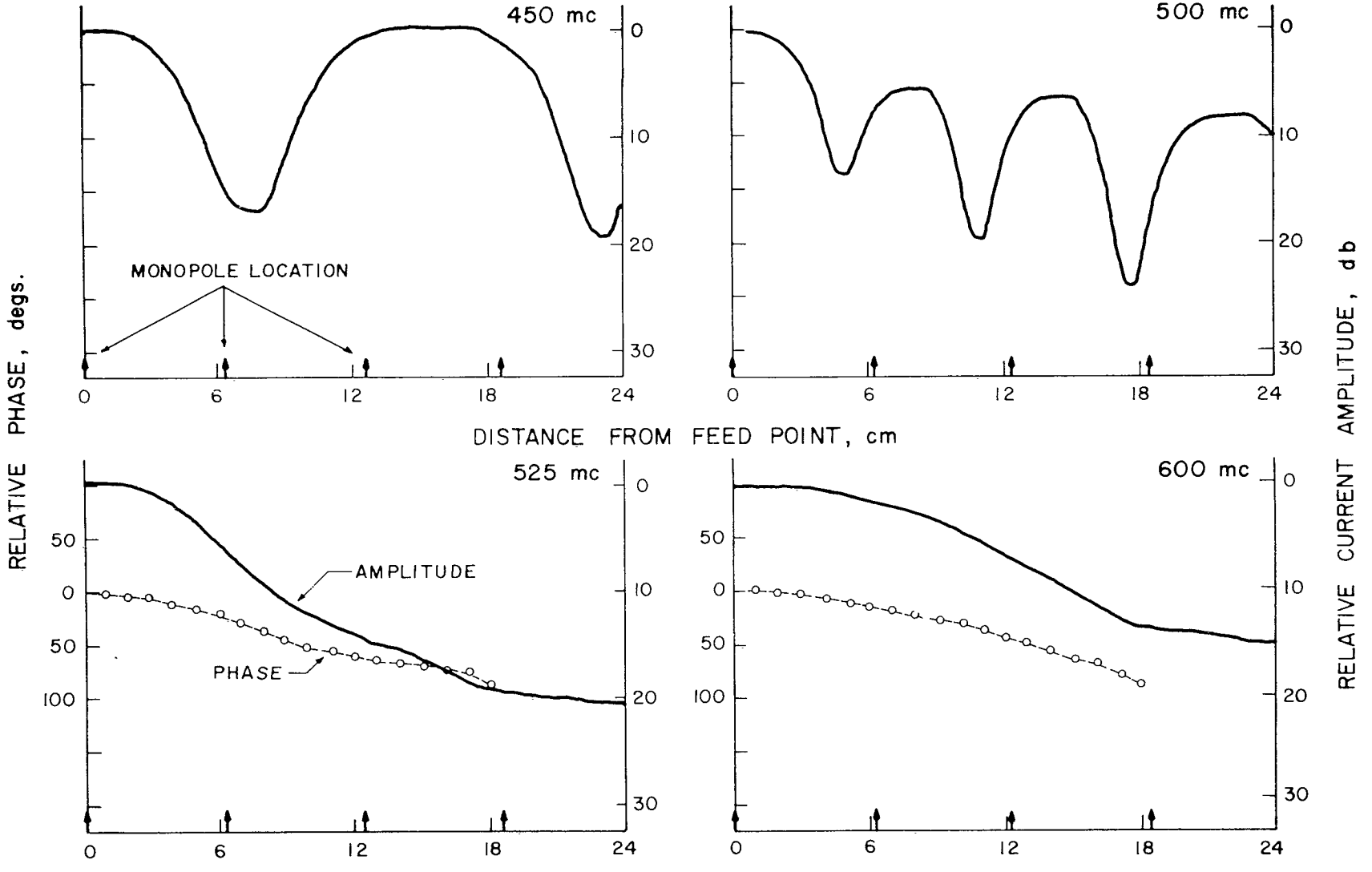

Figure 10. Measured Amplitude and Phase Distributions for UPM(2)C.

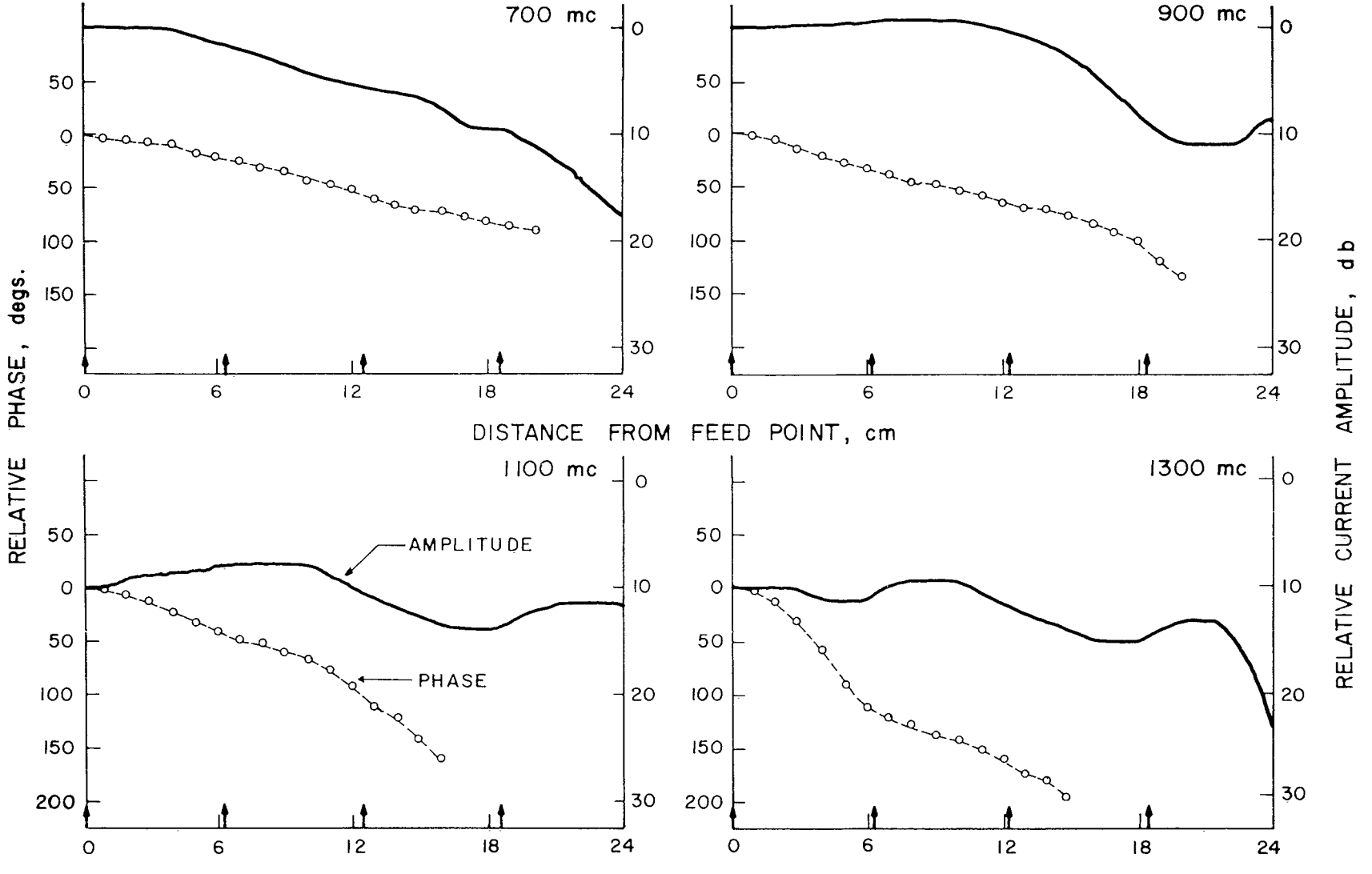

Figure 11. Measured Amplitude and Phase Distributions for UPM(2)C.

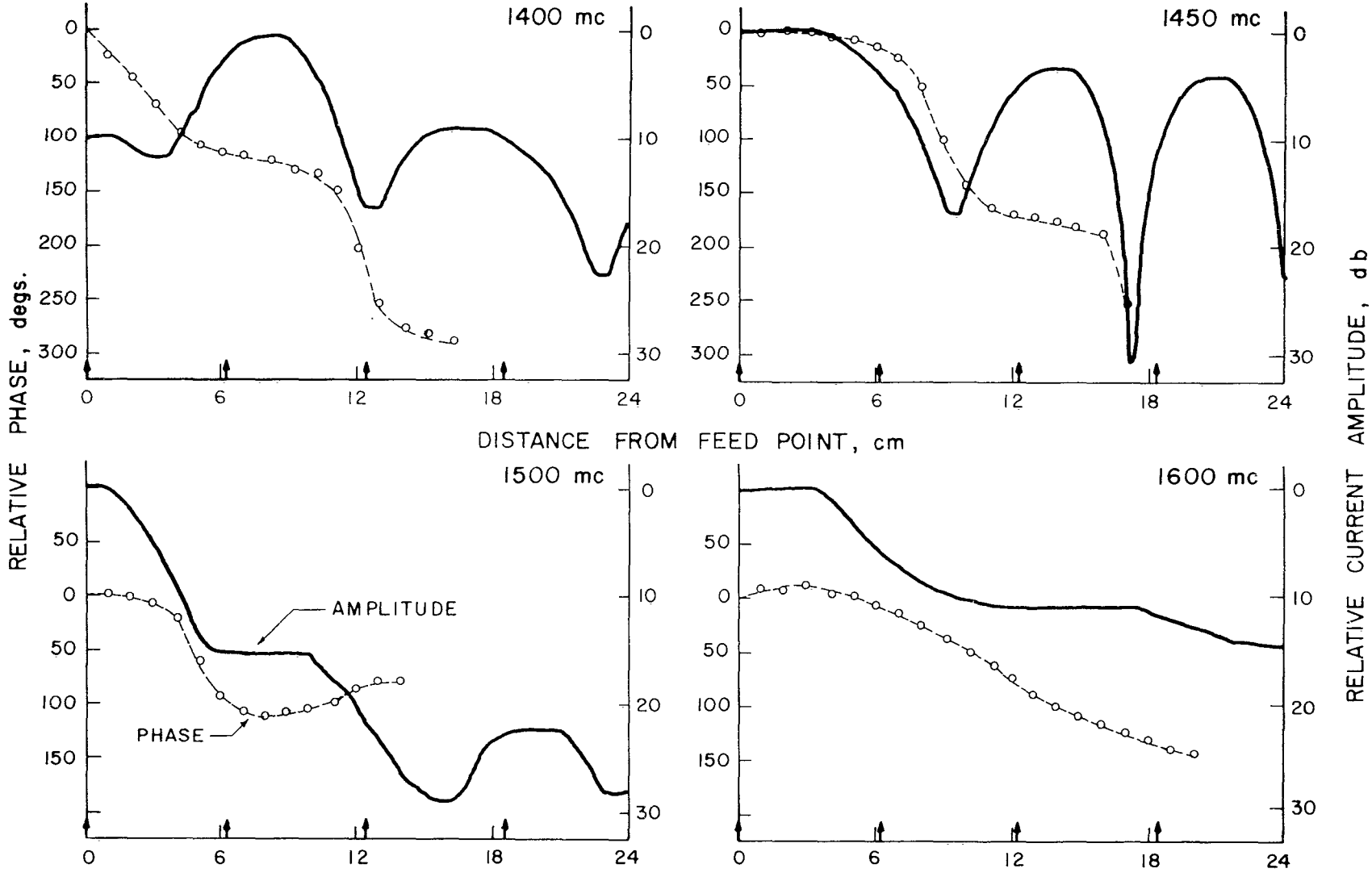

Figure 12. Measured Amplitude and Phase Distributions for UPM(2)C.

with the first monopole at the extreme left (ie., at 0-cm). Each diagram represents a different frequency of operation. For obvious practical reasons, only a portion of the total data acquired from the numerous measurements are included in this report. The data shown are generally those which correspond to the more significant points on the k-β curve.

Beginning with the amplitude plot at 450 Mc shown in Figure 10, it is seen that the amplitude distribution of current along the structure is of the form of a fairly well-defined and uniform standing wave. Here the value of the phase constant can be readily determined by noting the spacing between the adjacent nulls, which, of course, is equivalent to a one-half guide-wavelength. This form of a standing wave pattern is typical for frequencies up to the region near turnover, which for UPM(2)C is slightly above 500 Mc. At frequencies near to and approaching turnover, the standing wave pattern becomes distorted. That is, the null separations and/or the maxima and minima of the standing wave are no longer uniform. Throughout this region a distinct value for the phase constant cannot be determined. The standing wave plot at 500 Mc borders on that from which an accurate value of the phase constant can or cannot be determined. At frequencies above 500 Mc and up to just below 525 Mc, a distinct value of the phase constant cannot be resolved from either the standing wave plot or the measurement of phase. As the frequency of 525 Mc is approached, the amplitude distribution gradually becomes smooth and exhibits attenuation. Thus, a distinct value of the phase constant at 525 Mc can be determined. A straight line drawn as an average through the phase curve yields a slope from which the phase change in degrees per cell is read. Similarly, an averaging line drawn through the amplitude plot yields the attenuation per cell. The phase and amplitude distributions for UPM(2)C are

seen from Figures 10 and 11 to remain relatively smooth through 1300 Mc. However, the data at 1400 Mc shown in Figure 12 indicate that the structure is approaching a frequency region of standing wave phase and amplitude distribution. Here the attenuation is negligible and effective radiation is not expected. This region of ineffective radiation remains for only a short period, for at 1500 and 1600 Mc it is observed that the attenuation rate becomes quite significant and the phase takes on the form of that for a traveling wave.

Subsequent analysis and reduction of the data shown in Figures 10, 11 and 12 (and those other data not included here) constitute the summary diagrams of Figure 9. In addition to the Brillouin or k-β diagram, which was introduced and discussed earlier in this report, Figure 9 also contains a diagram which illustrates the rate of decay of the wave on the structure as a function of frequency. The attenuation curve is drawn such that it can be directly related to the k-β curve. However, since the attenuation data are shown as attenuation per cell, care must be taken not to be misled when comparing the attenuation rates of the various structures. Obviously, for large cell dimensions the rate of attenuation also will appear large. It would have been better to have otherwise normalized the rate of decay, perhaps as attenuation per guide-wavelength. Unfortunately, this hindsight was formulated after the attenuation data were condensed and drawn as shown. Of prime interest in the k-β curve of Figure 9 is the rather abrupt change in the locus of points at about 500 Mc. Here the monopoles are near their quarter-wavelength resonance and as a result create an impedance condition for the incident feeder wave to couple strongly to the monopoles. At frequencies below this resonance the structure functions simply as a loaded transmission line. That is, the

monopoles are electrically short and effect an impedance condition for the feeder wave to propagate along the structure as a slow wave. Whereas, at frequencies near and above quarter-wavelength resonance the phase velocity of the wave is fast, or at least near to that of a free space wave. Accompanying the fast wave characteristic is a decay or attenuation of the wave as it travels along the structure away from the feed point. This attenuation is generally attributed to radiation. As can be seen from the plots of amplitude distribution, the rate of attenuation is greatest just above "turnover", that is, where the k-β curve alters its trend from slow to fast. The rate of attenuation then decreases as the frequency of excitation is increased. Note that during this time the progression of phase is relatively smooth, lagging in sense, and is of the velocity such to locate the k-β curve near to the k=+β line of the Brillouin triangle. It is expected, therefore, that the structure should be radiating and predominantly in the endfire direction. That this is essentially so can be seen from the measured H-plane voltage patterns shown in Figure 13. Indeed, the patterns from UPM(2)C are not highly unidirectional. Other structures of the simple monopole variety, but with apparently better length-to-spacing ratios, have exhibited more directive endfire patterns. See, for example, the data reported in Reference 6. However, it has been the author's experience that no uniformly periodic monopole structure investigated exhibited ideally unidirectional endfire radiation. This might be expected from the interference offered by the "cold" monopole elements which are in the line of fire of the forward radiated wave.

As the frequency of excitation is further increased, the attenuation becomes negligible and the wave on the structure is once again of the standing wave form. Then as the monopoles approach three-quarter-wavelength resonance

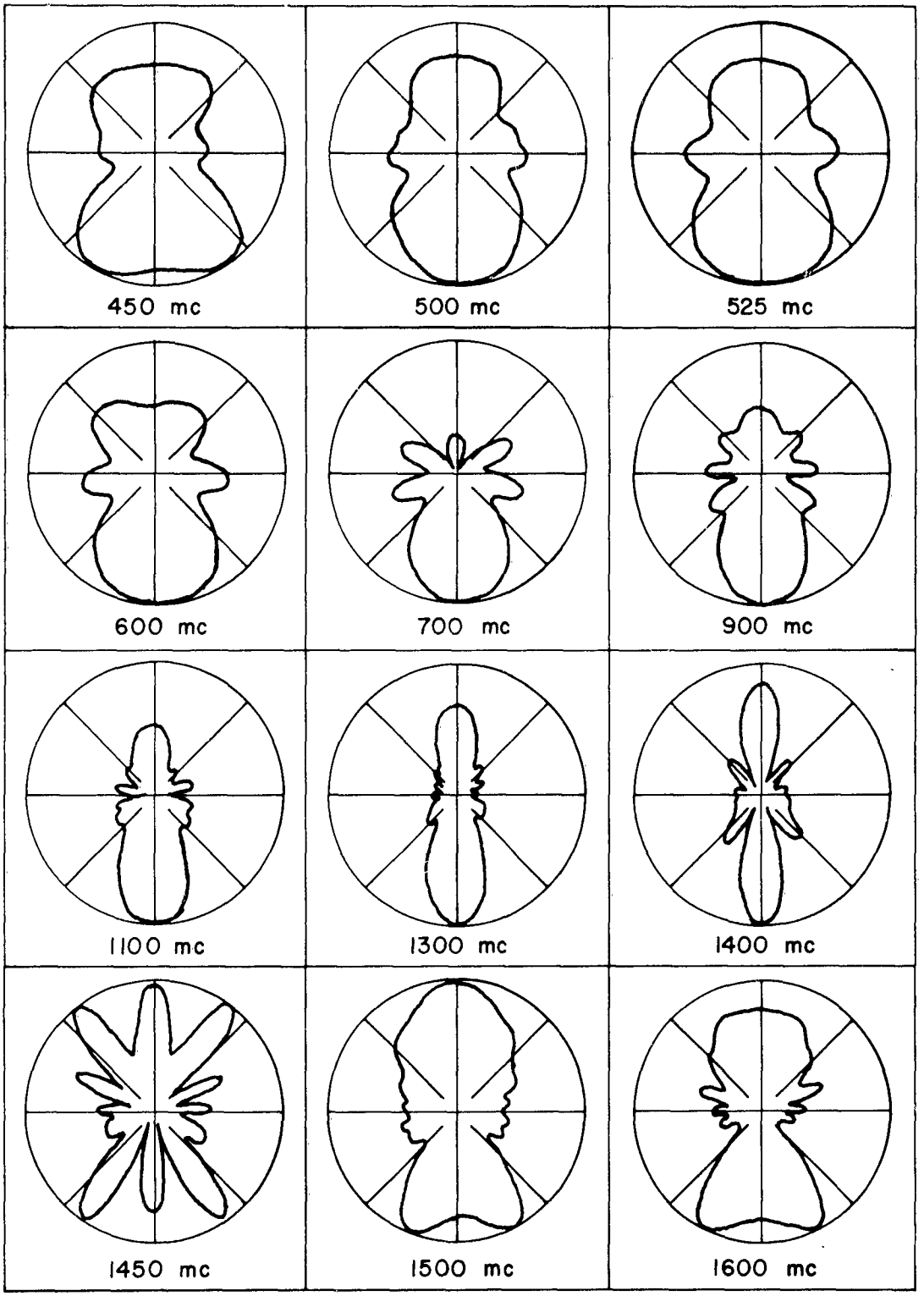

Figure 13. Measured H-Plane Voltage Patterns for UPM(2)C.

the structure exhibits phase and amplitude characteristics similar to those observed at the first quarter-wavelength resonance. The patterns observed at this second resonance are more bidirectional than unidirectional. This is undoubtedly due to the increased electrical spacing (ie., βa large) between the adjacent monopoles. The βa factor also may account for the bidirectional tendency of the H-plane patterns at frequencies where the k-β curve is nearing its entrance to the Brillouin triangle (eg., 1200 and 1300 Mc). As will be seen from the discussion of the various other monopole structures, this latter bidirectional tendency of the H-plane patterns is consistently observed.

To end the discussion of the simple monopole array, attention is called to the fact that this type of periodic structure, when tapered, has not been known to yield successful frequency independent performance.

4.2 UPM(2), UPM(2)A, UPM(2)B --- Stub-Loaded Monopole Array, Type-I

This series of monopole arrays is illustrated in the upper right of Figure 1. It is seen that this version differs from UPM(2)C discussed above only by the addition of the horizontal elements or, equivalently, open-circuited stubs. These stubs are connected to the single-wire feed line to offer additional and purely reactive shunt loading of the line. UPM(2), UPM(2)A and UPM(2)B differ only by the length of their stubs. The respective stub lengths, L_s, are indicated below the detailed sketch. In each case the stubs are located midway between the monopole elements and are spaced one-quarter inch above the ground plane.

The log-periodic counterpart of this structure has been known to yield farily successful frequency independent performance and was reported in 1960 by Ore and Berry[6]. It has also been found through experiment on scale model

and full scale work with this type of log-periodic structure that it was very difficult to tune for wideband operation. In other words, the system-Q was extremely high. As will be seen from the following data, the uniform structure exhibits the same high-Q property. The length of the stub plays a very important part in controlling the directional characteristics of the array. The stub length, of course, also effects the impedance properties of the structure, but as mentioned in the beginning of this report, the subject investigation was not concerned with impedance.

The k-β /attenuation diagram and corresponding experimental data for the stub-loaded structures are shown in Figures 14 through 22. In order that the amount of experimental data displayed in this report be maintained at a minimum, only the data for UPM(2)A is shown in detail. Except for the relative frequencies, the amplitude, phase and pattern data for the other two structures are quite similar. After having associated the location of points on the k-β diagram for UPM(2)A with the corresponding amplitude, phase and pattern data, the performance of UPM(2) and UPM(2)B may be readily deduced from their respective k-β diagrams. This, in fact, will be seen to be one of the virtues of the Brillouin diagram. The k-β curves for the stub-loaded structures are seen to differ markedly from that of the simple monopole array. Besides the perturbations in the curve in the lagging phase region (ie., to the right of $\beta a = 0$ axis), the curve extends into the leading phase region (ie., to the left of $\beta a = 0$ axis) of the Brillouin diagram. The leading phase condition corresponds to a backward traveling wave and should, therefore, lead to directivity which is predominantly backfire. The H-plane patterns at 545 to 600 Mc indicate that this is definitely so. Indicative of the high Q-factor and the sensitivity of the structure at turnover is the sudden

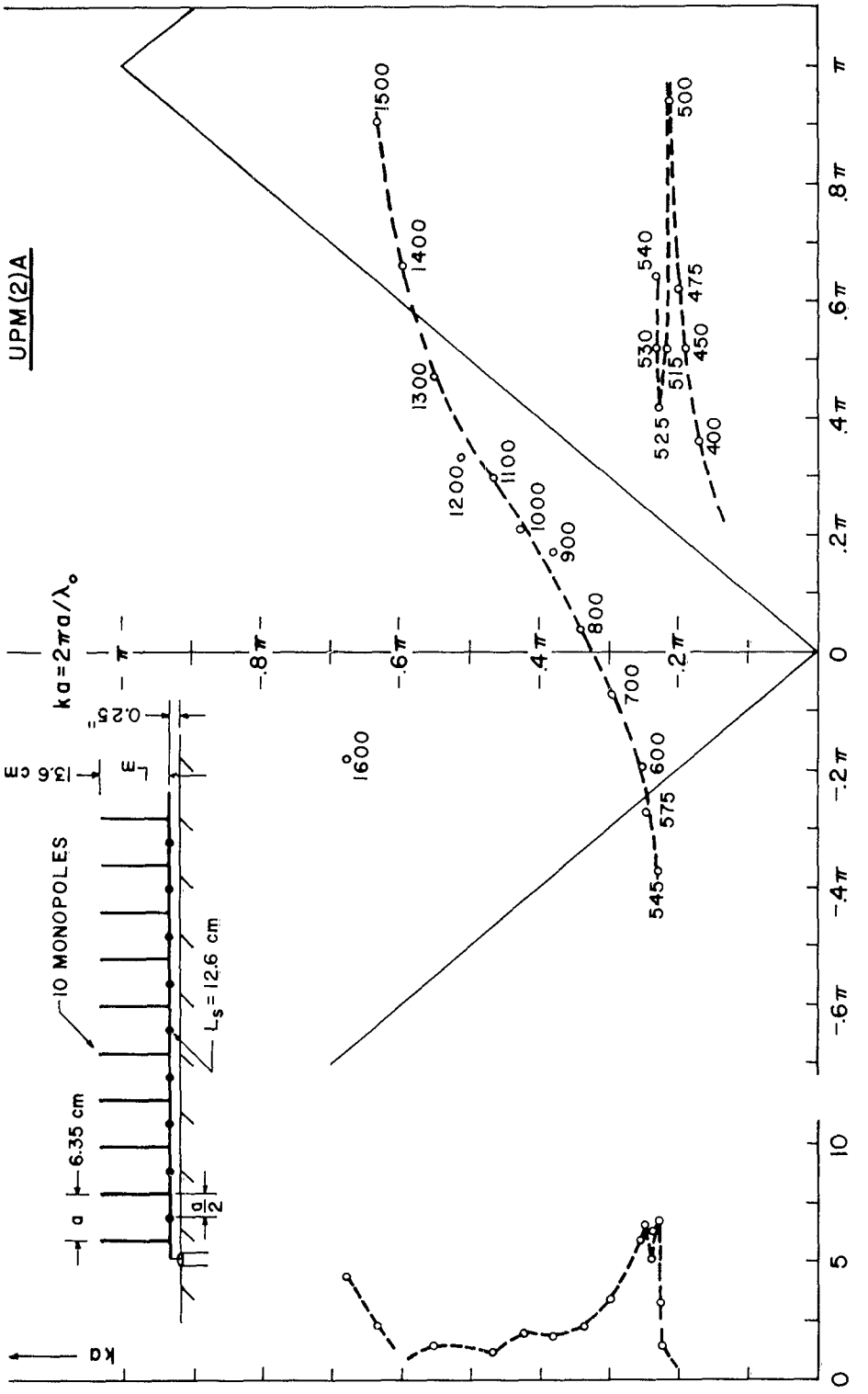

Figure 14. The k-β /Attenuation Diagram for the Stub-Loaded Monopole Array, Type-I, UPM(2)A.

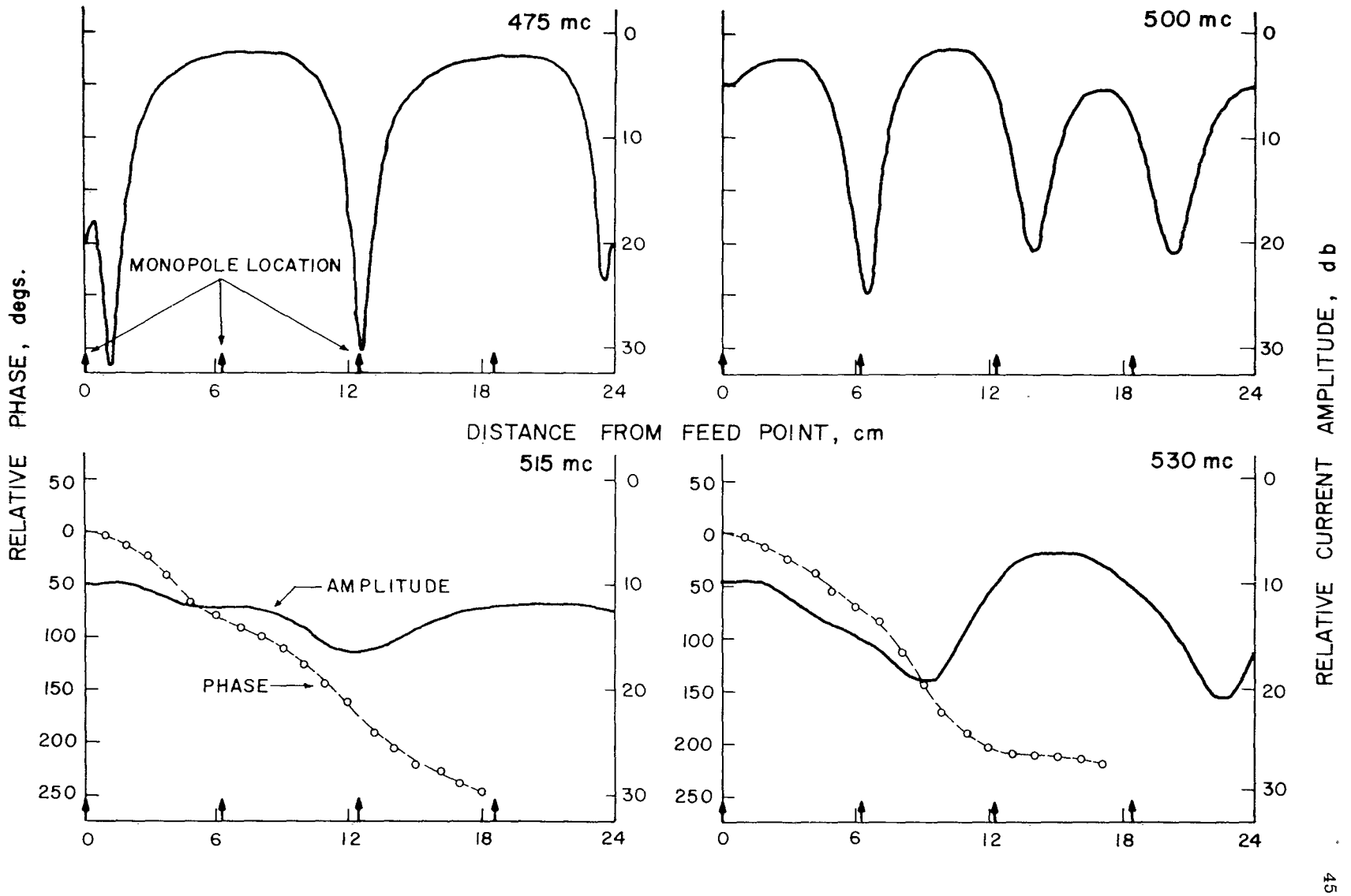

Figure 15. Measured Amplitude and Phase Distributions for UPM(2)A.

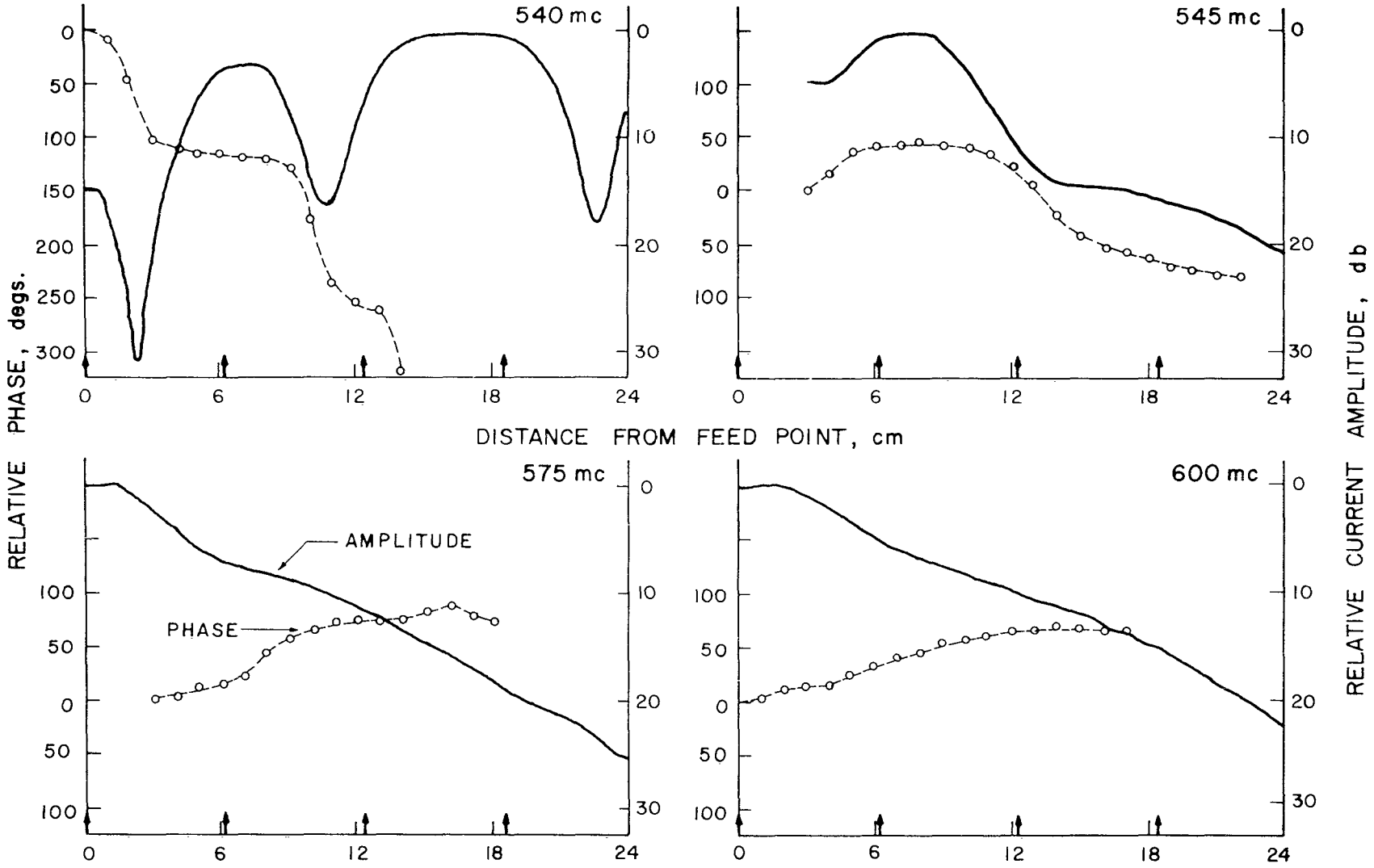

Figure 16. Measured Amplitude and Phase Distributions for UPM(2)A.

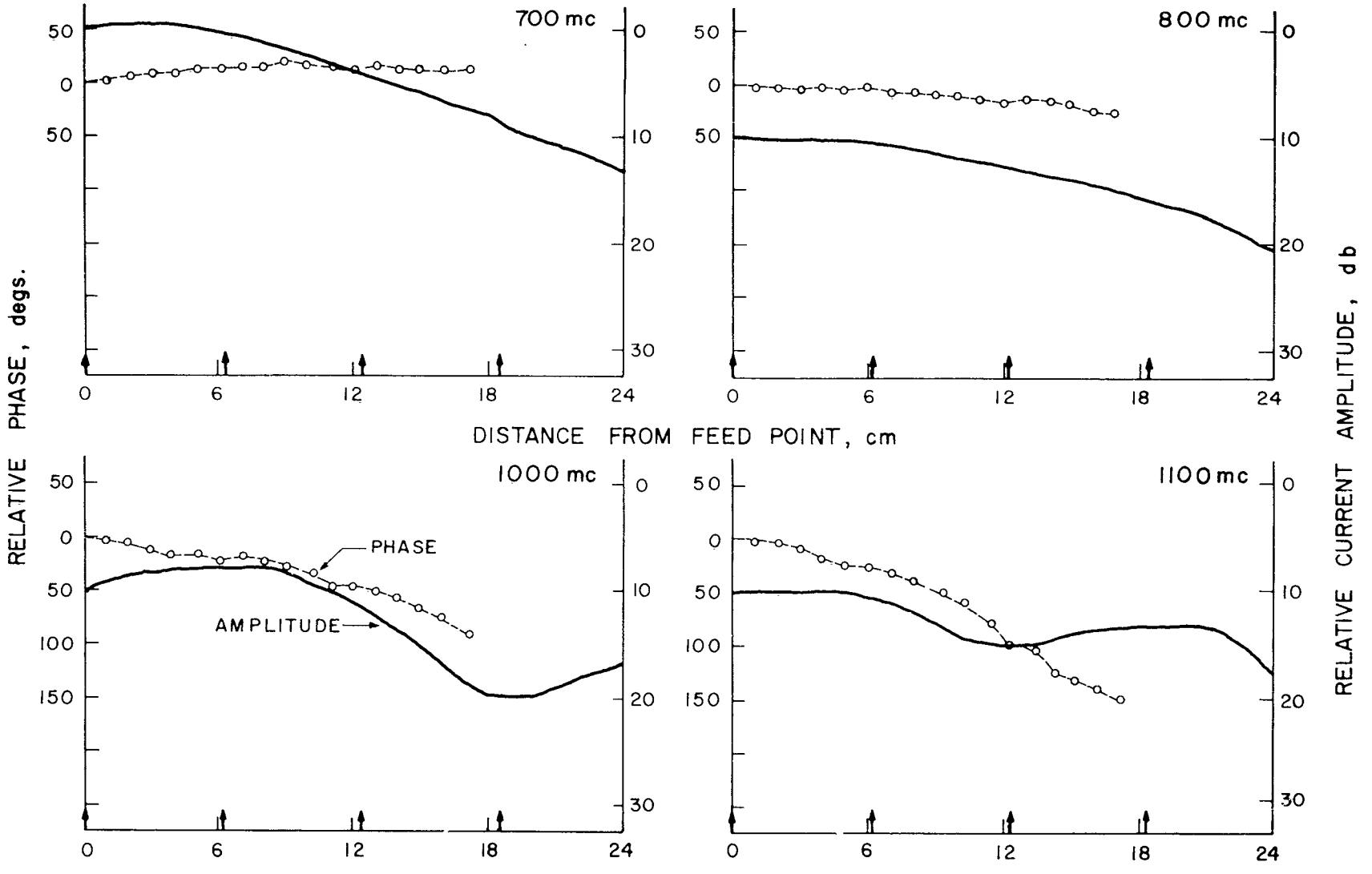

Figure 17. Measured Amplitude and Phase Distributions for UPM(2)A.

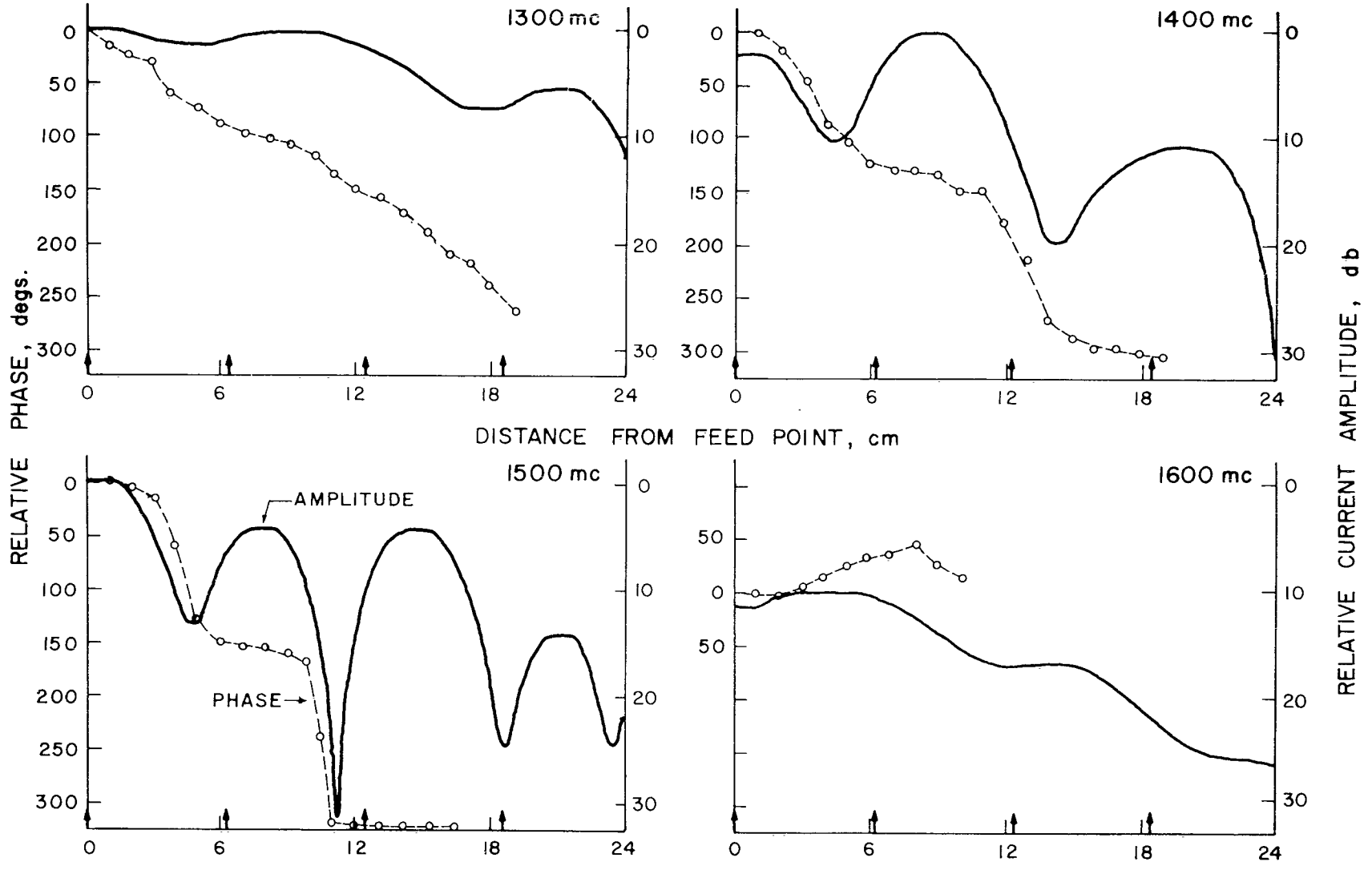

Figure 18. Measured Amplitude and Phase Distributions for UPM(2)A.

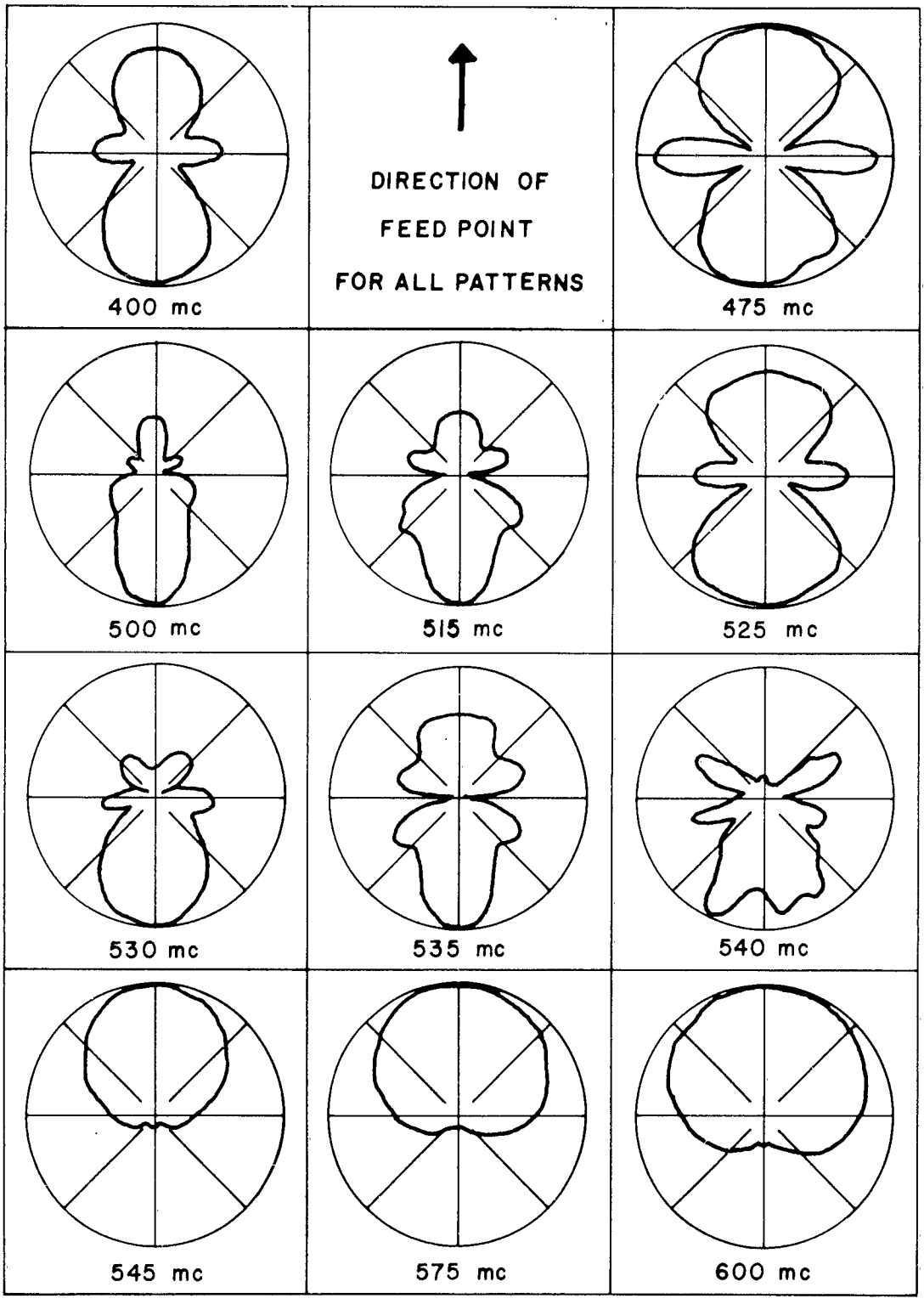

Figure 19. Measured H-Plane Voltage Patterns for UPM(2)A.

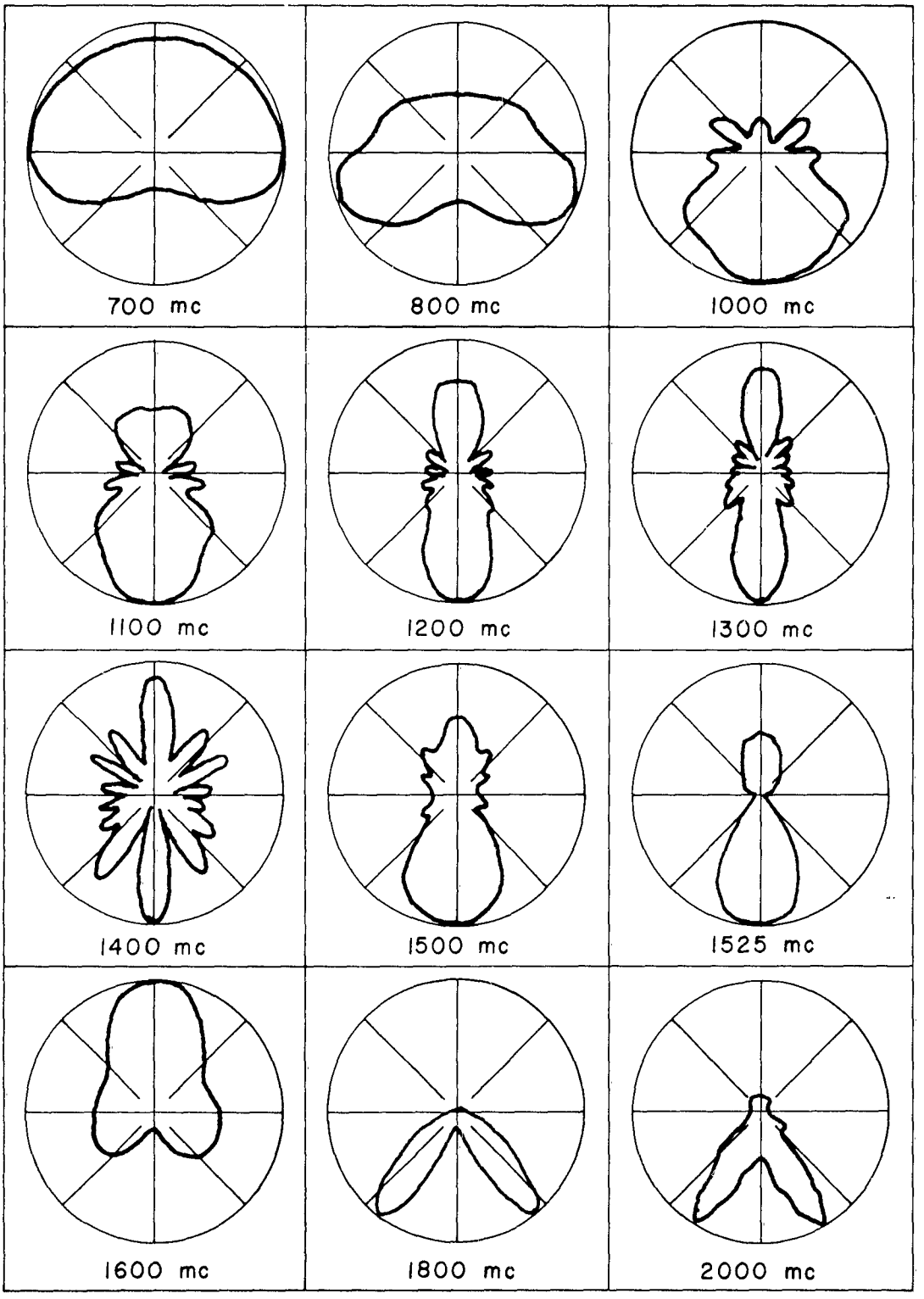

Figure 20. Measured H-Plane Voltage Patterns for UPM(2)A.

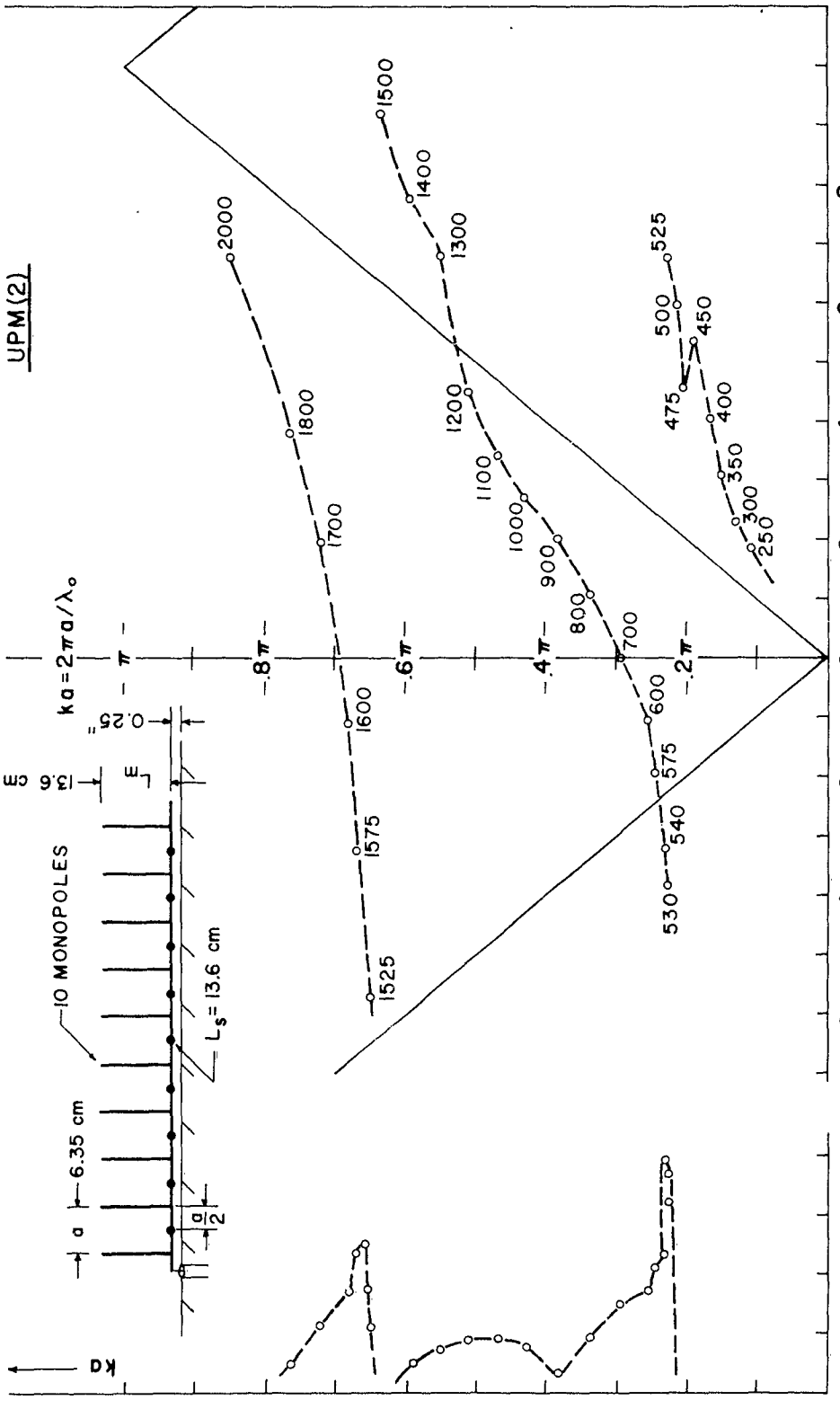

Figure 21. The k-β /Attenuation Diagram for the Stub-Loaded Monopole Array, Type-I UPM(2).

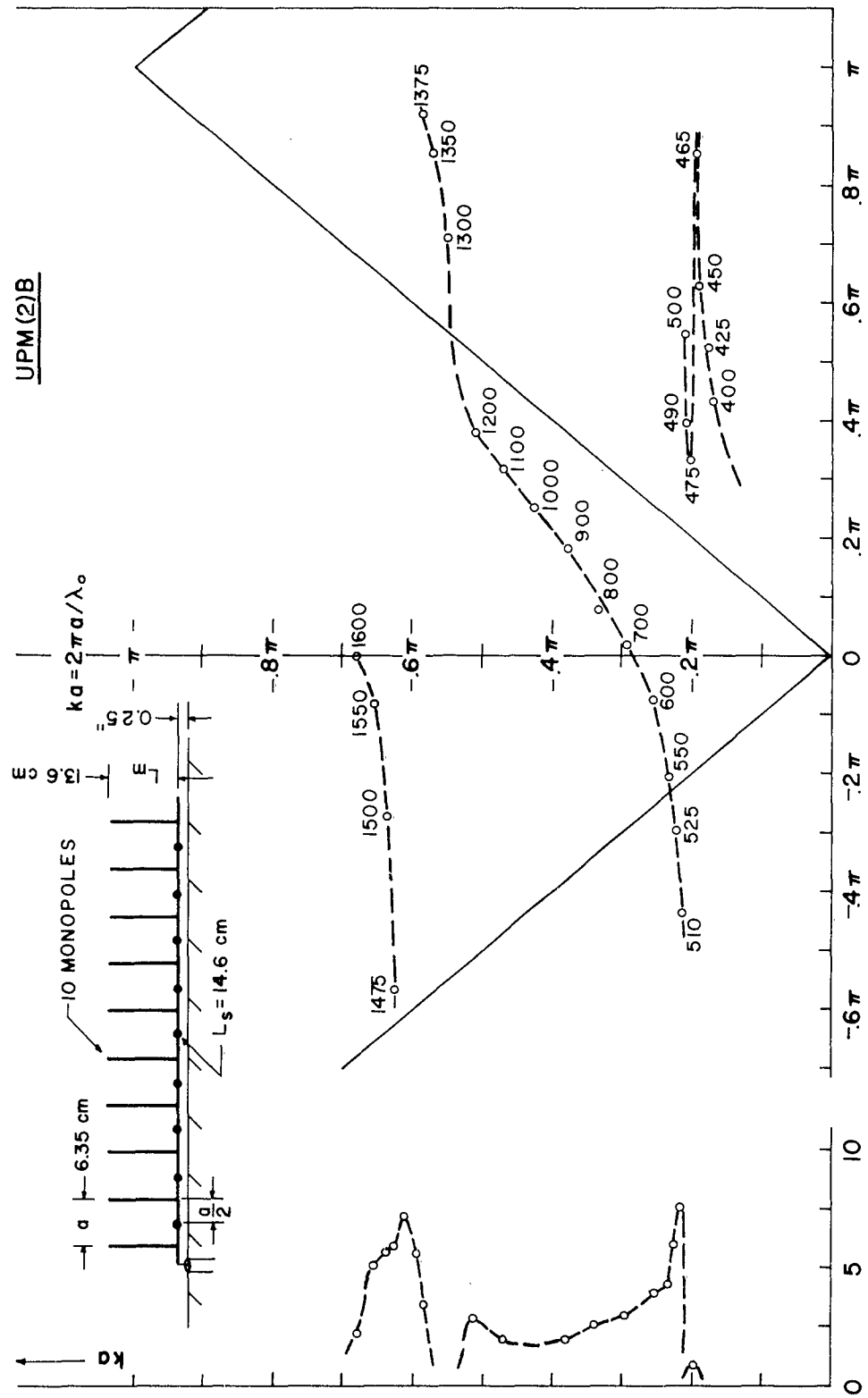

Figure 22. The k-β /Attenuation Diagram for the Stub-Loaded Monopole Array, Type-I, UPM(2)B.

change in radiation patterns between the frequencies of 540 and 545 Mc. Strictly speaking, there are two turnover regions here, one near 500 Mc and the other near 540 Mc. The most significant one, of course, is that which just precedes backfire radiation. The perturbations in the lagging phase portion of the k-β curve are due to the multi-resonance effects of the monopoles and stubs. It will be seen from the k-β diagrams for UPM(2) and UPM(2)B that the regions of turnover and the degree of distortion in the characteristic curve are influenced considerably by the length of the stubs. Although the effect of monopole length was not investigated here, it is postulated that this parameter would not be as critical, since the Q-factor of the monopole is not as great as that of the stub.

Here, as with the simple monopole array, the attenuation rate is greatest just beyond turnover (ie., the second turnover) and decreases with increase in frequency up to the region of three-quarter-wavelength resonance. It is important to note the trend of the H-plane patterns as the k-β curve passes from the backward wave region of the Brillouin diagram across to the forward wave region. This is another characteristic of the uniformly periodic monopole array. The dependence of the oblique angle, θ, on the ratio β/k was discussed earlier in the report. From this it was anticipated that beam scanning would occur in the H-plane patterns as the k-β curve passed across the radiation region of the Brillouin diagram. From the patterns shown for UPM(2)A it is seen that there is a scanning tendency. Beam scanning is more distinct over the second pass of the k-β curve, that is, at frequencies above the three-quarter-wavelength resonance. To see this, reference must be made to both the UPM(2)A and UPM(2) data. Phase and amplitude measurement on UPM(2)A were not made at the higher frequencies.

Another significant fact to note is the nature of the phase distribution on the structure at the region of turnover, specifically, at 540 and 545 Mc. The phase sense over the first few centimeters of the array changes from lagging at 540 Mc to leading at 545 Mc. This sudden change in phase sense at turnover was observed also with UPM(2) and UPM(2)B; and, as will be seen from the phase data of the various other structures, this phenomenon is consistent with the transition to backfire directivity. In this frequency region, it is only the first cell or two which exhibits the leading phase property. Beyond that the phase assumes a lagging sense. However, as the frequency is increased slightly both the amplitude and phase distribution become relatively smooth. Then as the frequency is increased to advance the k-β curve across the Brillouin diagram into the triangle, the amplitude and phase distributions gradually change from attenuation and leading to less attenuation and lagging, and then again to distributions which correspond to the standing wave condition.

The effect of the stub length on the directional performance of the stub-loaded monopole array can be deduced from the respective Brillouin diagrams for UPM(2) and UPM(2)B. It is evident from these that turnover occurs at frequencies lower than that for UPM(2)A which employed the shortest stubs. Far-field pattern measurements confirmed this. If time would have permitted, it would be interesting to have determined the extent to which the stub reactance could control backfire radiation. The effect of the stub reactance is also evident in the perturbations of the k-β curve prior to turnover. For UPM(2) the degree of distortion to the k-β curve is the least of the three models. Here the length of the stubs is just slightly shorter than the effective length of the monopoles. It is not known whether or not the amount

of distortion to the phase curve lends any insight to the optimum length for the stub. However, the optimum stub length for the log-periodic structure would almost certainly be based on impedance as well as pattern performance.

4.3 UPM(2)D — Stub-Loaded Monopole Array, Type - II

Except for locating the horizontal stubs at the monopole position rather than between the monopoles, UPM(2)D is precisely the same as UPM(2) discussed above. A detailed sketch of UPM(2)D is shown in the lower left of Figure 1. This experimentation was carried out to determine whether or not backfire radiation could be achieved by locating the stub reactance other than midway between the monopoles. During the course of the original work with the log-periodic counter-part*, it was believed that this additional shunt reactance should be positioned between the adjacent monopoles in accordance with the log-periodic taper. But near and far-field measurements on UPM(2)D illustrated that this structure possessed essentially the same directional properties as did the Type-I array. Here again, however, the problem of impedance has not been considered. The k-β / attenuation diagram for this array is shown in Figure 23.

4.4 UPM(15) — Shunt-Fed Solid Tooth Monopole Array, Type - I

The detailed sketch of UPM(15) is illustrated in the lower right of Figure 1. The monopole elements are solid sheet conductors grounded at their lower ends and shunt fed by proximity coupling to the conducting strip as shown. With the dimensions shown, the magnitude of capacitive reactance across each feed junction is approximately 7 ohms at 500 Mc. As reported in 1961 by Wickersham and Franks,[7] the log-periodic version of this structure is known to yield successful frequency independent performance. The Brillouin

*Antenna Dept., Collins Radio Co., Cedar Rapids, Iowa, 1960.

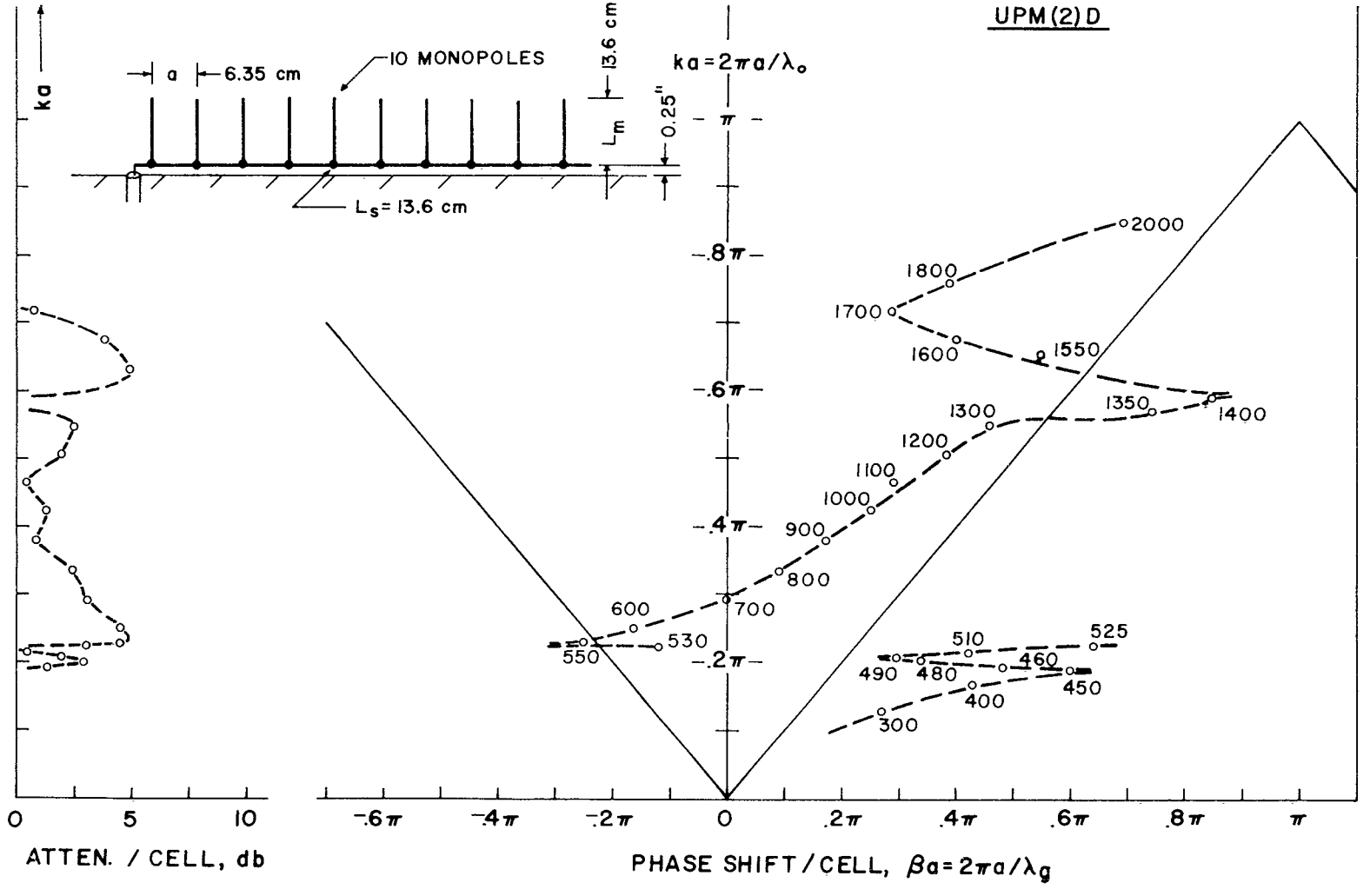

Figure 23. The k-β /Attenuation Diagram for the Stub-Loaded Monopole Array, Type-II, UPM(2)D.

diagram of Figure 24 summarizes the results of near-field measurements on UPM(15). Some of the corresponding data is shown in Figures 25 through 30. Although the data for this array resemble, in general, those of the stub-loaded monopole structure, there are several significant points of difference. Perhaps the point most noteworthy is that of the apparent lower system-Q. The transition to the condition of backward directivity is seen to be more gradual than was that of the stub-loaded structure. This tends to indicate that the parameters of the tapered counterpart would not be so critical for a successful design. Experiment with the log-periodic version confirms this — at least insofar as achieving satisfactory frequency independent unidirectional patterns. Another point of interest is the attainment of backfire directivity while the amplitude distribution is still predominantly of the standing wave form. But it must be noted, also, that associated with the backfire directivity is a leading phase over the first cell or two, even though the phase distribution corresponds to that of a standing wave. This phenomenon will be seen to occur with several of the other structures discussed later.

As the frequency is increased, the phase and amplitude distributions become fairly smooth. Note that the attenuation rate is markedly greater than that for the stub-loaded array.

The reason for the endfire tendency and the rather high rate of attenuation at the lower frequencies, where only transmission is to be expected, is not clearly known. These characteristics, as well as the failure of the structure to enter the three-quarter-wavelength resonance condition, are most likely due to the effect of the "fatness" of the elements and to the method of feeding them.

Before passing on to the next structure, it may be of interest to note that the feed capacitance per element of UPM(15) was reduced by one-half and

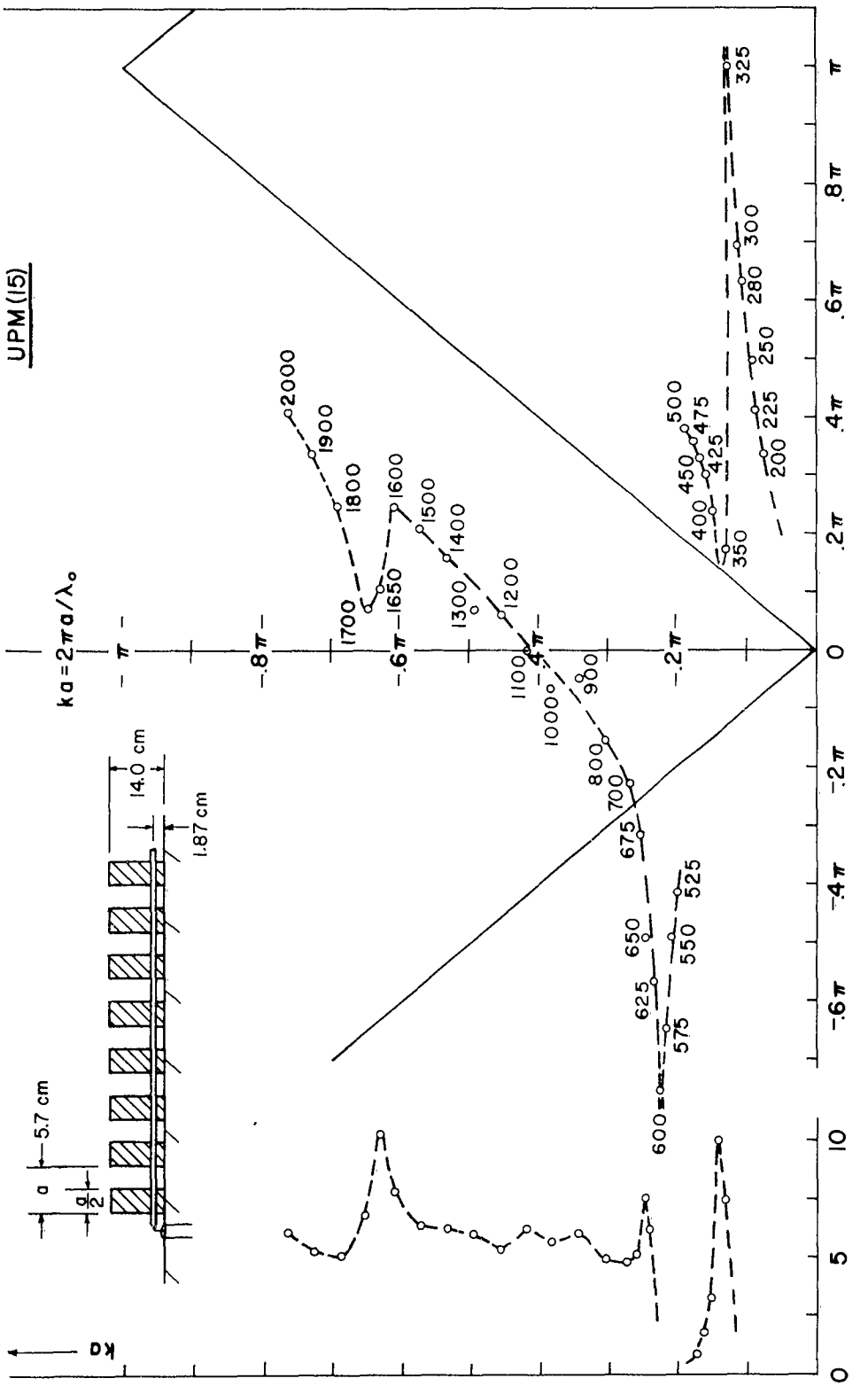

Figure 24. The k-β /Attenuation Diagram for the Shunt-Fed, Solid Tooth Monopole Array, Type-I, UPM(15).

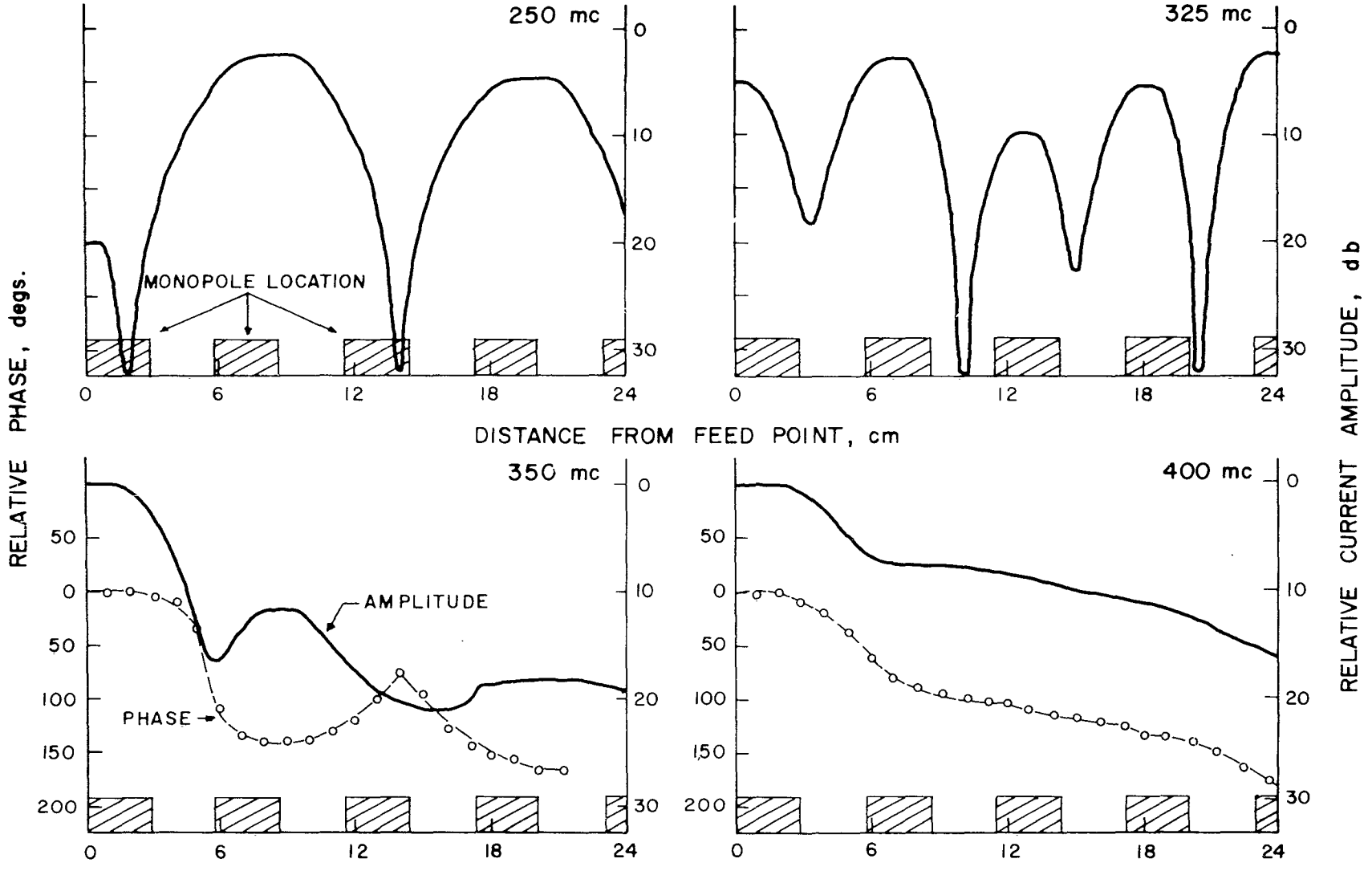

Figure 25. Measured Amplitude and Phase Distributions for UPM(15).

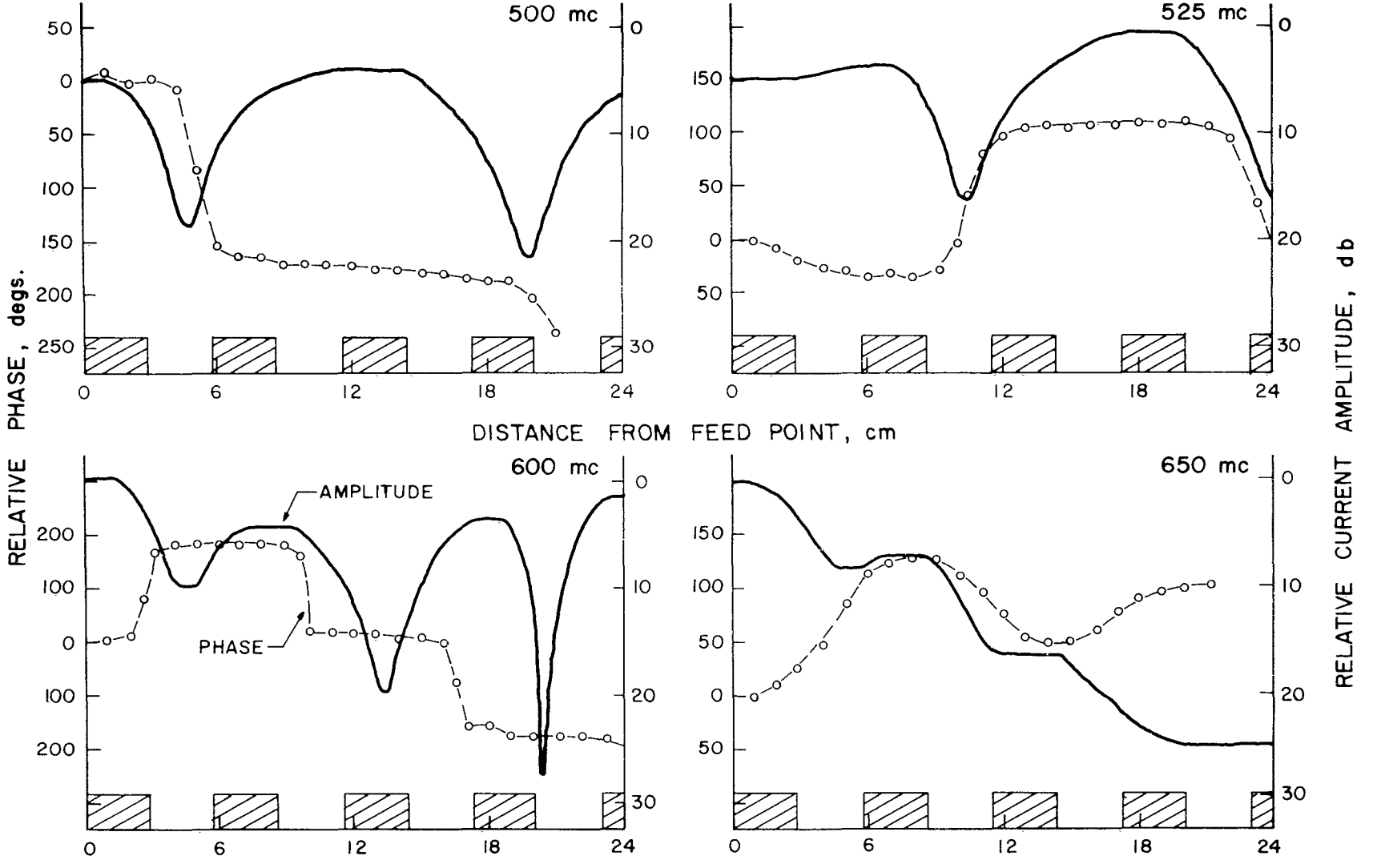

Figure 26. Measured Amplitude and Phase Distributions for UPM(15).

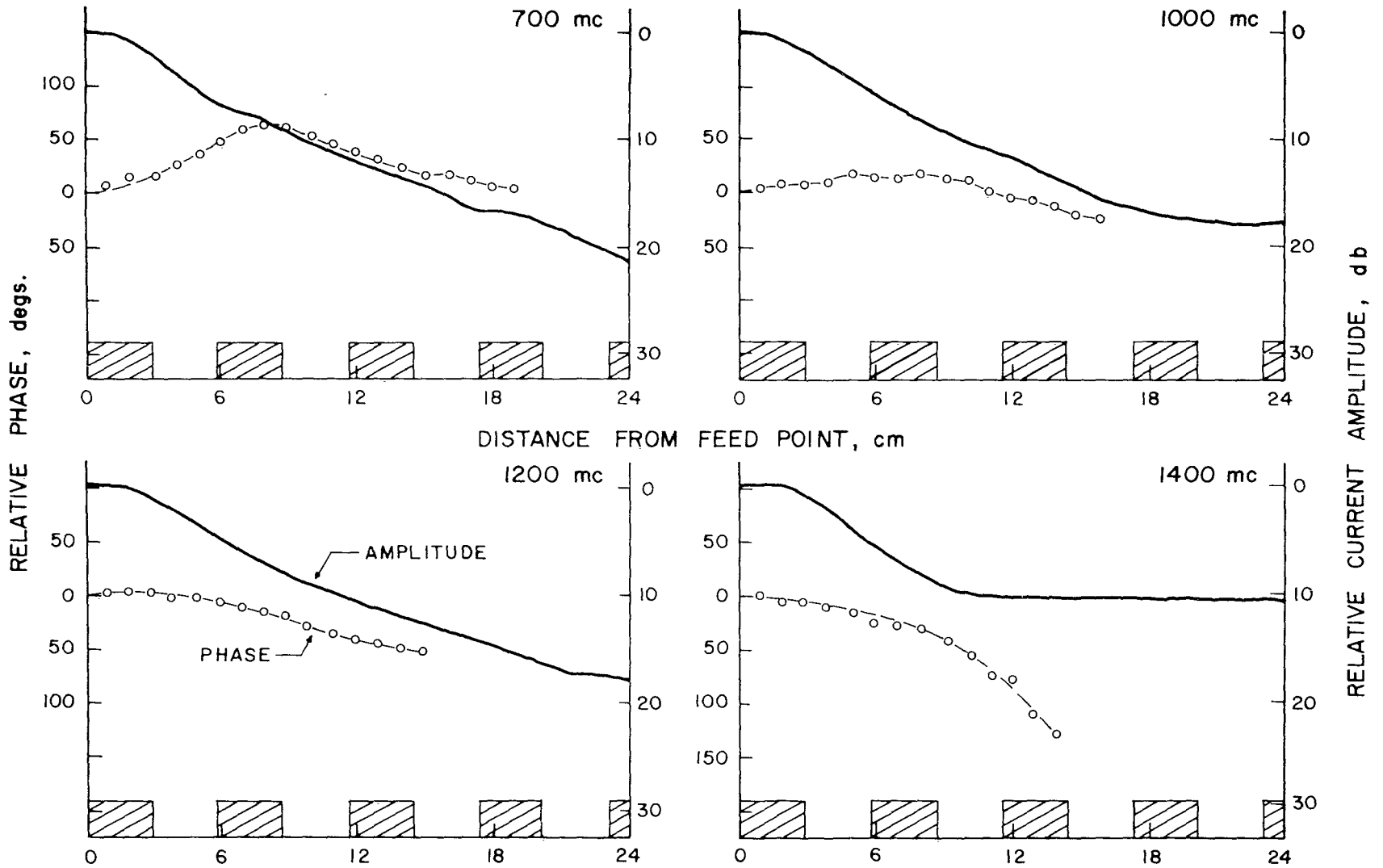

Figure 27. Measured Amplitude and Phase Distributions for UPM(15).

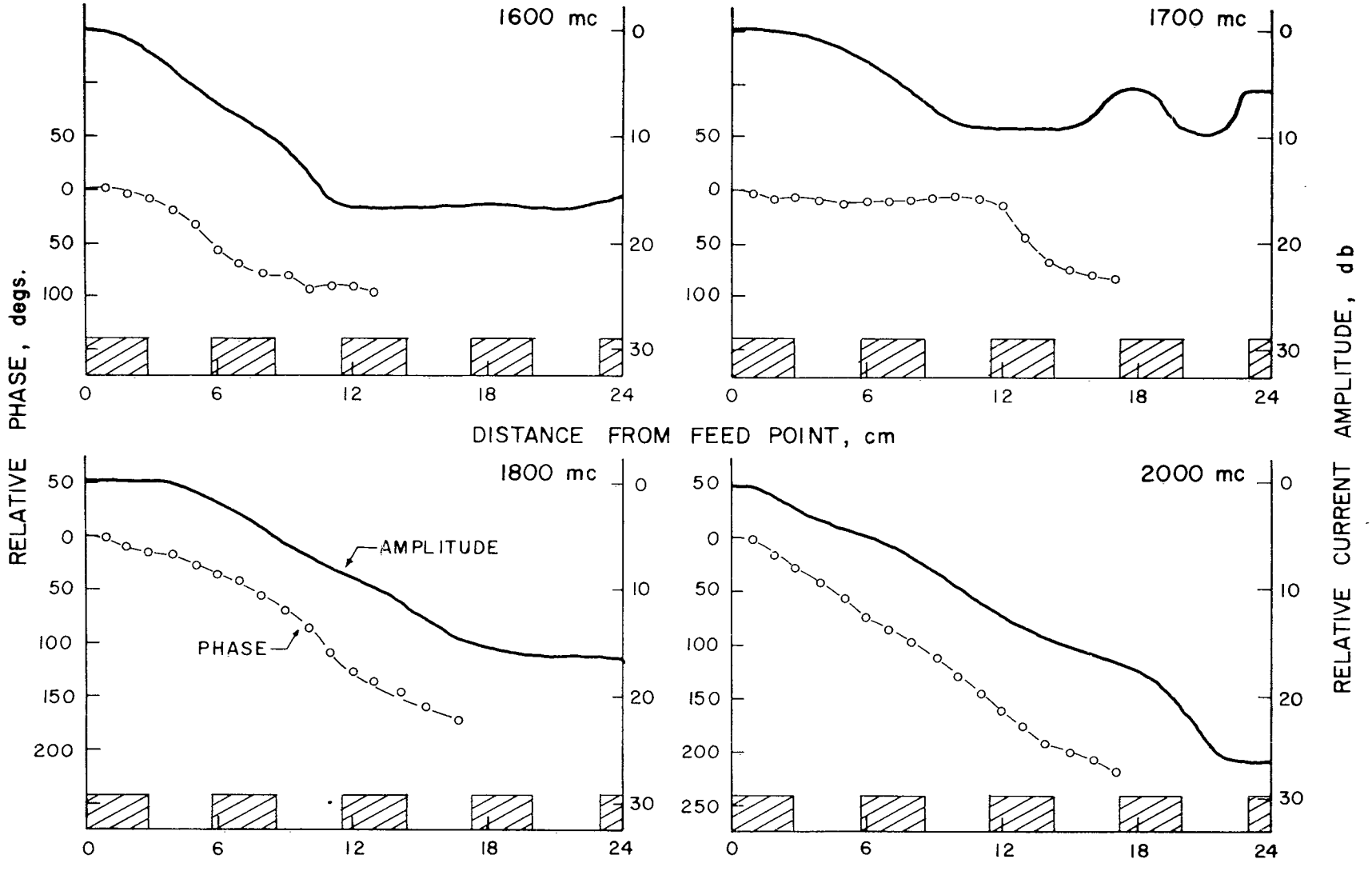

Figure 28. Measured Amplitude and Phase Distributions for UPM(15).

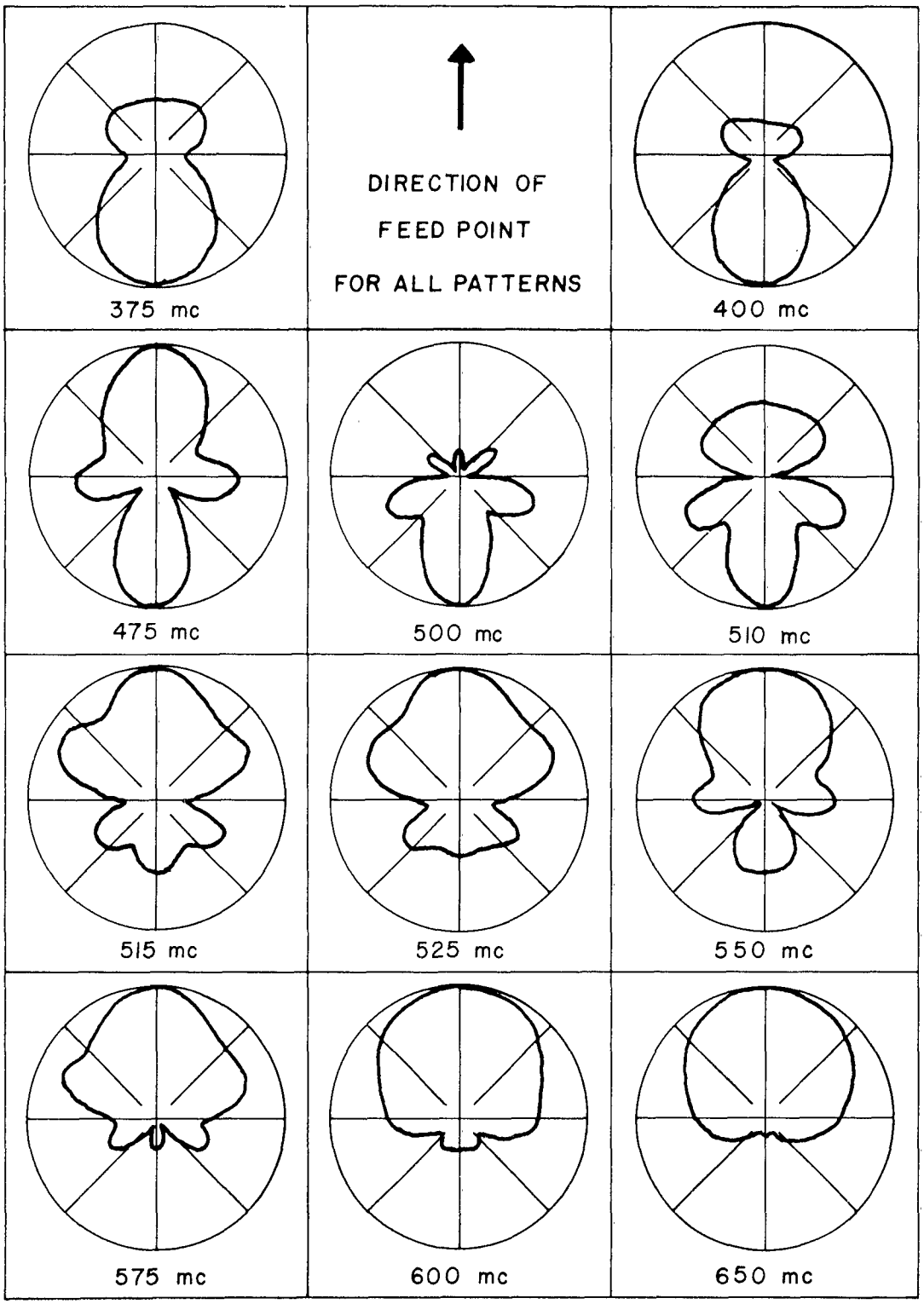

Figure 29. Measured H-Plane Voltage Patterns for UPM(15).

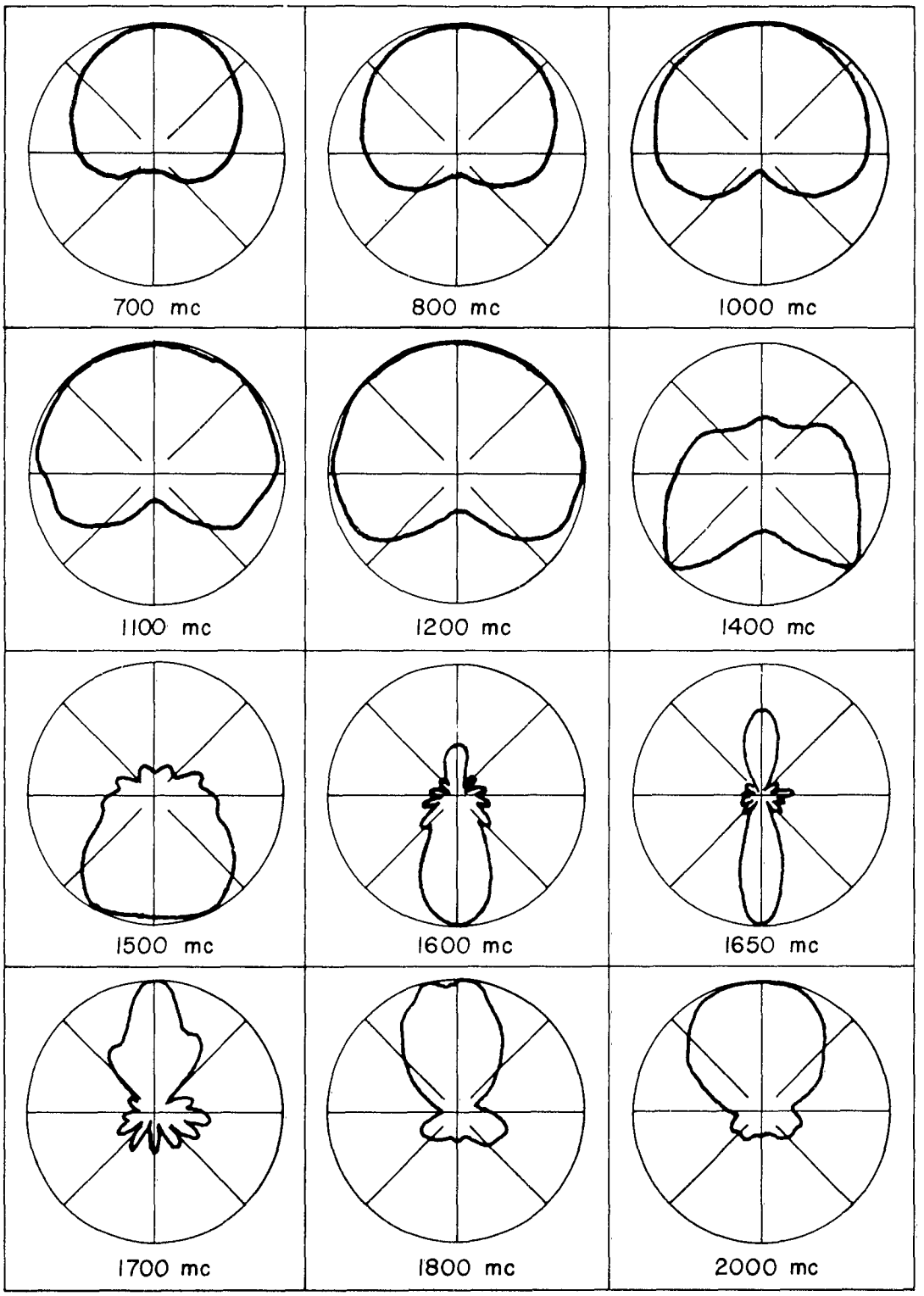

Figure 30. Measured H-Plane Voltage Patterns for UPM(15).

H-plane pattern measurements repeated. The patterns remained essentially unchanged from those in the original case.

4.5 UPM(14) — Shunt-Fed Solid Tooth Monopole Array, Type - II

The UPM(14) model is similar in construction to UPM(15), but employs monopole elements twice the width of those in the UPM(15). Hence, the period is also twice as large. Details of UPM(14) are shown in the upper left of Figure 2. The feed capacitance per element is approximately the same as that incorporated in UPM(15). The prime reason for reporting on this particular structure is that its basic parameters correspond to those of UPM(13) which is reviewed next, and, thus, offers a basis for comparison. Since the characteristics of UPM(14) are quite similar to those of UPM(15) discussed above, it is not necessary to elaborate on the results of the measurements on this wider tooth version. The results of near-field measurements are summarized in the k-β / attenuation diagram of Figure 31. Figures 32 through 37 illustrate some of the corresponding experimental data. Attention is called to the fact that although the overall attenuation rate appears greater here than for the UPM(15) structure, it must be remembered that the cell dimension is twice that of UPM(15).

4.6 UPM(13)—Shunt-Fed Wire Tooth Monopole Array, Type - II

UPM(13) is a wire outline of the UPM(14) monopole array and is also shunt fed by proximity coupling to the feed line. Here, the feeding system consists of an interrupted coaxial cable as indicated in the detailed sketch at the upper right of Figure 2. The log-periodic counter-part of this structure is known to yield satisfactory frequency independent operation*. This structure

*Antenna Dept., Collins Radio Co., Cedar Rapids, Iowa, 1961, and private communications with F.R. Ore, Antenna Laboratory, University of Illinois, 1962.

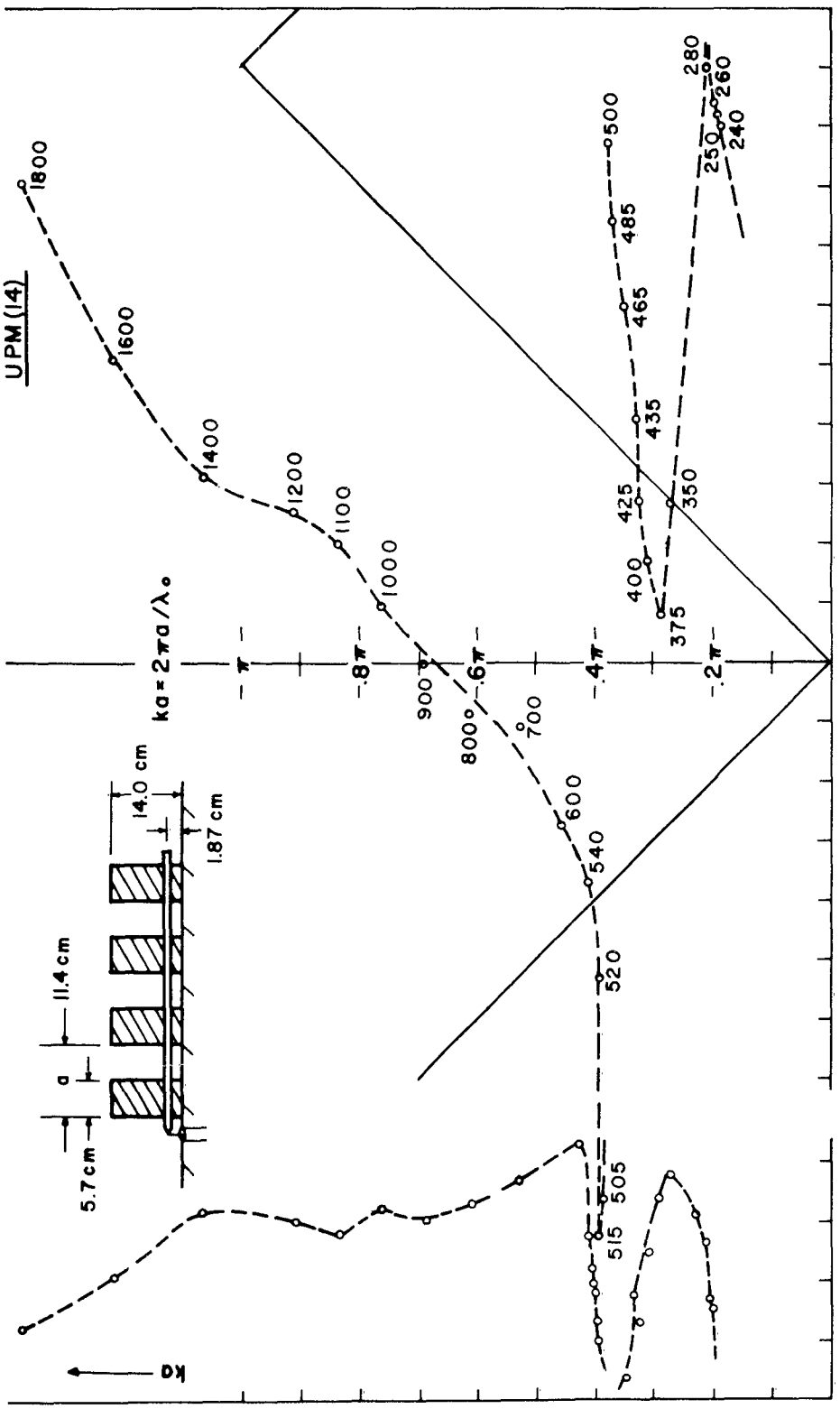

Figure 31. The k-β /Attenuation Diagram for the Shunt-Fed, Solid Tooth Monopole Array, Type-II, UPM(14).

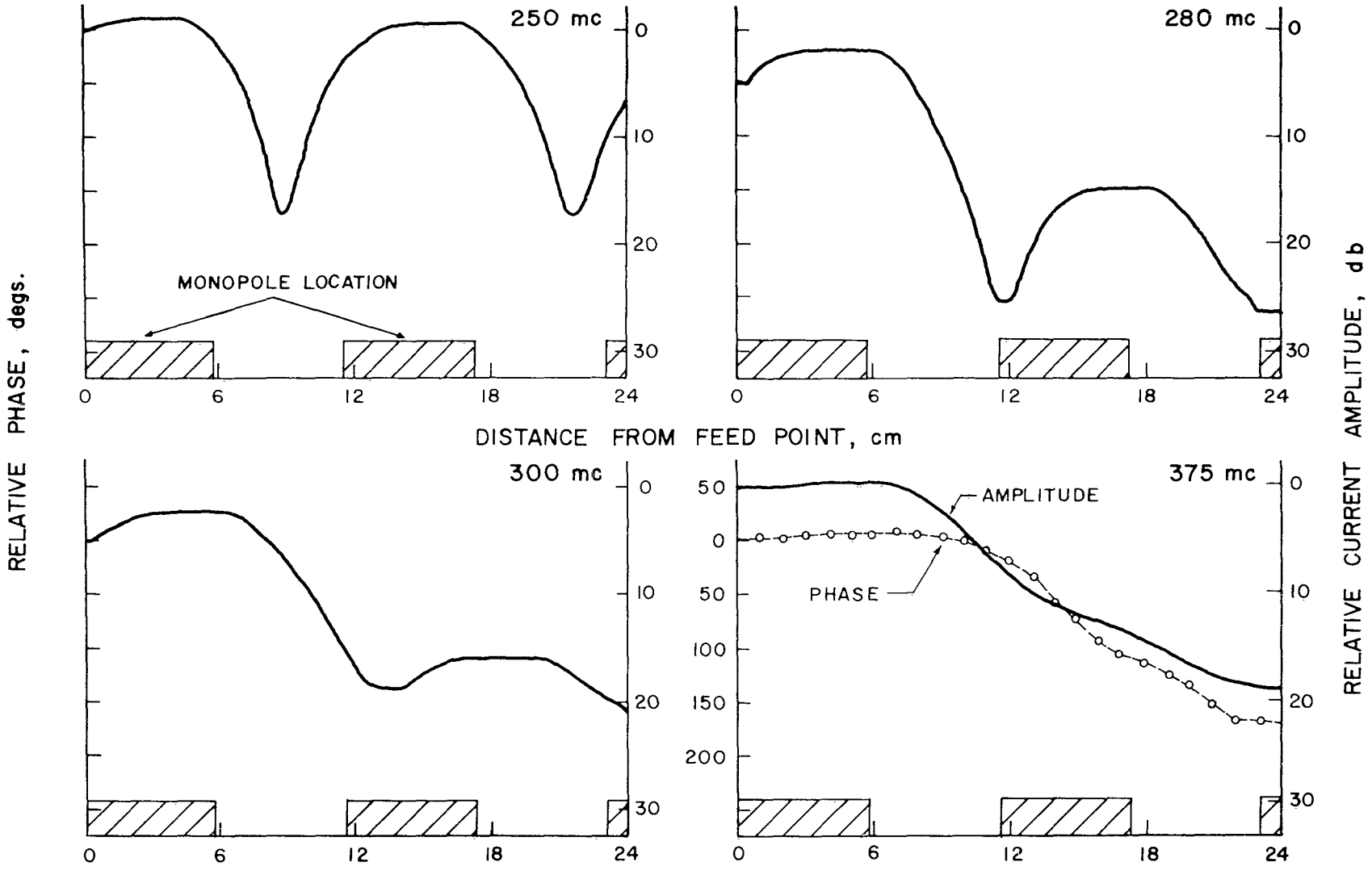

Figure 32. Measured Amplitude and Phase Distributions for UPM(14).

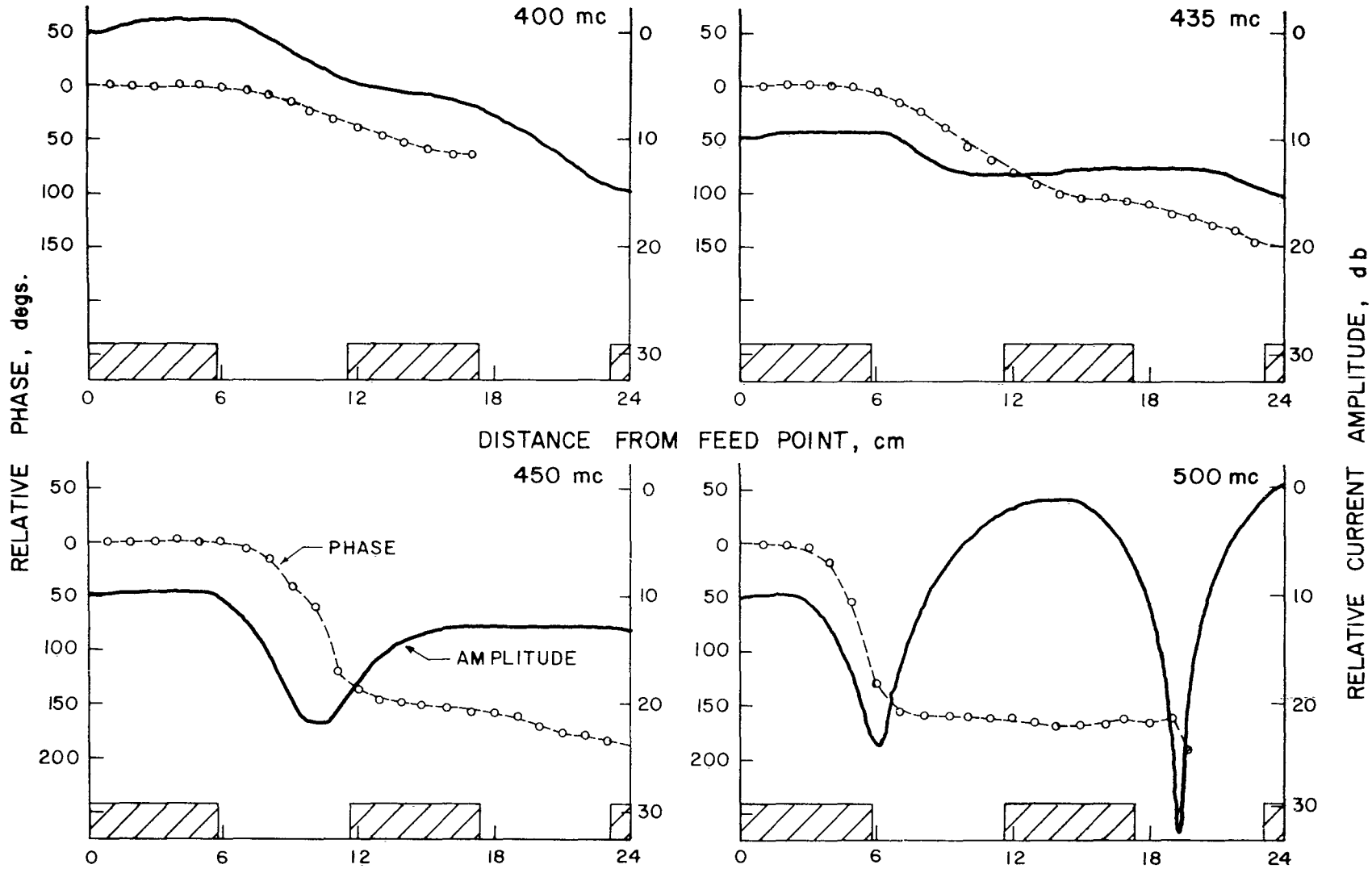

Figure 33. Measured Amplitude and Phase Distributions for UPM(14).

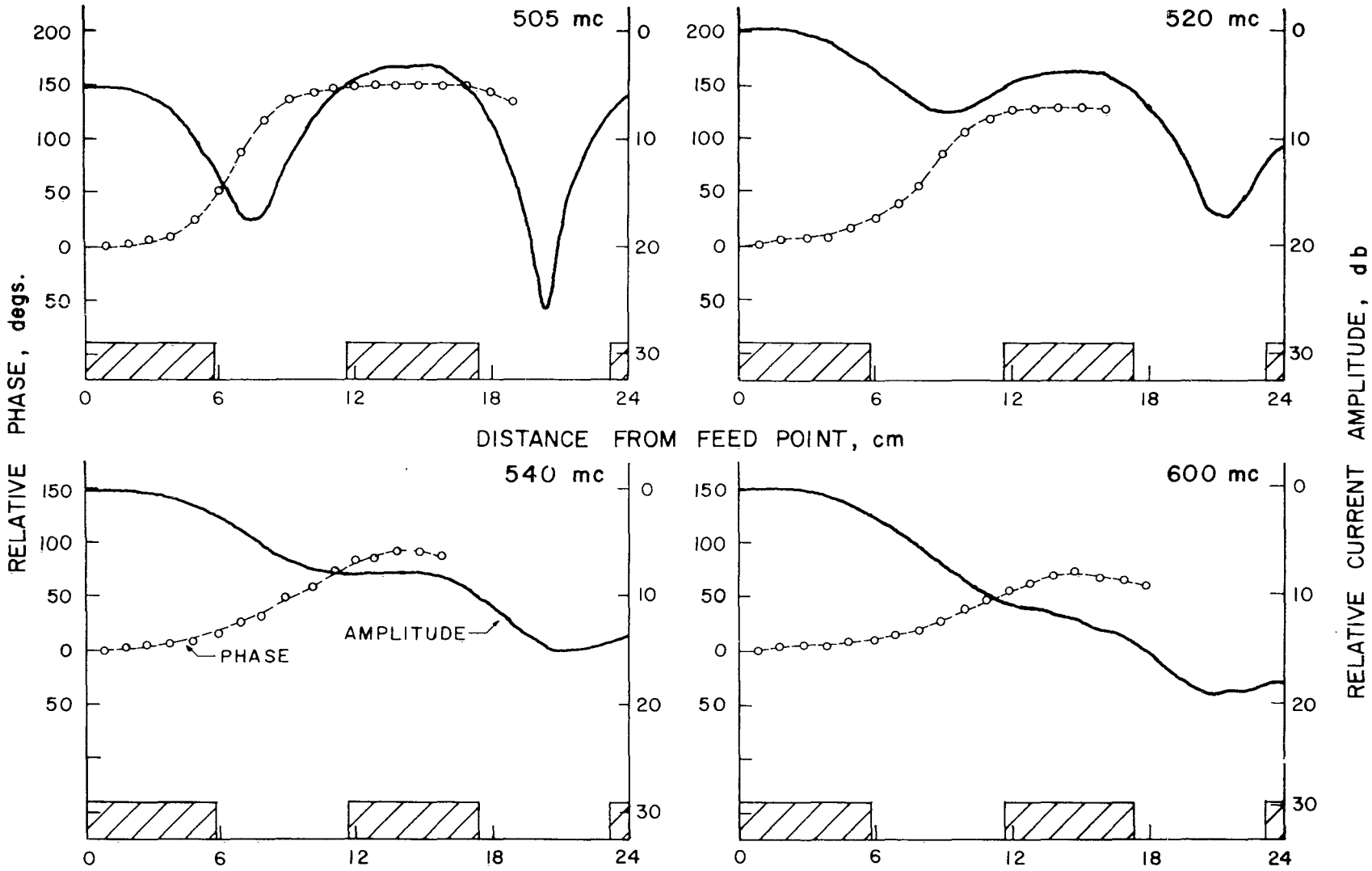

Figure 34. Measured Amplitude and Phase Distributions for UPM(14).

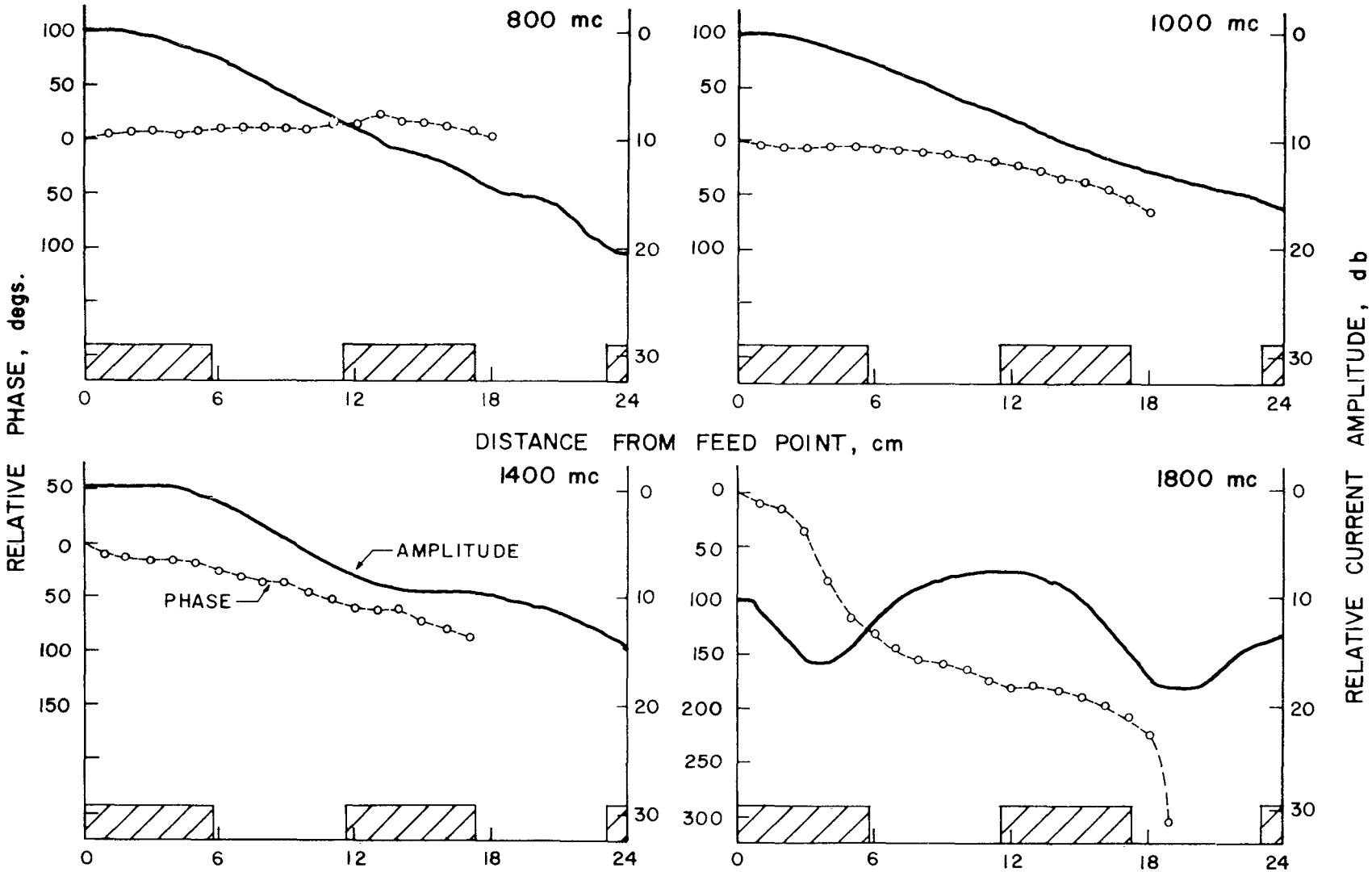

Figure 35. Measured Amplitude and Phase Distributions for UPM(14).

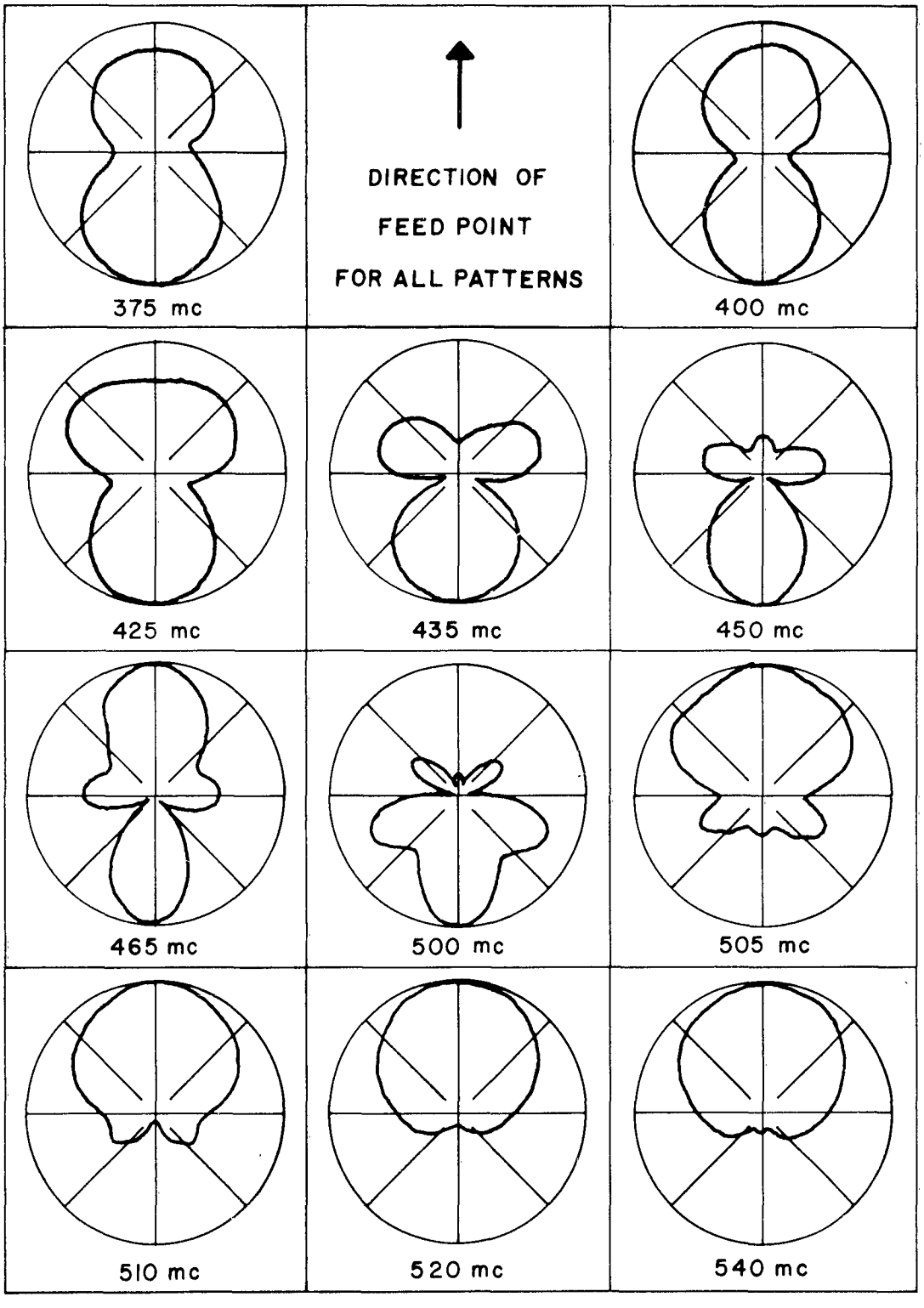

Figure 36. Measured H-Plane Voltage Patterns for UPM(14).

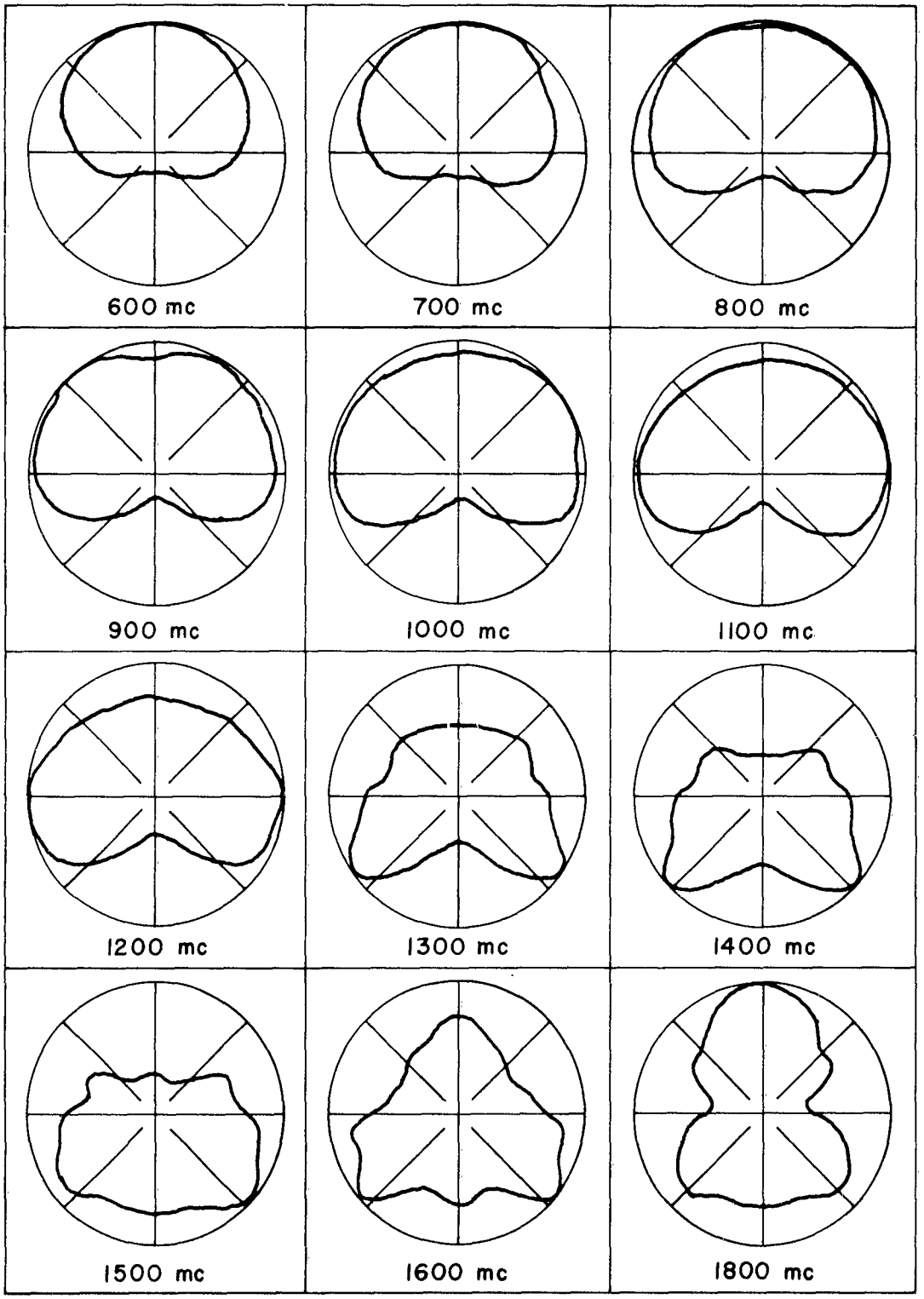

Figure 37. Measured H-Plane Voltage Patterns for UPM(14).

is of interest because its construction and geometry are suitable for practical full scale h-f antennas. The k-β'/ attenuation diagram for UPM(13) is shown in Figure 38, and asserts that through the frequency range of most interest the near-field and directional characteristics of this array are quite similar to those of the solid tooth version. The differences which do exist are largely at the higher frequencies (above about 900 Mc) as might be expected from the respective structure designs. Note that the scale on the attenuation-per-cell axis of Figure 38 is expanded over the previous diagrams by a factor or two. This was done to eliminate interference with the k-β curve. Figures 39 through 41 illustrate some of the amplitude and phase data. Figure 42 illustrates measured H-plane voltage patterns. From these it can be seen that the patterns are much the same as those for UPM(14) up to about 900 Mc.

4.7 UPM(10)C —Balanced-Fed Dual Monopole Array

A somewhat different approach to the attempt to achieve backfire radiation was made with the periodic structure illustrated in the lower left of Figure 2. Here two simple monopole arrays, each similar to the UPM(2)C structure described above, are arranged in collinear fashion and fed balanced, that is, π radians out of phase. The balun action is achieved through the twin line of parallel tubing, one of which contains the coax feed cable. This feed configuration is often referred to as an infinite-type balun since its balance-to-unbalance action is achieved when the twin line appears infinite in length, which is the case during the regions of amplitude attenuation. The two lines are equally spaced one-quarter inch (from their lower edges) above the ground plane. UPM(10)C is only one uniformly periodic model of about six in this class which were investigated. Pattern measurements were also made on the log-periodic counter-part of those structures which exhibited backfire tendencies.

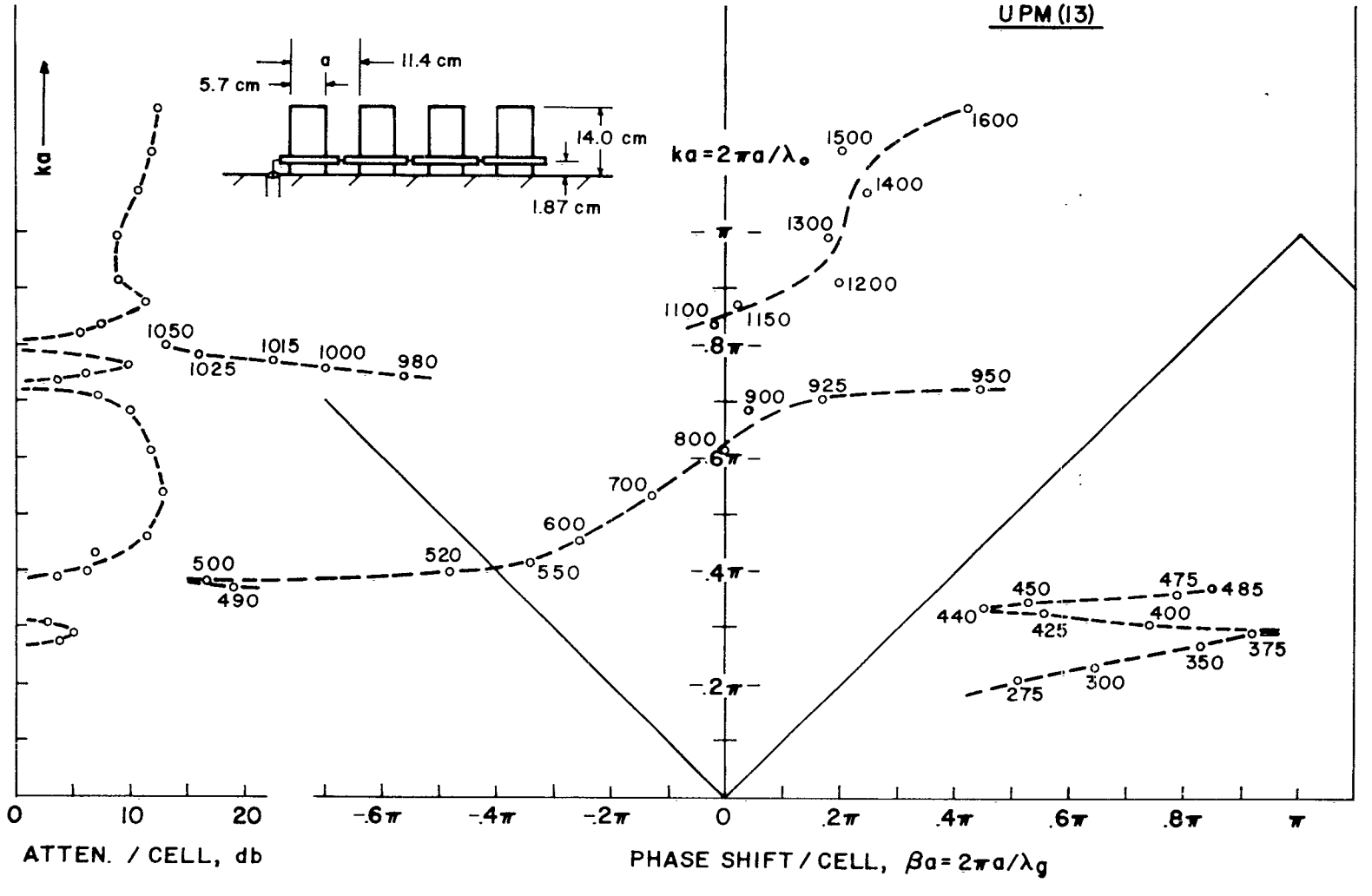

Figure 38. The k-β /Attenuation Diagram for the Shunt-Fed, Wire Tooth Monopole Array, Type-II, UPM(13).

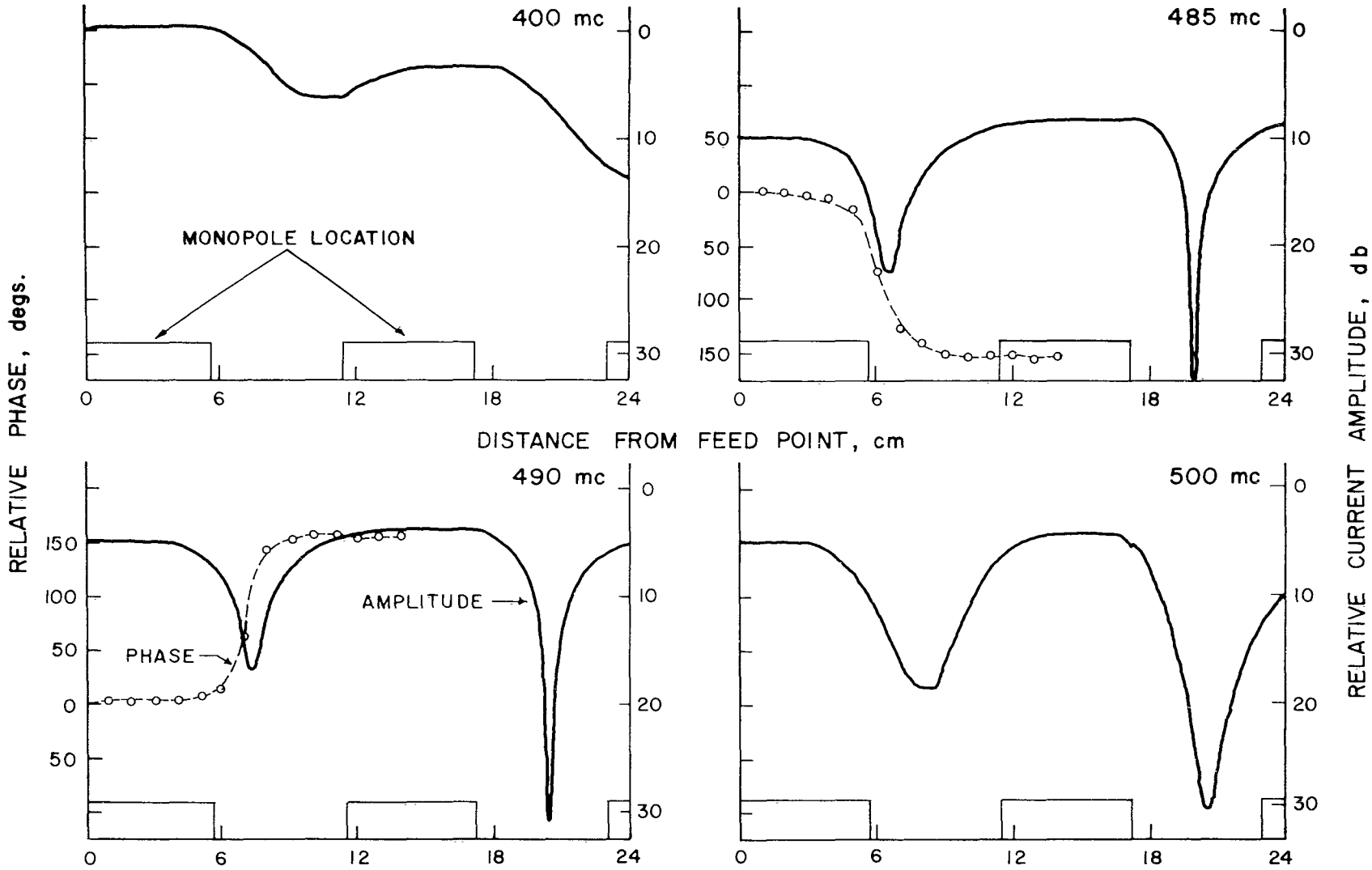

Figure 39. Measured Amplitude and Phase Distributions for UPM(13).

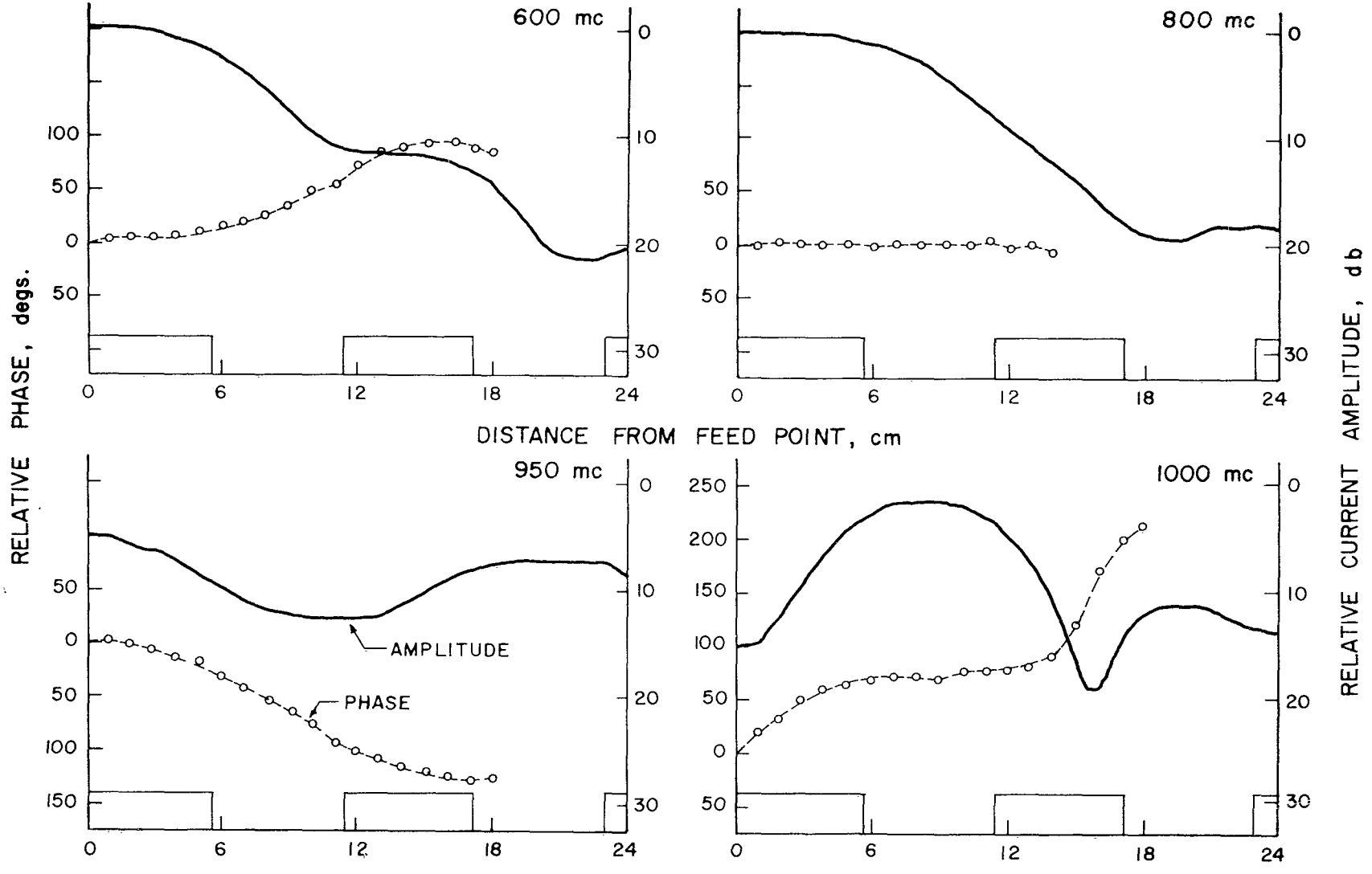

Figure 40. Measured Amplitude and Phase Distributions for UPM(13).

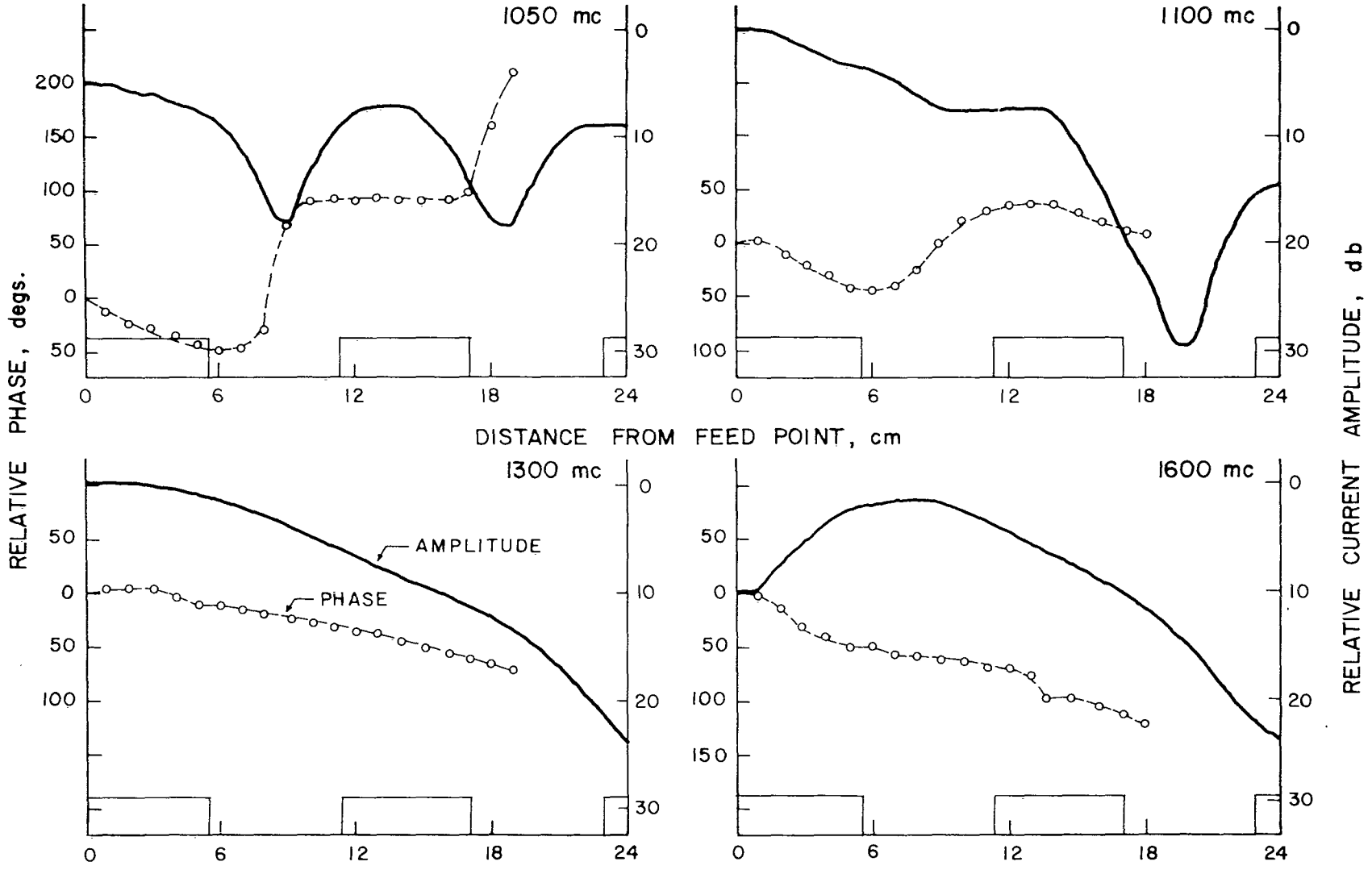

Figure 41. Measured Amplitude and Phase Distributions for UPM(13).

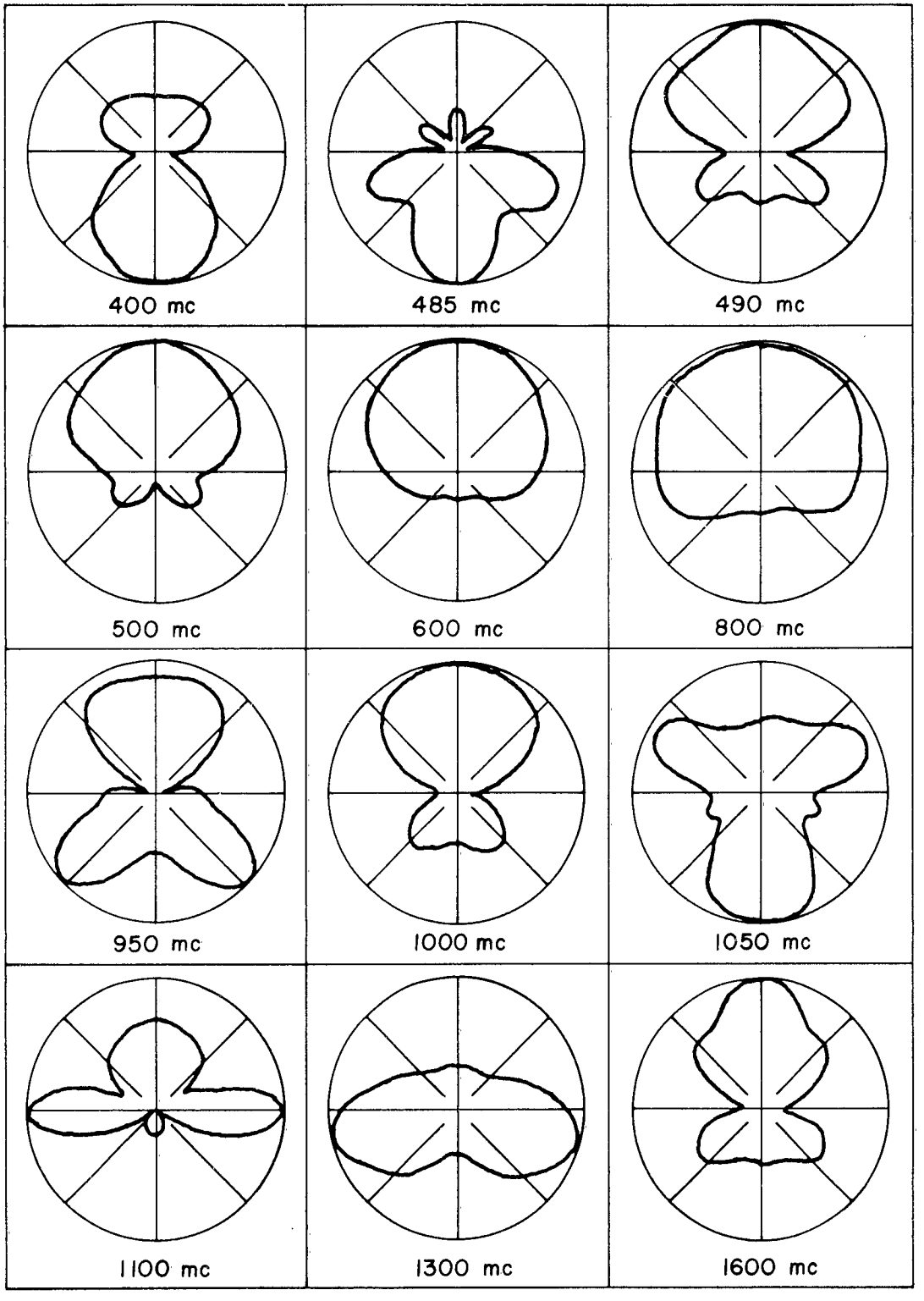

Figure 42. Measured H-Plane Voltage Patterns for UPM(13).

UPM(10)C is one of these models, but as can be seen from the H-plane patterns of Figure 43, none are truly unidirectional. However, the backward direction is generally favored. Patterns observed from the tapered counterpart of UPM(10)C were of the same general nature, perhaps somewhat broader but more unidirectional, and not sufficiently independent of frequency. The other structures of this class incorporated additional loading or "slowing" in attempts to improve the phasing conditions and thereby enhance backward wave radiation. It was postulated that if a leading phase condition were achieved (with associated attenuation) over a greater distance along the structure, the backfire directivity would be improved. However, the several attempts made yielded no further and, in fact, usually no less success than that shown for UPM(10)C in Figures 44 through 46. Specific attempts included increasing the monopole length-to-spacing ratio, varying the ratio of line impedance to monopole impedance and applying several different magnitudes of zigzag to the feed line. It is apparent from the amplitude and phase data for UPM(10)C that a significant amount of guess work would have to go into determining representative values of the phase constant. For this reason a k-β curve is not included with the discussion of this structure.

Although the particular models investigated in this class of monopole arrays did not yield entirely satisfactory directional performance, their general backfire tendency should motivate further study of these structures.

4.8 HFUPM(5)—Helix Fed Monopole Array

The helix fed monopole array HFUPM(5) is the last periodic structure to be covered in this report. It is only one of several of its kind on which both near-field and far-field measurements were made. This particular structure was selected to report on because of the character of its k-β curve,

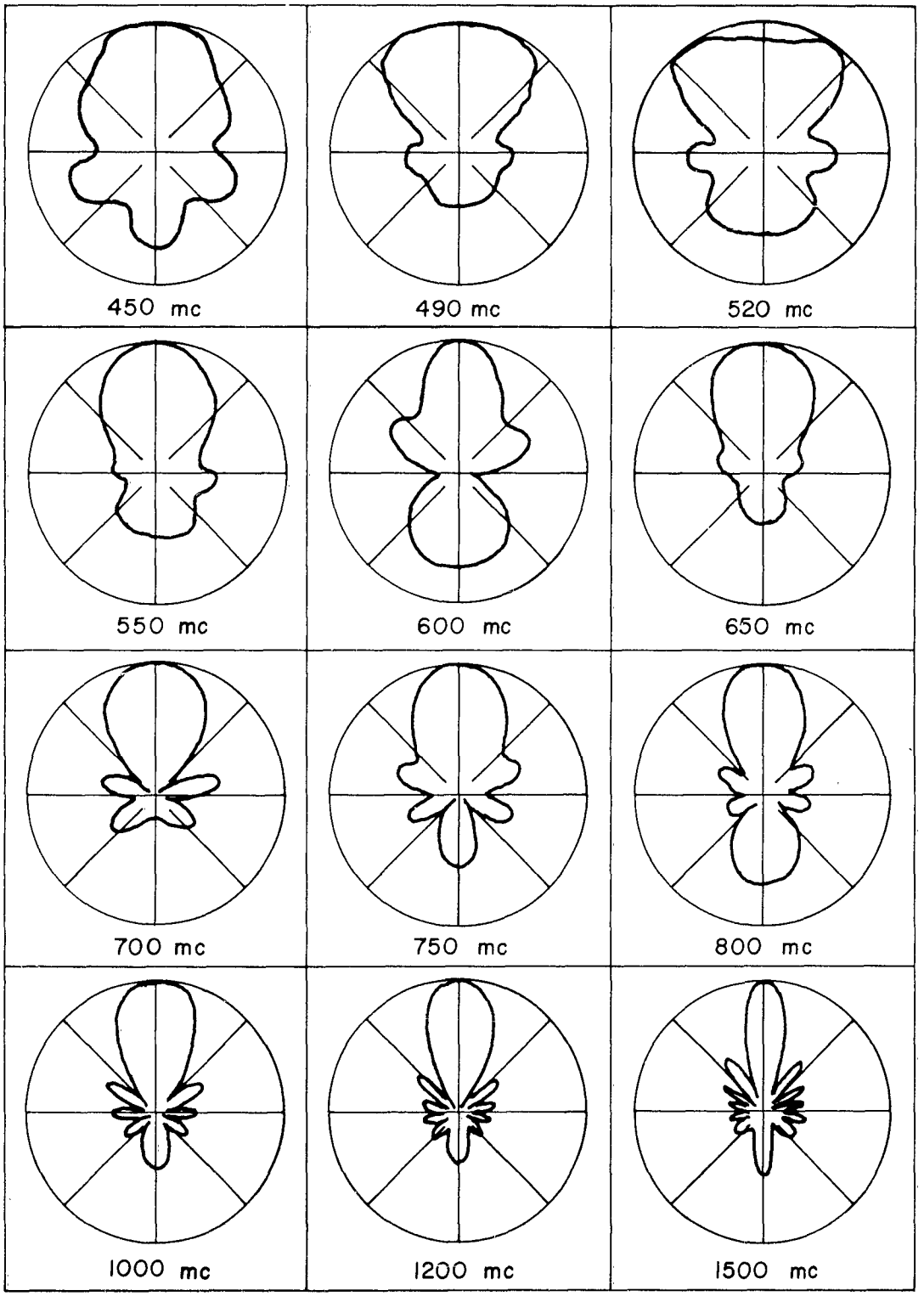

Figure 43. Measured H-Plane Voltage Patterns for UPM(10)C.

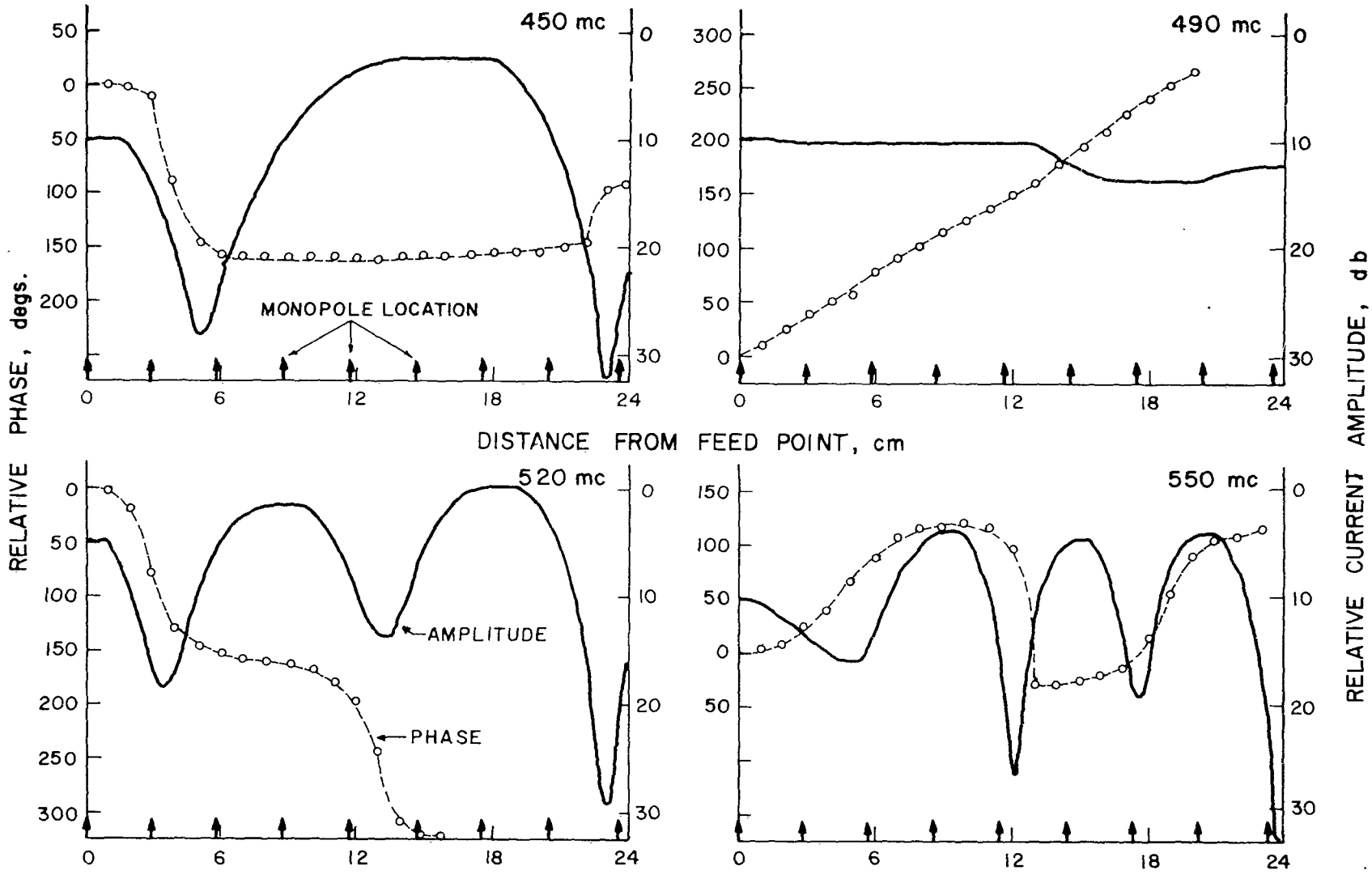

Figure 44. Measured Amplitude and Phase Distributions for UPM(10)C.

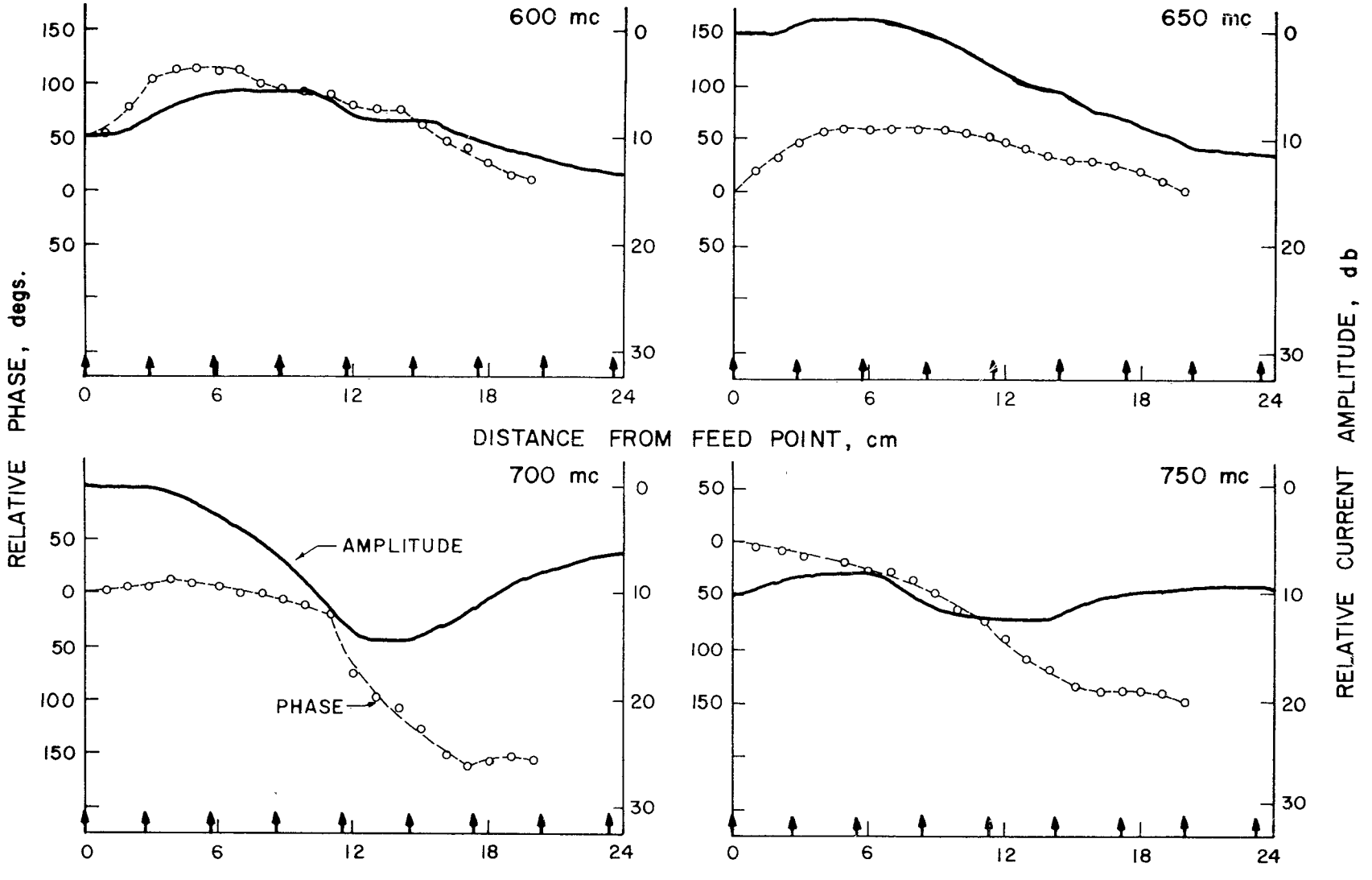

Figure 45. Measured Amplitude and Phase Distributions for UPM(10)C.

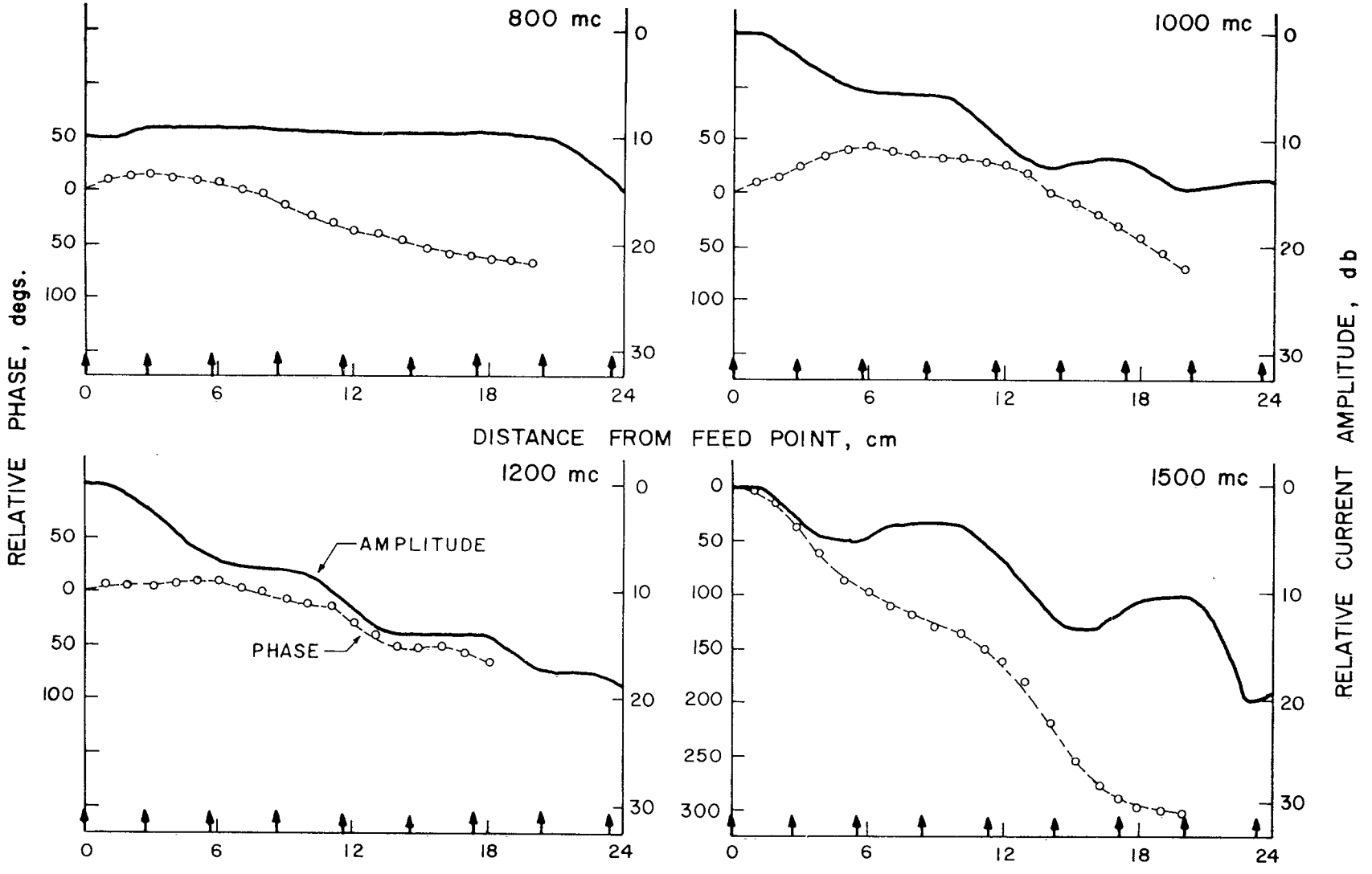

Figure 46. Measured Amplitude and Phase Distributions for UPM(10)C.

and not because of any potential usefulness it has in h-f frequency independent antennas. If one were interested in only demonstrating the utility of the Brillouin diagram in analyzing near-field data, he would need to investigate solely a model similar to HFUPM(5). For here the structure exhibits most all forms of directivity and illustrates well the extent to which the Brillouin diagram may be used to predict the radiation properties of a given monopole array.

The pertinent details of the HFUPM(5) model are shown in the lower right of Figure 2. Attention is called to the use of a good lossless dielectric material to support the helix. Early work with this type of structure employed dielectric forms such as wood dowel and fiber tubing. It was discovered, however, that these materials were too lossy and as a result would have as much or more control over the current distribution along the array as did the structure itself.

The k-β / attenuation diagram for HFUPM(5) is shown in Figure 47 and some of the corresponding measured amplitude and phase data in Figures 48 through 51. Figures 52 and 53 illustrate most of the measured H-plane radiation patterns. Because of the rather full coverage which this particular structure exhibits, it is instructive to review briefly the near-field data and to correlate these data with the k-β curve and far-field patterns. In this way some of the points of significance discussed heretofore will be reiterated. However, no attempt is made to analyze the mechanisms which take place to effect the various gyrations in amplitude and phase distribution nor in the achievement of the various pattern directivities.

Beginning with the amplitude and phase distributions along the structure at the lower frequencies, it is seen that these are simply of the standing wave form. Likewise, there exists no decay in the amplitude with distance

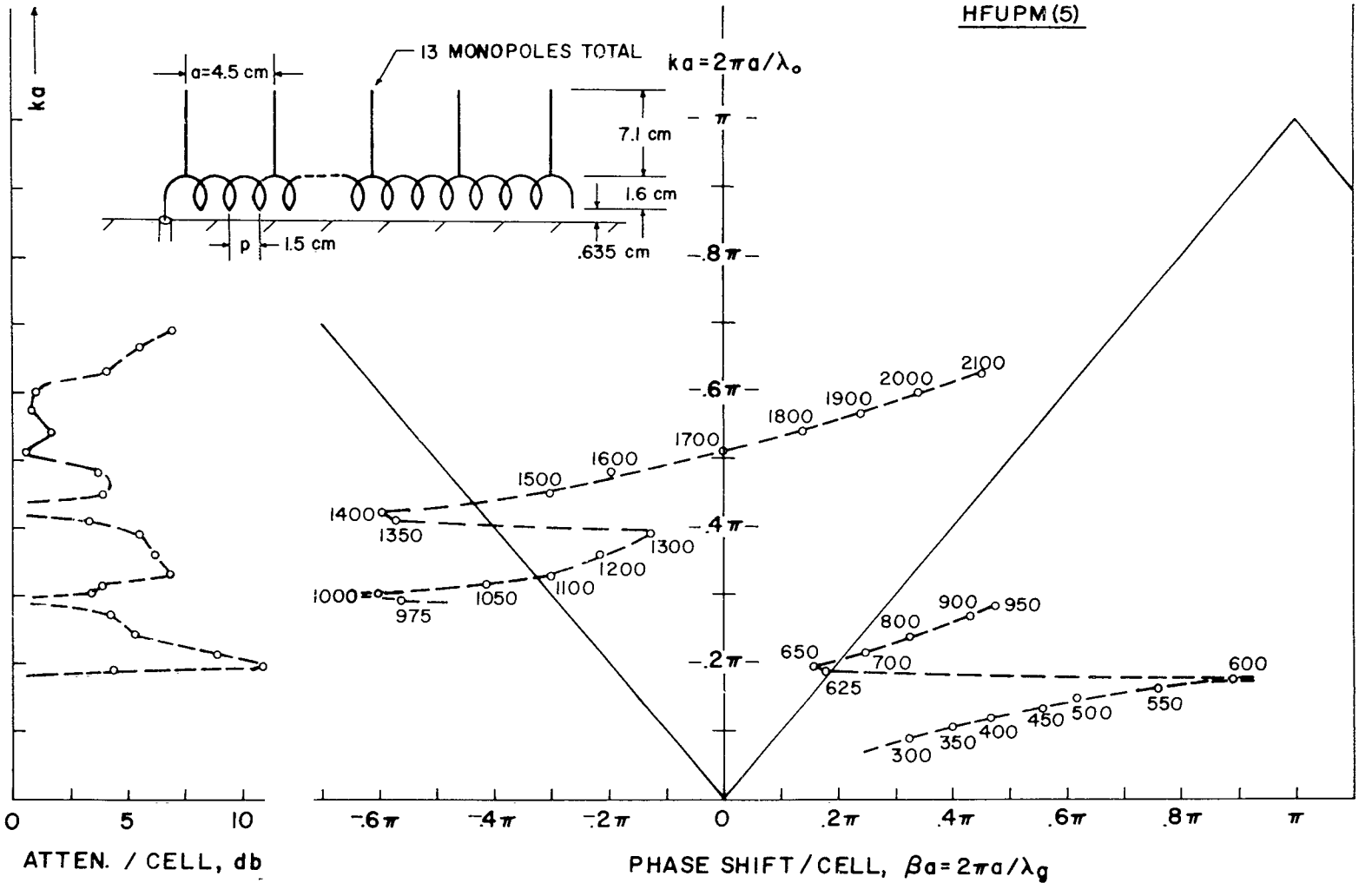

Figure 47. The k-β /Attenuation Diagram for the Helix-Fed Monopole Array. HFUPM(5).

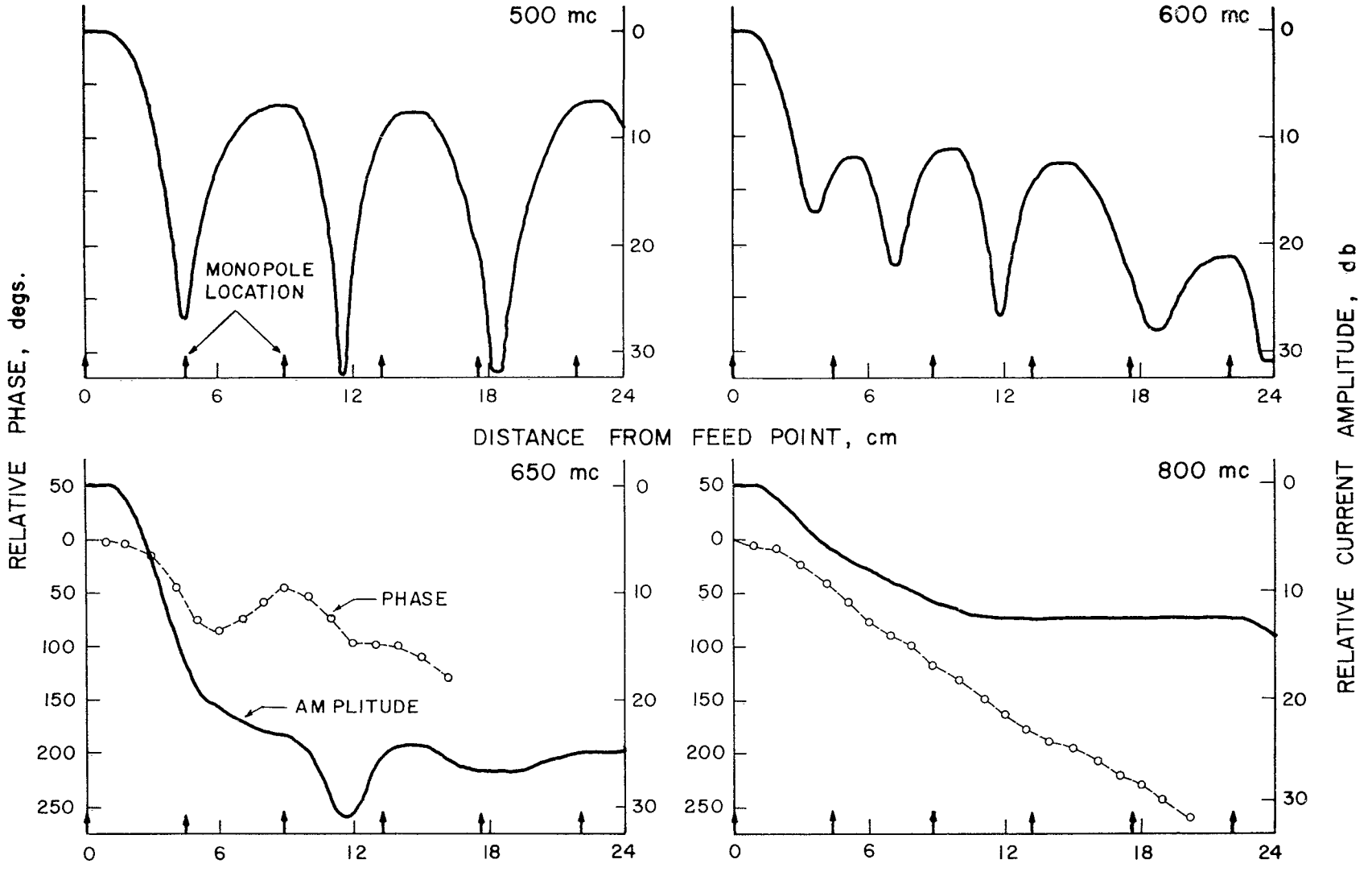

Figure 48. Measured Amplitude and Phase Distributions for HFUPM(5).

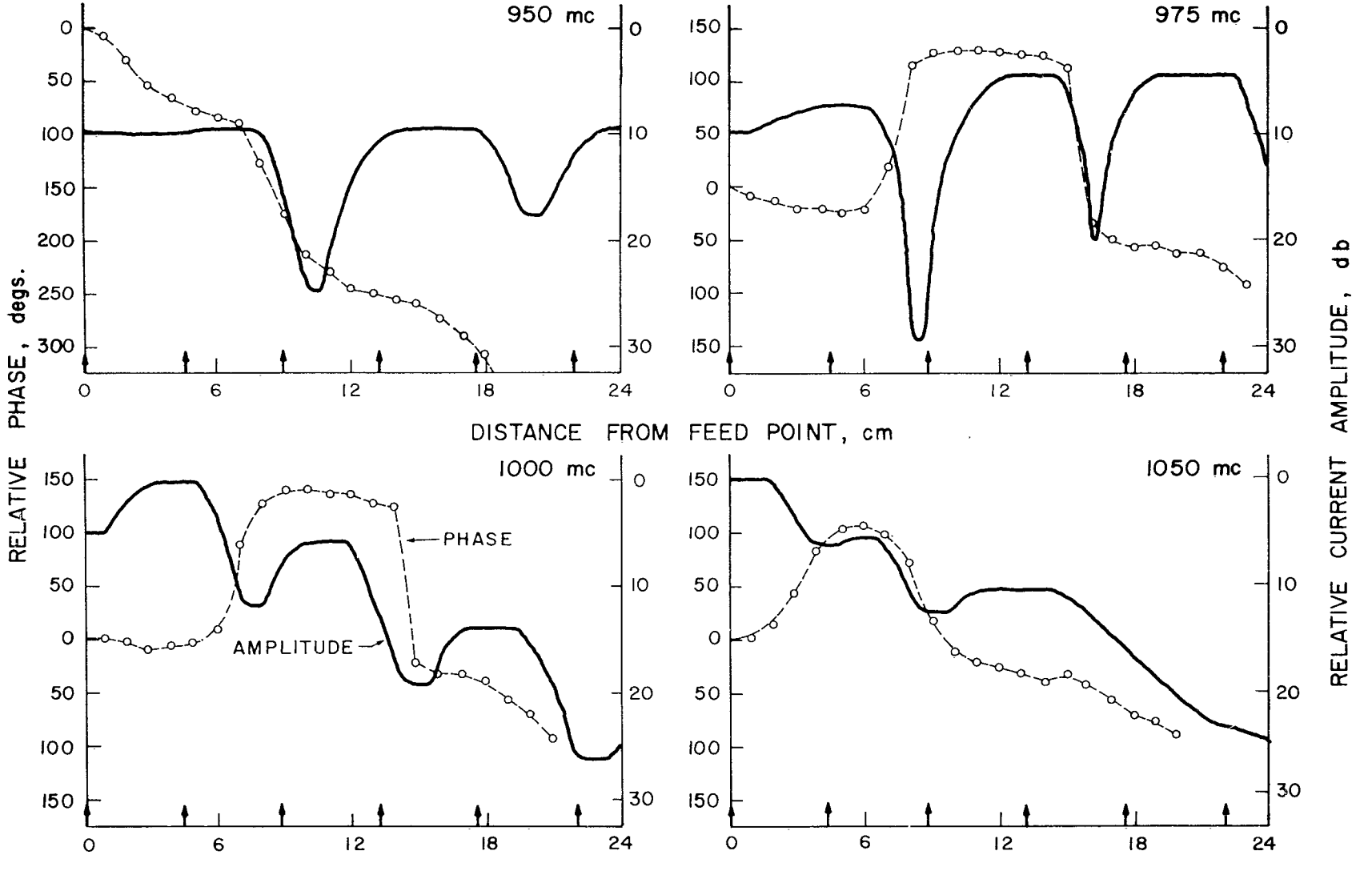

Figure 49. Measured Amplitude and Phase Distributions for HFUPM(5).

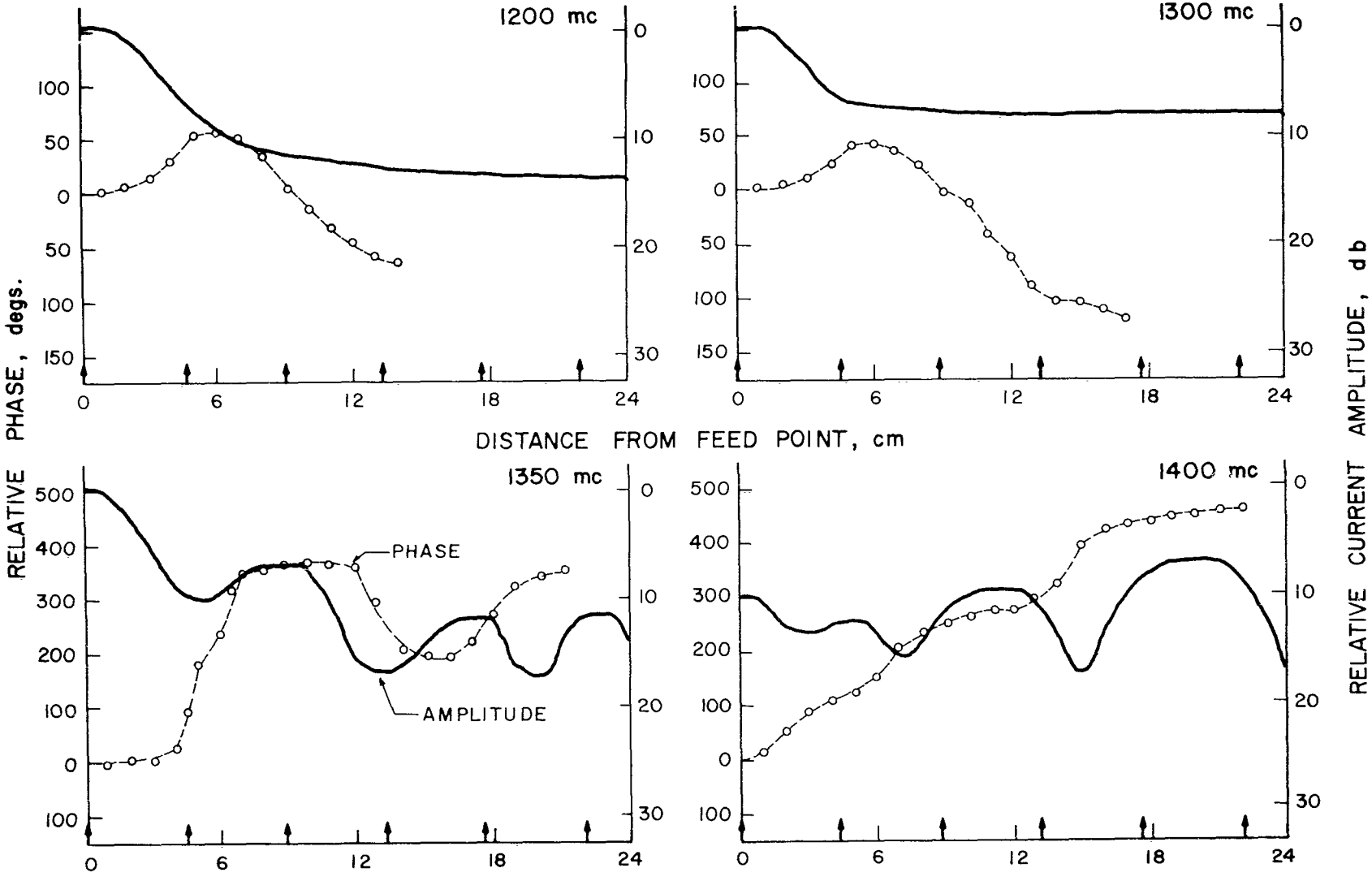

Figure 50. Measured Amplitude and Phase Distributions for HFUPM(5).

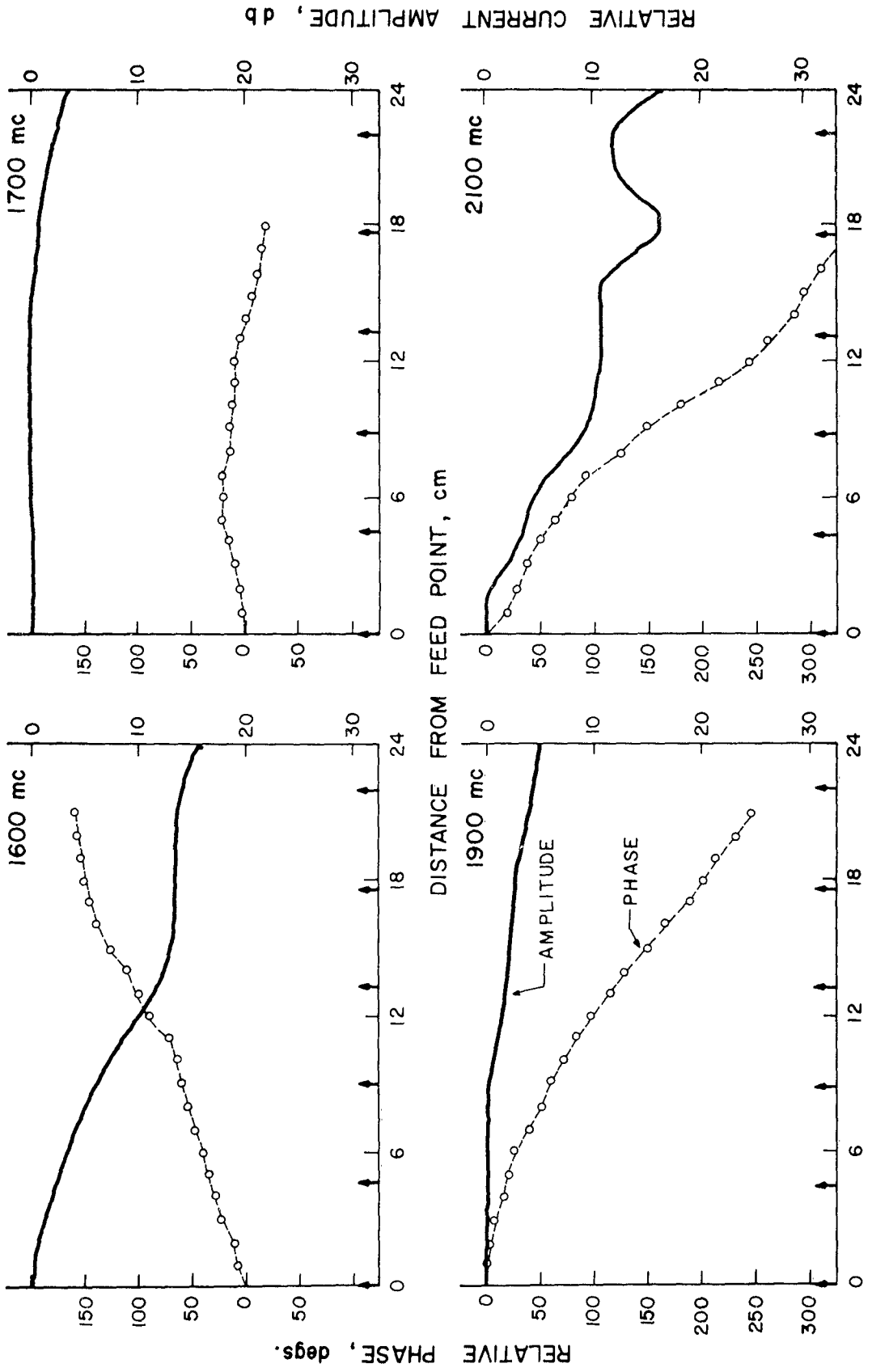

Figure 51. Measured Amplitude and Phase Distributions for HFUPM(5).

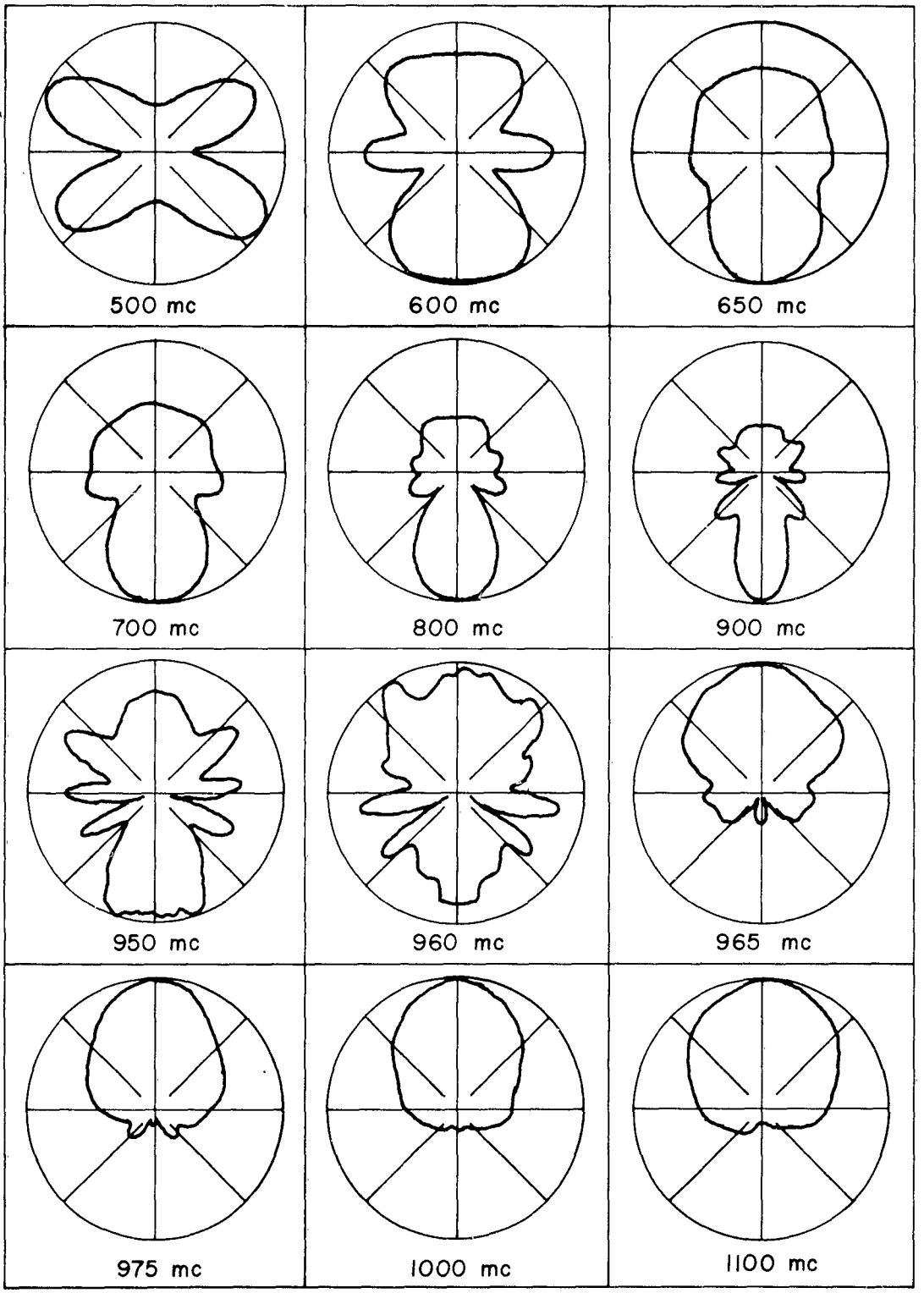

Figure 52. Measured H-Plane Voltage Patterns for HFUPM(5).

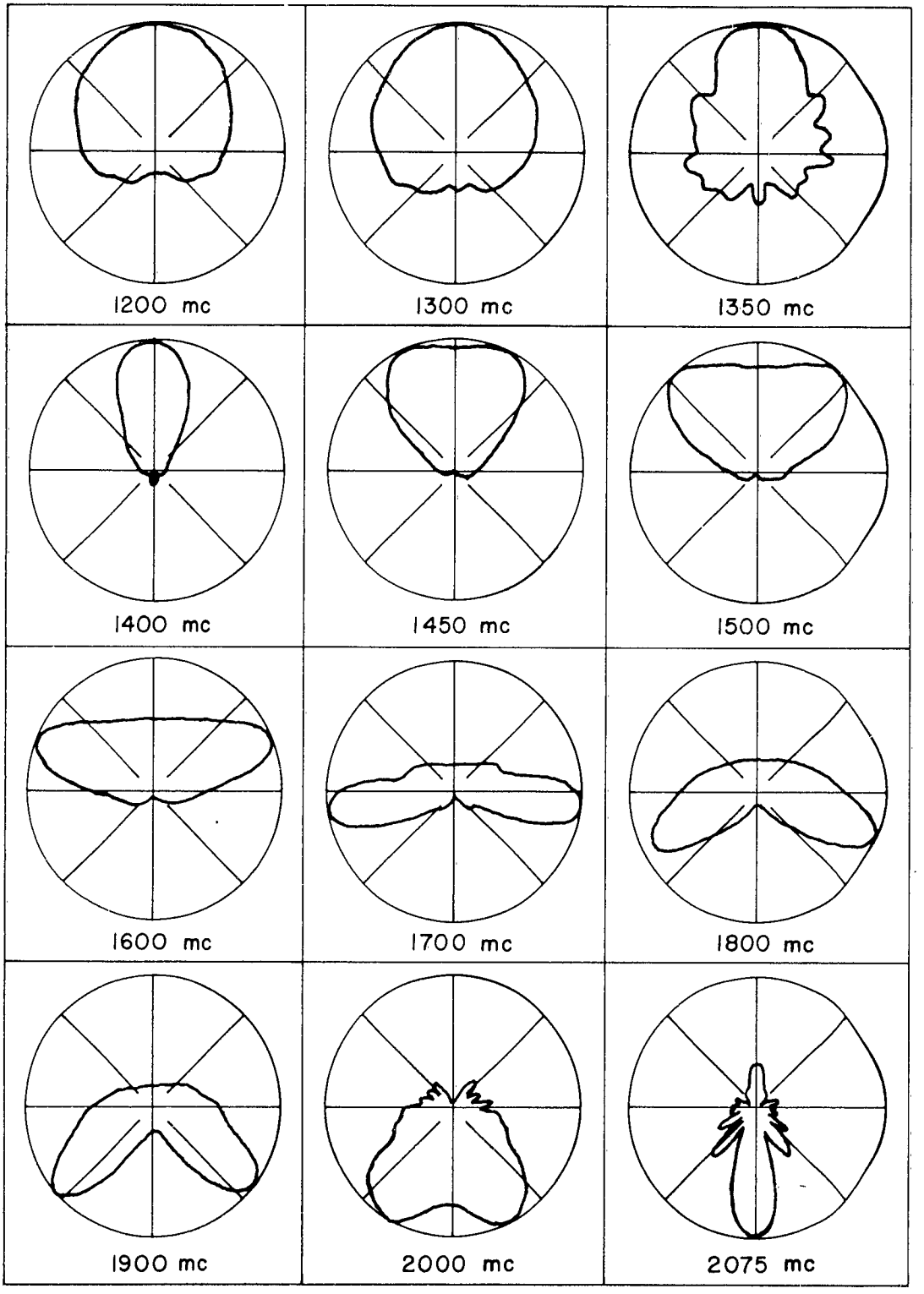

Figure 53. Measured H-Plane Voltage Patterns for HFUPM(5).

along the structure, and the directional properties correspond to those of a standing wave current distribution. This exists up to about 600 Mc. The equivalent length of the monopoles is approximately 10.5 cm and, hence, should resonate at about 680 Mc. Apparently, however, the effect of the helix causes the first resonance to occur somewhat lower in frequency, for near 600 Mc the typical distorted standing wave is observed at the approach of turnover. There then follows a narrow region of frequencies in which a unique value for the phase constant cannot be measured. As the frequency of excitation is increased the amplitude and phase distributions gradually become smooth and correspond to those of a predominantly traveling wave. Associated with this condition are attenuation of the traveling wave and endfire tendency in the radiation pattern. Note the k-β curve in this frequency region and observe also the fact mentioned previously regarding the degree of endfire directivity; that is, the pattern is not ideally unidirectional. Above about 900 Mc the structure undergoes a change to effect another region of standing wave amplitude and phase distributions, and a corresponding change in pattern takes place. The next turnover region occurs between 950 and 975 Mc. Note here the significant change in the structure's directional properties and the distinct backfire patterns which occur immediately after turnover. It is interesting to note again the phenomenon occurring at, for example, 975 Mc. Here the pattern is definitely unidirectional, yet the amplitude distribution is that of a standing wave. However, as also observed before, the character of the phase over the first cell or two is of a leading nature. Then as the frequency is further increased the amplitude distribution becomes smoother and undergoes decay. Attention is called to the relatively short distance along which the structure exhibits a leading phase. This together with the rate of amplitude attenuation is

indicative of the importance of the first cell or two of these uniform structures. At about 1300 Mc, rather than continuing across the radiation region of the Brillouin diagram as might be expected, the k-β curve is perturbed and returns to the backfire region of the Brillouin triangle. The measured patterns correspond well to this minor turnover. The pattern at 1400 Mc demonstrates the achievement of higher directive gain by illuminating a greater portion of the structure; that is, the rate of decay is slower than that for the preceding backfire frequencies. Finally, as the frequency is increased to where the k-β curve passes across the $\beta a \simeq 0$ axis into the forward wave domain of the radiation region, there occurs the characteristic scanning of the beam.

As a matter of interest here, the slope of the k-β curve between 1500 and 2100 Mc is approximately 0.27, which corresponds to a slowness factor of 3.7. The theoretical slowness factor for the subject helix itself is 3.5. This indicates, therefore, that in this frequency region the inherent slowness of the helix predominates, as might be expected since here the monopoles themselves are on the order of one-half wave in length. Calculations of the beam angle θ, according to the expression $\cos \theta = \beta/k$, as the beam scans with frequency over this range, shows agreement to within about 10° of the measured angles.

5. CONCLUSION

The purpose of this experimental research effort was to learn more about the fundamental principles which underlie successful frequency independent antennas, which, in turn, would hopefully lead to the most adequate state-of-the-art design for use in the wideband h-f radio direction finding system. This objective was accomplished through a comprehensive investigation of the near-field characteristics of various periodic monopole arrays. The study was based on the theory that knowledge of the properties of the uniformly periodic structure whose geometry is the counter part of that of the log-periodic structure would offer an insight to the basic principles of frequency independence. Hence, the major portion of the effort involved monopole structures whose periodicity was uniform and, consequently, their near-field characteristics were observed as a function of frequency. This led to extensive use of the Brillouin diagram, and its utility in the analysis and summation of the measured near-field data was shown.

In this effort, studies were made on periodic monopole structures whose designs were known to offer successful frequency independent performance as well as on structures whose designs do not. Results of the studies made on several specific and representative structures were reported. In correlating the various near-field data, it was shown that the character of the amplitude and phase distributions along the structure, particularly that of the phase, over the first cell or two controlled to a large extent the directional properties of the structure. Specifically, if the phase of the wave on the structure assumed a leading sense over only the first cell or two, and even if the amplitude distribution corresponded to that of a standing wave, distinct backward directivity was established. However, it is assumed that effective

radiation does not take place until the feeder wave undergoes substantial decay with distance along the structure. Relative gain observations during far-field pattern measurements indicated that this was so. At the near-field frequency of turnover to backward directivity it usually was difficult to deliver enough power to the structure for adequate signal detection. In other words, there appeared to exist a condition of almost complete reflection of the generator power incident at the feed terminal of the array. This condition, however, would exist for only a very narrow region of frequencies, depending on the Q of the structure, before substantial attenuation of the feeder wave would take place. Backward directed radiation is an inherent trait in all known unidirectional log-periodic antennas, and, therefore, the establishment of this condition seems imperative for achieving successful frequency independent antenna designs —— at least for the vertically polarized monopole array class of structures. The leading phase and associated backward traveling wave property was the distinguishing difference between the successful and unsuccessful designs for frequency independence.

From the many near-field measurements of amplitude and phase, and from the corresponding far-field measurements of radiation patterns, analysis of the near-field data by use of the Brillouin or k-β diagram was found to be very effective. The display of H-plane radiation patterns on the Brillouin diagram of Figure 54 illustrates the general directional characteristics which can be expected as a function of the k-to-β relation. In like manner, typical amplitude and phase distributions are exemplified in Figure 55. Included also in Figure 55 are typical patterns and relative locations of the phase constant which correspond to the respective plots of amplitude and phase.

The rate of decay of the wave propagating along the structure was illustrated in the report as attenuation (in db) per cell. Displaying the attenu-

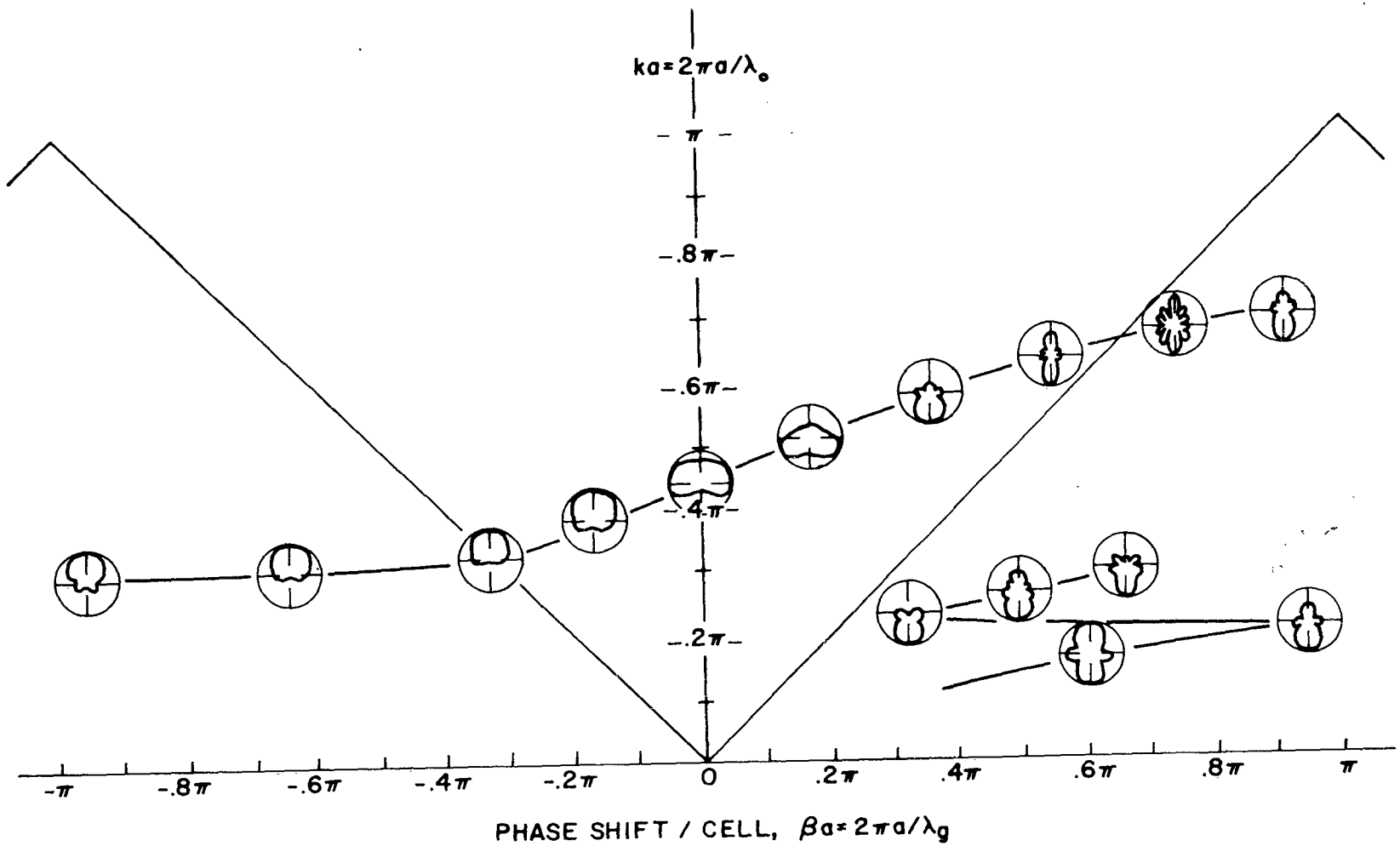

Figure 54. Display of H-Plane Directional Characteristics on the Brillouin Diagram for a Typical Uniform Periodic Monopole Array.

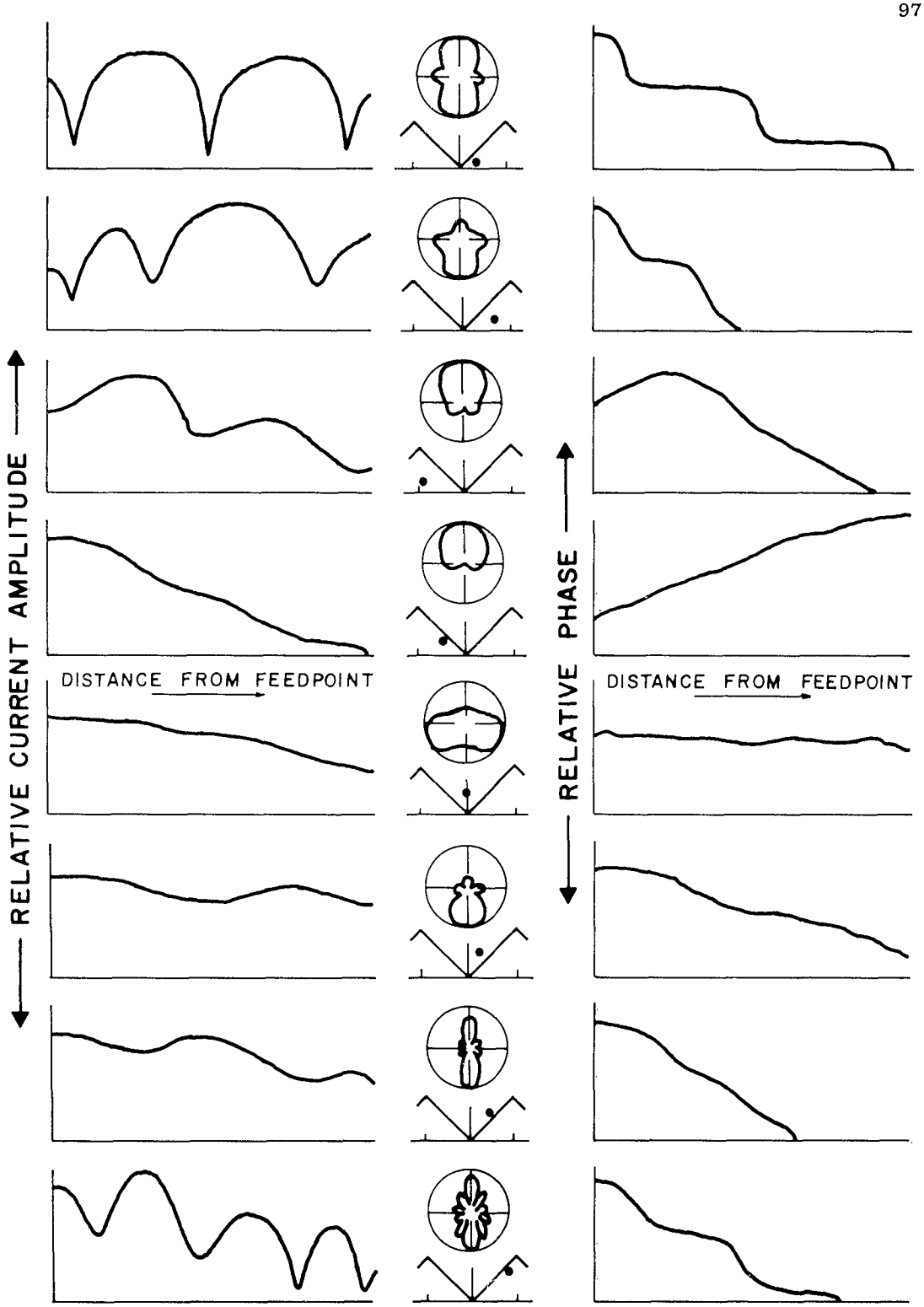

Figure 55. Relative Amplitude and Phase Characteristics of a Typical Uniform Periodic Monopole Array.

ation rate in this manner, however, may prove misleading since the attenuation rate becomes a function of cell dimension. As an aftermath of this work, it is suggested that the attenuation rate be otherwise normalized, perhaps to guide-wavelength. A further suggestion, one made by Professor G. A. Deschamps, is that of plotting the propagation constnat (ie., attenuation and phase) in the complex plane rather than displaying the real and imaginary components as separate data. By so doing, the locus of points in the complex plane should establish a smooth curve, and, hence, not exhibit any gaps or regions of uncertainty.

It is hoped that the results of this effort have afforded useful experimental evidence to the hypothesized relation between backward wave radiation and the log-periodic antenna, and, further, that the data contained herein will offer supplemental aid to those who may be engaged in the further development of such theories.

BIBLIOGRAPHY

1. Mayes, P. E., Deschamps, G. A., and Patton, W. T., "Backward-Wave Radiation from Periodic Structures and Applications to the Design of Frequency-Independent Antennas", Proc. IRE, (correspondence), Vol. 49, No. 5, pp. 962-963, May, 1961, and Mayes, P. E., Deschamps, G. A., and Patton, W. T., "Backward-Wave Radiation from Periodic Structures and Application to the Design of Frequency-Independent Antennas", Tech. Report No. 60, Contract No. AF33(657)8460, Antenna Laboratory, University of Illinois, Urbana, Illinois, October, 1962.

2. Mayes, P. E. and Ingerson, P. G., "Near-Field Measurements on Backfire Periodic Dipole Arrays", Proc. Twelfth Symp. USAF Antenna Res. and Dev. Symp., Allerton Park, Monticello, Illinois, October, 1962.

3. Deschamps, G. A., "Symmetry, As Applied to Periodic Structures", Antenna Laboratory Seminar, University of Illinois, Urbana, Illinois, December, 1962.

4. Watkins, D. A., Topics in Electromagnetic Theory, John Wiley and Sons, Inc., New York, 1958.

5. Interim Engineering Report No. 6, "Broadband Wide Aperture Radio Location Antenna System", Contract No. NOBSR 85243, Electrical Engineering Research Laboratory, Engineering Experiment Station, University of Illinois, Urbana, Illinois, December, 1962.

6. Berry, D. G. and Ore, F. R., "Log-Periodic Monopole Array", CRR No. 220, Collins Radio Company, Cedar Rapids, Iowa, October, 1960.

7. Wickersham, A. F. and Franks, R. E., "Further Developments in Tapered Ladder Antennas", Proc. IRE, (correspondence), Vol. 49, No. 1, p. 378, January, 1961.

APPENDIX

Phase Measurement Error Due to Mismatched Load on Slotted-Line

Shown below is a simple derivation of a useful expression which relates the phase variation along a slotted line to the VSWR on the line. This situation is of general interest in phase measurement set-ups which employ the terminated slotted line as the source of variable reference phase. Since most commercially available terminations do not offer a perfect impedance match to the slotted line, an error in the phase measurement can be expected. However, as the example below illustrates, this particular source of error is not serious in the measurements of interest here, for most good quality terminations do not create a VSWR much in excess of 1:1.

With reference to Figure 7, and assuming that the input end of the slotted line is matched, we have

$$\bar{E}_i = E_i \exp [j(\omega t - \beta x)] \tag{7}$$

and

$$\bar{E}_r = E_r \exp [j(\omega t + \beta x + \alpha)] \tag{8}$$

where $\bar{E}_i$ = complex incident voltage.

$\bar{E}_r$ = complex reflected voltage.

E_i = magnitude of the incident voltage.

E_r = magnitude of the reflected voltage.

$\omega t = 2\pi$ ft, time phase angle.

β = phase constant of the slotted line medium.

x = distance along the slotted line with positive direction toward the load.

α = phase angle of the load.

The argument will not be deterred if we assume that the load is purely resistive; therefore, $\alpha = 0$. Hence, the reflection coefficient, $\overline{\Gamma}$, can be written as

$$\overline{\Gamma} = \frac{\overline{E}_r}{\overline{E}_i} = \frac{E_r}{E_i} \exp [j(2\beta x)] \tag{9}$$

or

$$= \Gamma \exp [j(2\beta x)] \tag{10}$$

The total voltage on the slotted-line, $\overline{E}_R$, is the phasor sum of $\overline{E}_i$ and $\overline{E}_r$. Letting θ be the phase angle of $\overline{E}_R$ and equating real and imaginary components, we have

$$E_T \cos (-\theta) = E_i \cos (-\beta x) + E_r \cos (\beta x) \tag{11}$$

and

$$E_T \sin (-\theta) = E_i \sin (-\beta x) + E_r \sin (\beta x) \tag{12}$$

For convenience let $E_i = 1$. Then the above reduces to

$$E_T \cos \theta = (1 + \Gamma) \cos \beta x \tag{13}$$

and

$$E_T \sin \theta = (1-\Gamma) \sin \beta x \tag{14}$$

or

$$\tan \theta = \frac{1 - \Gamma}{1 + \Gamma} \tan \beta x \tag{15}$$

Since VSWR = $\rho = \frac{1 + \Gamma}{1 - \Gamma}$

we have finally that

$$\theta = \arctan \left[\frac{1}{\rho} \tan \beta x \right] \tag{16}$$

The maximum magnitude of the VSWR observed for the load used in this work was about 1.07:1. Using the expression (16), the phase correction curve of Figure 56 was calculated. As it can be seen, the degree of error was insignificant insofar as the data of interest in this work was concerned.

In a similar manner, an expression for the maximum phase error as a function of the VSWR on the slotted line can be derived. Thus, we are interested in an expression of the form

$$(\theta - \beta x)_{max.} = f(\rho)$$

From (16) above and by trigonometric identity, we can write

$$(\theta - \beta x) = \arctan \left[\frac{(1 - \rho) \tan \theta}{(1 + \rho \tan^2 \theta} \right] \tag{17}$$

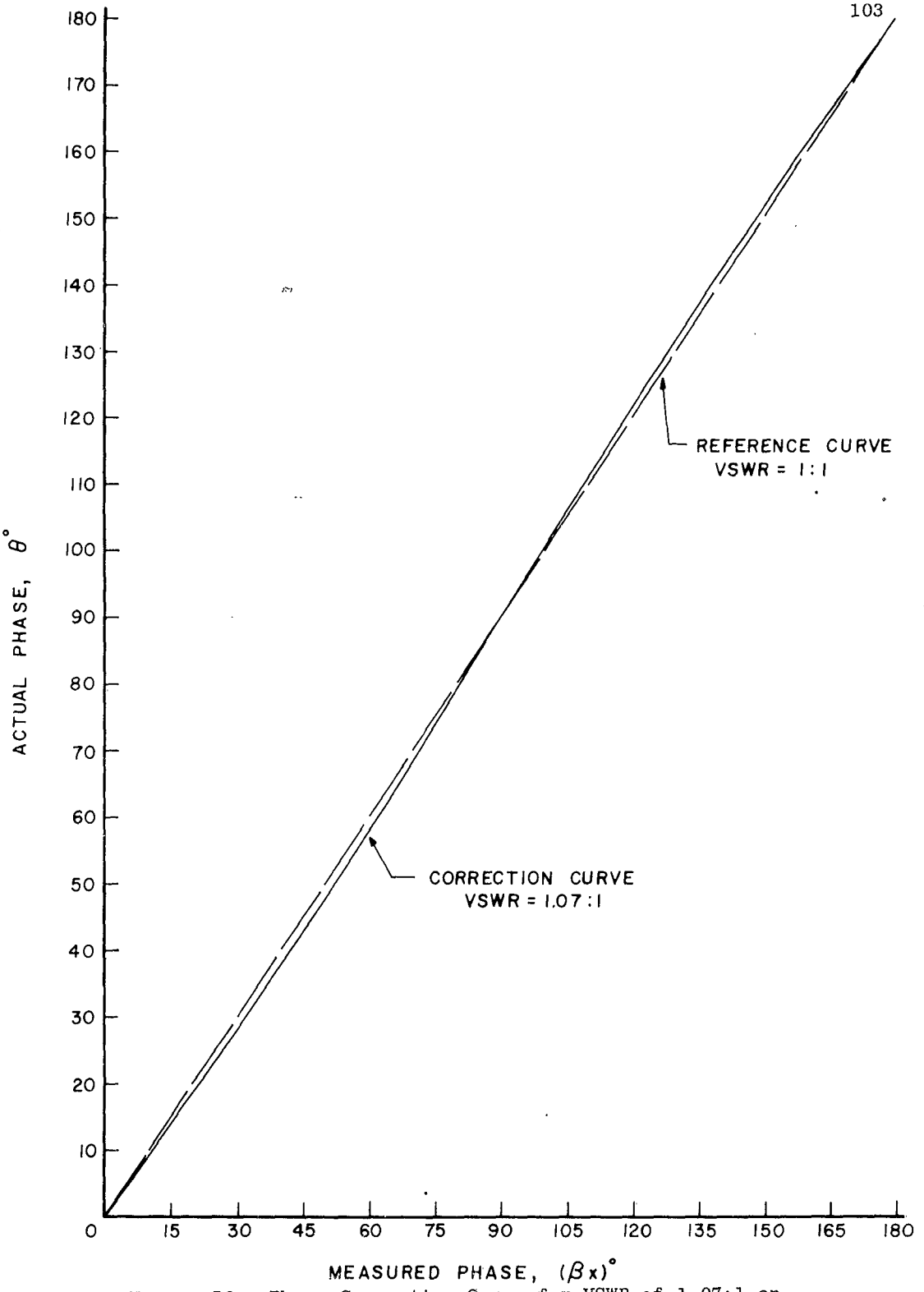

Figure 56. Phase Correction Curve for VSWR of 1.07:1 on the Slotted Line.

and from

$$\frac{d(\theta - \beta x)}{d\theta} = \frac{(1-\rho)\sec^2\theta\,(1+\rho\tan^2\theta - 2\rho\tan^2\theta)}{(1+\rho\tan^2\theta)^2 + (1-\rho)^2\tan\theta} \tag{18}$$

it is found that

$$\tan\theta = \sqrt{\frac{1}{\rho}} \tag{19}$$

for the condition of maximum difference. Hence

$$(\theta - \beta x)_{max.} = \arctan\left[\frac{\sqrt{\rho}}{2}\left(1 - \frac{1}{\rho}\right)\right] \tag{20}$$

Using Equation (2C), the plot of maximum phase error shown in Figure 57 was calculated.

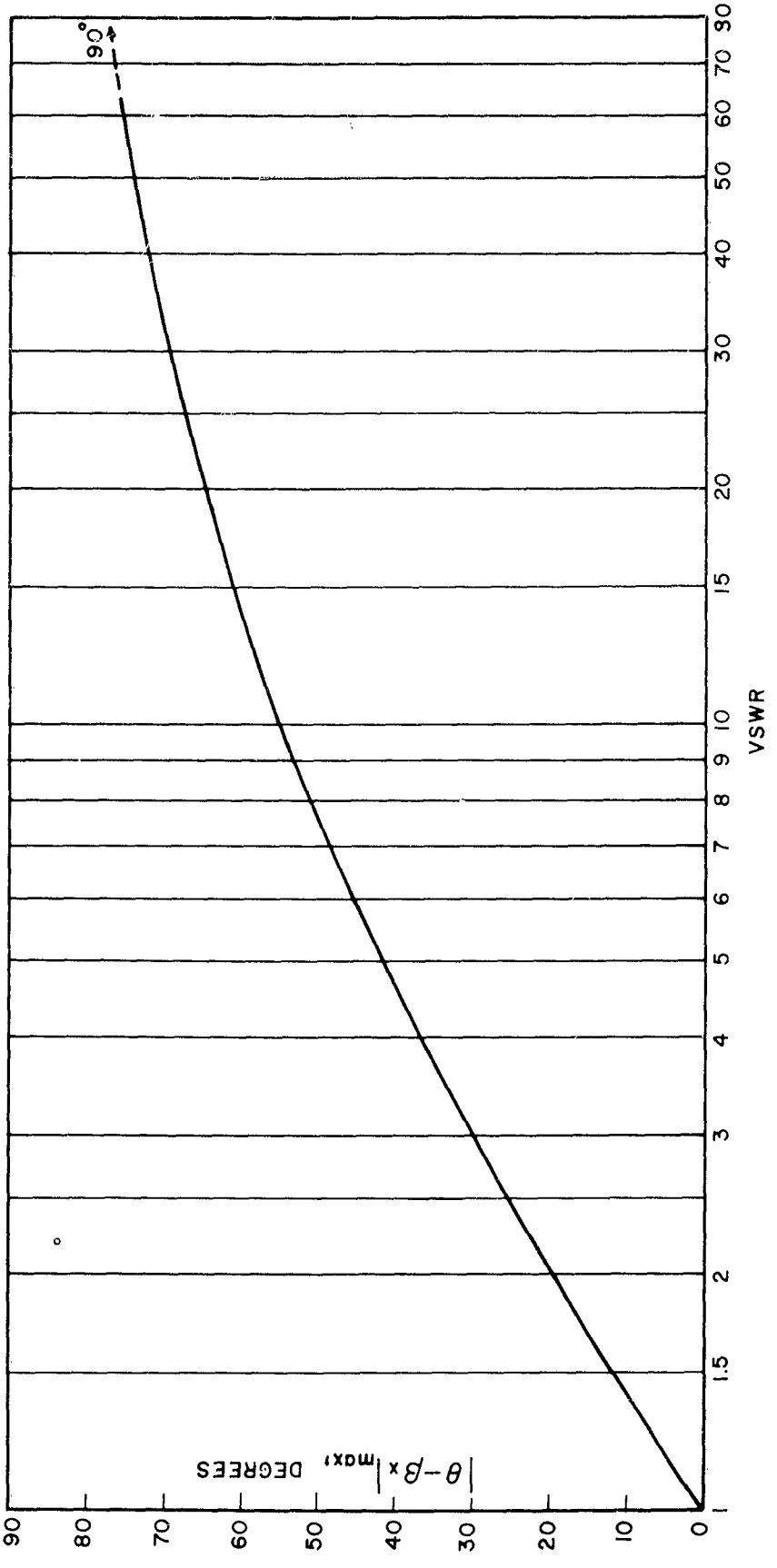

Figure 57. Maximum Phase Error as a Function of VSWR on the Slotted Line.